

BULLETIN OF RUSSIAN STATE MEDICAL UNIVERSITY

BIOMEDICAL JOURNAL OF PIROGOV RUSSIAN NATIONAL RESEARCH MEDICAL UNIVERSITY

EDITOR-IN-CHIEF Denis Rebrikov, DSc, professor

DEPUTY EDITOR-IN-CHIEF Alexander Oettinger, DSc, professor

EDITORS Valentina Geidebrekht, PhD; Nadezda Tikhomirova

TECHNICAL EDITOR Evgeny Lukyanov

TRANSLATORS Nadezda Tikhomirova, Vyacheslav Vityuk

DESIGN AND LAYOUT Marina Doronina

EDITORIAL BOARD

Averin VI, DSc, professor (Minsk, Belarus)
Alipov NN, DSc, professor (Moscow, Russia)
Belousov VV, DSc, professor (Moscow, Russia)
Bogomilskiy MR, corr. member of RAS, DSc, professor (Moscow, Russia)
Bozhenko VK, DSc, CSc, professor (Moscow, Russia)
Bylova NA, CSc, docent (Moscow, Russia)
Gainetdinov RR, CSc (Saint-Petersburg, Russia)
Gendlin GYe, DSc, professor (Moscow, Russia)
Ginter EK, member of RAS, DSc (Moscow, Russia)
Gorbacheva LR, DSc, professor (Moscow, Russia)
Gordeev IG, DSc, professor (Moscow, Russia)
Gudkov AV, PhD, DSc (Buffalo, USA)
Gulyaeva NV, DSc, professor (Moscow, Russia)
Gusev EI, member of RAS, DSc, professor (Moscow, Russia)
Danilenko VN, DSc, professor (Moscow, Russia)
Zarubina TV, DSc, professor (Moscow, Russia)
Zatevakhin II, member of RAS, DSc, professor (Moscow, Russia)
Kagan VE, professor (Pittsburgh, USA)
Kzyzhkowska YuG, DSc, professor (Heidelberg, Germany)
Kobriniskii BA, DSc, professor (Moscow, Russia)
Kozlov AV, MD PhD (Vienna, Austria)
Kotelevtsev YuV, CSc (Moscow, Russia)
Lebedev MA, PhD (Darem, USA)
Manturova NE, DSc (Moscow, Russia)
Milushkina OYu, DSc, professor (Moscow, Russia)
Mitupov ZB, DSc, professor (Moscow, Russia)
Moshkovskii SA, DSc, professor (Moscow, Russia)
Munblit DB, MSc, PhD (London, Great Britain)

Negrebetsky VV, DSc, professor (Moscow, Russia)
Novikov AA, DSc (Moscow, Russia)
Pivovarov YuP, member of RAS, DSc, professor (Moscow, Russia)
Polunina NV, corr. member of RAS, DSc, professor (Moscow, Russia)
Poryadin GV, corr. member of RAS, DSc, professor (Moscow, Russia)
Razumovskii AYU, corr. member of RAS, DSc, professor (Moscow, Russia)
Rebrova OYu, DSc (Moscow, Russia)
Rudoy AS, DSc, professor (Minsk, Belarus)
Rylova AK, DSc, professor (Moscow, Russia)
Savelieva GM, member of RAS, DSc, professor (Moscow, Russia)
Semiglazov VF, corr. member of RAS, DSc, professor (Saint-Petersburg, Russia)
Skoblina NA, DSc, professor (Moscow, Russia)
Slavyanskaya TA, DSc, professor (Moscow, Russia)
Smirnov VM, DSc, professor (Moscow, Russia)
Spallone A, DSc, professor (Rome, Italy)
Starodubov VI, member of RAS, DSc, professor (Moscow, Russia)
Stepanov VA, corr. member of RAS, DSc, professor (Tomsk, Russia)
Suchkov SV, DSc, professor (Moscow, Russia)
Takhchidi KhP, member of RAS, DSc, professor (Moscow, Russia)
Trufanov GE, DSc, professor (Saint-Petersburg, Russia)
Favorova OO, DSc, professor (Moscow, Russia)
Filipenko ML, CSc, leading researcher (Novosibirsk, Russia)
Khazipov RN, DSc (Marsel, France)
Chundukova MA, DSc, professor (Moscow, Russia)
Shimanovskii NL, corr. member of RAS, DSc, professor (Moscow, Russia)
Shishkina LN, DSc, senior researcher (Novosibirsk, Russia)
Yakubovskaya RI, DSc, professor (Moscow, Russia)

SUBMISSION <http://vestnikrgmu.ru/login?lang=en>

CORRESPONDENCE editor@vestnikrgmu.ru

COLLABORATION manager@vestnikrgmu.ru

ADDRESS ul. Ostrovityanova, d. 1, Moscow, Russia, 117997

Indexed in Scopus. CiteScore 2022: 0.5

Scopus[®]

SCImago Journal & Country Rank 2020: 0.14

SJR

Scimago Journal & Country Rank

Indexed in WoS. JCR 2021: 0.5

WEB OF SCIENCE[™]

Listed in HAC 31.01.2020 (№ 507)



ВЫСШАЯ
АТТЕСТАЦИОННАЯ
КОМИССИЯ (ВАК)

Five-year h-index is 8

Google
scholar

Open access to archive

CYBERLENINKA

Issue DOI: 10.24075/brsmu.2023-01

The mass media registration certificate № 012769 issued on July 29, 1994

Founder and publisher is Pirogov Russian National Research Medical University (Moscow, Russia)

The journal is distributed under the terms of Creative Commons Attribution 4.0 International License www.creativecommons.org



Approved for print 28.02.2023
Circulation: 100 copies. Printed by Print.Formula
www.print-formula.ru

ВЕСТНИК РОССИЙСКОГО ГОСУДАРСТВЕННОГО МЕДИЦИНСКОГО УНИВЕРСИТЕТА

НАУЧНЫЙ МЕДИЦИНСКИЙ ЖУРНАЛ РНИМУ ИМ. Н. И. ПИРОГОВА

ГЛАВНЫЙ РЕДАКТОР Денис Ребриков, д. б. н., профессор

ЗАМЕСТИТЕЛЬ ГЛАВНОГО РЕДАКТОРА Александр Эттингер, д. м. н., профессор

РЕДАКТОРЫ Валентина Гейдебрект, к. б. н.; Надежда Тихомирова

ТЕХНИЧЕСКИЙ РЕДАКТОР Евгений Лукьянов

ПЕРЕВОДЧИКИ Надежда Тихомирова, Вячеслав Виток

ДИЗАЙН И ВЕРСТКА Марины Дорониной

РЕДАКЦИОННАЯ КОЛЛЕГИЯ

В. И. Аверин, д. м. н., профессор (Минск, Белоруссия)
Н. Н. Алипов, д. м. н., профессор (Москва, Россия)
В. В. Белоусов, д. б. н., профессор (Москва, Россия)
М. Р. Богомилский, член-корр. РАН, д. м. н., профессор (Москва, Россия)
В. К. Боженко, д. м. н., к. б. н., профессор (Москва, Россия)
Н. А. Былова, к. м. н., доцент (Москва, Россия)
Р. Р. Гайнетдинов, к. м. н. (Санкт-Петербург, Россия)
Г. Е. Гендлин, д. м. н., профессор (Москва, Россия)
Е. К. Гинтер, академик РАН, д. б. н. (Москва, Россия)
Л. Р. Горбачева, д. б. н., профессор (Москва, Россия)
И. Г. Гордеев, д. м. н., профессор (Москва, Россия)
А. В. Гудков, PhD, DSc (Буффало, США)
Н. В. Гуляева, д. б. н., профессор (Москва, Россия)
Е. И. Гусев, академик РАН, д. м. н., профессор (Москва, Россия)
В. Н. Даниленко, д. б. н., профессор (Москва, Россия)
Т. В. Зарубина, д. м. н., профессор (Москва, Россия)
И. И. Затевахин, академик РАН, д. м. н., профессор (Москва, Россия)
В. Е. Каган, профессор (Питтсбург, США)
Ю. Г. Кжышковска, д. б. н., профессор (Гейдельберг, Германия)
Б. А. Кобринский, д. м. н., профессор (Москва, Россия)
А. В. Козлов, MD PhD (Вена, Австрия)
Ю. В. Котелевцев, к. х. н. (Москва, Россия)
М. А. Лебедев, PhD (Дарем, США)
Н. Е. Мантурова, д. м. н. (Москва, Россия)
О. Ю. Милушкина, д. м. н., доцент (Москва, Россия)
З. Б. Митупов, д. м. н., профессор (Москва, Россия)
С. А. Мошковский, д. б. н., профессор (Москва, Россия)
Д. Б. Мунблит, MSc, PhD (Лондон, Великобритания)

В. В. Негребский, д. х. н., профессор (Москва, Россия)
А. А. Новиков, д. б. н. (Москва, Россия)
Ю. П. Пивоваров, д. м. н., академик РАН, профессор (Москва, Россия)
Н. В. Полунина, член-корр. РАН, д. м. н., профессор (Москва, Россия)
Г. В. Порядин, член-корр. РАН, д. м. н., профессор (Москва, Россия)
А. Ю. Разумовский, член-корр., профессор (Москва, Россия)
О. Ю. Реброва, д. м. н. (Москва, Россия)
А. С. Рудой, д. м. н., профессор (Минск, Белоруссия)
А. К. Рылова, д. м. н., профессор (Москва, Россия)
Г. М. Савельева, академик РАН, д. м. н., профессор (Москва, Россия)
В. Ф. Семиглазов, член-корр. РАН, д. м. н., профессор (Санкт-Петербург, Россия)
Н. А. Скоблина, д. м. н., профессор (Москва, Россия)
Т. А. Славянская, д. м. н., профессор (Москва, Россия)
В. М. Смирнов, д. б. н., профессор (Москва, Россия)
А. Спаллоне, д. м. н., профессор (Рим, Италия)
В. И. Стародубов, академик РАН, д. м. н., профессор (Москва, Россия)
В. А. Степанов, член-корр. РАН, д. б. н., профессор (Томск, Россия)
С. В. Сучков, д. м. н., профессор (Москва, Россия)
Х. П. Тахчиди, академик РАН, д. м. н., профессор (Москва, Россия)
Г. Е. Труфанов, д. м. н., профессор (Санкт-Петербург, Россия)
О. О. Фаворова, д. б. н., профессор (Москва, Россия)
М. Л. Филипенко, к. б. н. (Новосибирск, Россия)
Р. Н. Хазипов, д. м. н. (Марсель, Франция)
М. А. Чундокова, д. м. н., профессор (Москва, Россия)
Н. Л. Шимановский, член-корр. РАН, д. м. н., профессор (Москва, Россия)
Л. Н. Шишкина, д. б. н. (Новосибирск, Россия)
Р. И. Якубовская, д. б. н., профессор (Москва, Россия)

ПОДАЧА РУКОПИСЕЙ <http://vestnikrgmu.ru/login>

ПЕРЕПИСКА С РЕДАКЦИЕЙ editor@vestnikrgmu.ru

СОТРУДНИЧЕСТВО manager@vestnikrgmu.ru

АДРЕС РЕДАКЦИИ ул. Островитянова, д. 1, г. Москва, 117997

Журнал включен в Scopus. CiteScore 2022: 0,5

Журнал включен в WoS. JCR 2021: 0,5

Индекс Хирша (h²) журнала по оценке Google Scholar: 8

Scopus®

WEB OF SCIENCE™

Google
scholar

Scimago Journal & Country Rank 2020: 0,14

Журнал включен в Перечень 31.01.2020 (№ 507)

Здесь находится открытый архив журнала

SJR
Scimago Journal & Country Rank

ВЫСШАЯ
АТТЕСТАЦИОННАЯ
КОМИССИЯ (ВАК)

CYBERLENINKA

DOI выпуска: 10.24075/vrgmu.2023-01

Свидетельство о регистрации средства массовой информации № 012769 от 29 июля 1994 г.

Учредитель и издатель — Российский национальный исследовательский медицинский университет имени Н. И. Пирогова (Москва, Россия)

Журнал распространяется по лицензии Creative Commons Attribution 4.0 International www.creativecommons.org



Подписано в печать 28.02.2023
Тираж 100 экз. Отпечатано в типографии Print.Formula
www.print-formula.ru

ORIGINAL RESEARCH**4****Development and characterization of a vector system based on the simian adenovirus type 25**

Ozharovskaya TA, Popova O, Zubkova OV, Vavilova IV, Pochtovyi AA, Shcheblyakov DV, Gushchin VA, Logunov DYU, Gintsburg AL

Разработка и характеристика векторной системы на основе аденовируса обезьян 25-го серотипа

Т. А. Ожаровская, О. Попова, О. В. Зубкова, И. В. Вавилова, А. А. Почтовый, Д. В. Щебляков, В. А. Гушин, Д. Ю. Логунов, А. Л. Гинцбург

ORIGINAL RESEARCH**12****Single-domain antibody for binding the conserved epitope in the SARS-COV-2 spike protein receptor-binding domain**

Vorobyev PO, Tilib SV

Однодоменное антитело для связывания консервативного эпитопа рецептор-связывающего домена белка Spike коронавируса SARS-COV-2

П. О. Воробьев, С. В. Тилиб

METHOD**21****The approach to patient clustering based on the microchip data confined to distinct loci using the combinations of variants**

Iulmetova LN, Kulemin NA, Sharova EI

Подход к кластеризации пациентов по микрочиповым данным внутри отдельных локусов с использованием комбинаций вариантов

Л. Н. Юльметова, Н. А. Кулемин, Е. И. Шарова

ORIGINAL RESEARCH**30****Survival of human cells in tissue-engineered constructs stored at room temperature**

Rogovaya OS, Alpeeva EV, Ruchko ES, Ereemeev AV, Vorotelyak EA

Выживаемость клеток человека в биомедицинских клеточных продуктах при хранении при комнатной температуре

О. С. Роговая, Е. В. Алпеева, Е. С. Ручко, А. В. Еремеев, Е. А. Воротеляк

ORIGINAL RESEARCH**38****Assessment of the zona pellucida microdissection on its thickness in mammalian embryos**

Sitnikov DS, Ilina IV, Filatov MA, Silaeva YuYu

Исследование влияния микродиссекции блестящей оболочки эмбрионов млекопитающих на ее толщину

Д. С. Ситников, И. В. Ильина, М. А. Филатов, Ю. Ю. Силаева

ORIGINAL RESEARCH**45****Adipokines and myokines as indicators of obese phenotypes and their association with the gut microbiome diversity indices**

Shestopalov AV, Ganenko LA, Grigoryeva TV, Laikov AV, Vasilyev IYu, Kolesnikova IM, Naboka YuL, Volkova NI, Roumiantsev SA

Адипокины и миокины как индикаторы фенотипов ожирения и их связь с показателями разнообразия микробиома кишечника

А. В. Шестопалов, Л. А. Ганенко, Т. В. Григорьева, А. В. Лайков, И. Ю. Васильев, И. М. Колесникова, Ю. Л. Набока, Н. И. Волкова, С. А. Румянцев

OPINION**55****Main state industrial policy measures for the pharmaceutical industry of the Russian Federation**

TY Gaydin, EV Geller, SA Rozhnova, TA Gaydina

Основные меры государственной промышленной политики в фармацевтической отрасли Российской Федерации

Т. Ю. Гайдин, Е. В. Геллер, С. А. Рожнова, Т. А. Гайдина

ORIGINAL RESEARCH**59****Midterm severe forefoot deformity treatment outcomes in elderly patients**

Egiazaryan KA, Ratyev AP, Miroshnikova EA, Zhavoronkov EA, Abilemets AS

Среднесрочные результаты лечения тяжелой деформации переднего отдела стопы у пациентов пожилого возраста

К. А. Егиазарян, А. П. Ратьев, Е. А. Мирошникова, Е. А. Жаворонков, А. С. Абилеметс

DEVELOPMENT AND CHARACTERIZATION OF A VECTOR SYSTEM BASED ON THE SIMIAN ADENOVIRUS TYPE 25

Ozharovskaia TA , Popova O, Zubkova OV, Vavilova IV, Pochtovyi AA, Shcheblyakov DV, Gushchin VA, Logunov DYU, Gintsburg AL

Gamaleya National Research Center for Epidemiology and Microbiology of the Ministry of Health of the Russian Federation, Moscow, Russia

Technological versatility and the humoral and cellular immune response induction capacity have conditioned wide spread of adenoviral vectors as vaccine and gene therapy drugs. However, vaccination with Sputnik V made a significant portion of the population immune to the types 5 and 26 (Ad5 and Ad26) recombinant human adenovirus vectors, which are some of the most frequently used bases for candidate vaccines. Today, vaccine designers tend to select alternative adenovirus serotypes as platforms to develop vaccines against new pathogens on. A good example is simian adenovirus type 25 (SAd25), which belongs to subgroup E. It is genetically distant from Ad5 and exhibits extremely low seroprevalence in human beings, which makes it an appealing alternative vaccine vector. The purpose of this work was to design and study a new vaccine platform based on simian adenovirus type 25. We relied on the advanced methods of molecular biology and virology to construct and make recombinant adenoviruses; the phylogenetic analysis in the context of this study was enabled with bioinformatic methods. The resulting recombinant adenoviral vector can effectively replicate itself in the HEK293 cell line (human embryonic kidney cells). This work substantiates the expediency of further investigation into the SAd25 vector as a platform for development of the prevention vaccines against various infectious diseases.


Keywords: adenovirus vector, vaccine platform, recombinant adenovirus, simian adenovirus type 25

Funding: the work is the result of the effort under the "Development of a recombinant vaccines platform (including live vaccines) enabling design of the infectious diseases prevention vaccines" task set by the Ministry of Health of the Russian Federation.

Acknowledgments: we express our sincere gratitude to AE Nikonova, a researcher with the Laboratory of Molecular Biotechnology of the NF Gamaleya National Research Center for Epidemiology and Microbiology for her help in conducting the phylogenetic analysis of adenovirus hexon sequences, as well as to research laboratory assistant D.D. Kustova for her help in obtaining the whole genome sequences.

Author contribution: Ozharovskaia TA, Zubkova OV, Logunov DYU, Gintsburg AL — conceptualization and planning of the experimental part; Popova O, Zubkova OV — production of genetically engineered constructs and recombinant simian adenovirus type 25; Ozharovskaia TA, Vavilova IV — phylogenetic analysis, virological experiments; Pochtovyi AA — whole genome sequencing of adenoviruses; Ozharovskaia TA, Zubkova OV — article preparation and authoring, interpretation of the results; Shcheblyakov DV, Gushchin VA — manuscript editing; Gushchin VA — state assignment project management.

Compliance with ethical standards: the work was carried out in accordance with the principles of the Declaration of Helsinki.

 **Correspondence should be addressed:** Tatiana A. Ozharovskaia
Gamalei, 18, Moscow, 123098, Russia; t.ozh@yandex.ru

Received: 29.12.2022 **Accepted:** 20.01.2023 **Published online:** 28.02.2023

DOI: 10.24075/brsmu.2023.006

РАЗРАБОТКА И ХАРАКТЕРИСТИКА ВЕКТОРНОЙ СИСТЕМЫ НА ОСНОВЕ АДЕНОВИРУСА ОБЕЗЬЯН 25-ГО СЕРОТИПА

Т. А. Ожаровская , О. Попова, О. В. Зубкова, И. В. Вавилова, А. А. Почтовый, Д. В. Щебляков, В. А. Гушчин, Д. Ю. Логунов, А. Л. Гинцбург

Национальный исследовательский центр эпидемиологии и микробиологии имени Н. Ф. Гамалеи Министерства здравоохранения Российской Федерации, Москва, Россия

В настоящее время аденовирусные векторы широко используют в качестве вакцинных и генотерапевтических препаратов благодаря их технологичности и способности индуцировать стойкий гуморальный и клеточный иммунный ответ. Однако одни из наиболее часто используемых векторов для разработки кандидатных вакцин — рекомбинантные аденовирусы человека 5-го и 26-го серотипов (Ad5 и Ad26) становятся менее привлекательными из-за высокого процента населения с иммунитетом к данным векторам, вызванным вакцинацией «Спутником V». На сегодняшний день появляется тенденция к выбору альтернативных серотипов аденовирусов в качестве платформ для разработки вакцин против новых патогенов. Например, аденовирус обезьян 25-го серотипа (SAd25), принадлежащий к подгруппе E, генетически отдален от Ad5 и проявляет крайне низкую серопревалентность у людей, что делает его привлекательным альтернативным вакцинным вектором. Целью работы было создать и исследовать новую вакцинную платформу на основе аденовируса обезьян 25-го серотипа. Для конструирования и получения рекомбинантных аденовирусов использовали современные молекулярно-биологические и вирусологические методы, для филогенетического анализа применяли биоинформатические методы. Полученный рекомбинантный аденовирусный вектор способен эффективно реплицироваться в производственной культуре клеток HEK293 (клетки почки эмбриона человека). Результаты работы обосновывают целесообразность дальнейшего исследования вектора SAd25 в качестве платформы для разработки вакцин для профилактики различных инфекционных заболеваний.


Ключевые слова: аденовирусный вектор, вакцинная платформа, рекомбинантный аденовирус, аденовирус обезьян 25-го серотипа

Финансирование: работа выполнена в рамках государственного задания Министерства здравоохранения Российской Федерации «Разработка технологической платформы для создания рекомбинантных, в том числе живых вакцин для профилактики инфекционных болезней».

Благодарности: выражаем искреннюю благодарность научному сотруднику А. Э. Никоновой из лаборатории молекулярной биотехнологии ФГБУ «НИЦЭМ им. Н. Ф. Гамалеи» за помощь в проведении филогенетического анализа последовательностей гексонов аденовирусов, а также лаборанту-исследователю Д. Д. Кустовой за помощь в получении полногеномных последовательностей.

Вклад авторов: Т. А. Ожаровская, О. В. Зубкова, Д. Ю. Логунов, А. Л. Гинцбург — концепция и план экспериментов; О. Попова, О. В. Зубкова — получение генно-инженерных конструкций и рекомбинантного аденовируса обезьян 25-го серотипа; Т. А. Ожаровская, И. В. Вавилова — филогенетический анализ, вирусологические эксперименты; А. А. Почтовый — полногеномное секвенирование аденовирусов; Т. А. Ожаровская, О. В. Зубкова — подготовка и написание статьи, интерпретация результатов; Д. В. Щебляков, В. А. Гушчин — редактирование рукописи; В. А. Гушчин — руководство проектом госзадания.

Соблюдение этических стандартов: работа проведена в соответствии с принципами Хельсинкской декларации.

 **Для корреспонденции:** Татьяна Андреевна Ожаровская
ул. Гамалеи, д. 18, г. Москва, 123098, Россия; t.ozh@yandex.ru

Статья получена: 29.12.2022 **Статья принята к печати:** 20.01.2023 **Опубликована онлайн:** 28.02.2023

DOI: 10.24075/vrgmu.2023.006

Recombinant adenoviral vectors (rAd) are a popular tool for gene delivery into mammalian cells; in particular, they are used in development of candidate vaccines [1–4]. Vaccines based on human adenovirus types 5 and 26 (Ad5 and Ad26, respectively) designed to counter Ebola and COVID-19 have proven to be effective [5, 6]. However, there is a need for new adenovirus vectors of other serotypes that can be alternatives to the existing ones, since vaccination of the large portion of the population translated into immunity to adenovirus vectors that can lower efficacy thereof. In this connection, human adenovirus types other than Ad5 and Ad26, as well as simian adenovirus serotypes, can facilitate development of the new drugs and heterologous prime-boost immunization patterns. There are over 80 serotypes of human adenoviruses; there are various approaches to their classification: they can be viewed as forming seven separate subgroups (A–G) or belonging to seven species of adenoviruses (*Human mastadenovirus A–G*) [7, 8].

Simian adenoviruses (SAd) are also being extensively investigated as vector vaccines. There is a considerably wide range of SAd-based adenoviral vectors currently being analyzed as vaccine candidates, including the chimpanzee adenoviruses (ChAd) ChAd3 [9], ChAd63 [10, 11], ChAd68 (also called SAd25) [12, 13], ChAd83 and ChAd155 [14, 15], as well as SAd22 [16], SAd23 [16, 17], SAd24 [16, 18]. These vectors have shown high immunogenicity in animal models and in clinical trials of candidate vaccines [13, 19, 20]. In addition, they are significantly similar to human adenoviruses biologically and exhibit low cross-activity of sera with virus-neutralizing antibodies to Ad5 and Ad26 [12, 21].

Simian adenovirus type 25 (SAd25) is one of the alternative serotypes used as a platform for therapeutic agents. It belongs to subgroup E, which makes it a potent vector in its own right and as part of heterologous immunization. In addition, antibodies to Ad2, Ad4, Ad5, Ad7, and Ad12 do not neutralize SAd25, therefore, this vector a promising vaccine platform candidate [12].

This study aimed to design a new vector platform based on SAd25 and study its biological and physical characteristics.

METHODS

Bacterial strains and cell lines

For this work, we used a laboratory strain of *Escherichia coli* DH5 α (New England Biolabs; USA), an *E. coli* BJ5183 strain (Stratagene; USA) and the HEK293 cell line, human embryonic kidney cells containing the Ad5 region in the E1 genome (Russian Collection of Vertebrate Cell Lines; Russia). We cultivated HEK293 in the DMEM1 \times medium (Dulbecco's Modified Eagle Medium; HyClone, USA) supplemented with 5% fetal bovine serum (HyClone; USA) and 25 ml of sodium bicarbonate 7.5% (PanEco; Russia), in the presence of 146 mg of L-glutamine (PanEco; Russia) and a mixture of penicillin and streptomycin (PanEco; Russia), at 37 °C, with CO₂ at 5%.

SAd25 genome sequencing

The SAd25 wild-type (wt-) virus strain was obtained from the State Collection of Viruses of II–IV Pathogenicity Groups of the D.I. Ivanovsky Institute of Virology, part of the N. F. Gamaleya National Research Center of Epidemiology and Microbiology. This virus was passaged on HEK293 cells and purified by cesium chloride (CsCl) density gradient ultracentrifugation. We used the standard technique [22] to isolate the genomic DNA from purified wt-SAd25. The nucleotide sequence of wt-SAd25

was determined using whole genome sequencing on the Oxford MinION sequencer (Oxford Nanopore Technologies; UK).

Designing the recombinant adenovirus vectors

Firstly, to create the pArms-SAd25-EGFP plasmid, we PCR-amplified the left homology arm (nucleotides 1–537 and 3406–3801 in accordance with the wt-SAd25 genome) and the right homology arm (nucleotides 35969–36519). The expression cassette, consisting of the cytomegalovirus early promoter (CMV promoter), the enhanced green fluorescent protein (EGFP) gene and the SV40 virus polyadenylation signal, is located at the site of the E1 deletion (nucleotides 538–3405). For further linearization of the pArms-SAd25-EGFP plasmid a Swal site was inserted between the homology arms.

To construct the plasmid pSAd25 Δ E1-EGFP carrying the full-length SAd25 genome and the expression cassette with the EGFP gene at the site of the deleted E1 region of the genome, we used the method of homologous recombination between the linearized pArms-SAd25-EGFP plasmid and wt-SAd25 genomic DNA in *E. coli* cells of the BJ5183 strain. The bacterial cells were transformed by electroporation with the MicroPulser (Bio-Rad, Hercules; USA), as prescribed by the manufacturer's instructions. We analyzed the resulting plasmid pSAd25 Δ E1-EGFP with PCR and restriction mapping.

For the E3 region modification, we designed the pBS-E3-SAd25 plasmid that carried a fragment of the SAd25 genome (12804 nucleotides) cloned by NheI. The E3 region of the genome (nucleotides 27131–31051) was deleted using the NcoI and SalI sites and with the help of the homologous recombination technique. The final pSAd25-EGFP plasmid contained deletions in the E1 and E3 regions of the genome. We resorted to restriction mapping and whole genome sequencing to analyze the resulting molecular clone.

Production of recombinant adenoviruses

We used the pSAd25-EGFP plasmid to obtain a pSAd25-EGFP recombinant adenovirus. HEK293 cells were seeded in six-well culture plates and incubated overnight to 80% confluence. To remove the bacterial part, we hydrolyzed the plasmid DNA with PacI and SspI restriction endonucleases and then transfected into HEK293 cells using the Lipofectamine 2000 reagent (Thermo Fisher Scientific; USA), as prescribed in the manual provided by the manufacturer. Once the CKX41 inverted microscope (Olympus; Japan) allowed a visual conformation of the viral cytopathic effect (CPE), the cells in the culture medium were subjected to three freeze-thaw cycles.

The Ad5-mCherry and Ad26-EGFP recombinant adenoviruses were obtained as described previously [23].

Accumulation and purification of recombinant adenoviruses

We produced the recombinant adenoviruses in the HEK293 cell line. The HEK293 cells were seeded into 10 culture dishes (diameter of 15 cm) in the amount of 15–17 \times 10⁶ per dish. The next day, a monolayer of cells with the confluence of 65–75% was infected with recombinant Ad at a dose of 107 PFU per dish. Two days later, when the CPE was at 90–100%, the infected cells were collected, concentrated by low-speed centrifugation, resuspended in buffer (0.01 M Tris-HCl pH 8.0, 0.01 M NaCl, 5 mM EDTA) and subjected to three freeze-thaw cycles to destroy cell and nuclear membranes and release the virus from the cells. Cell lysates were centrifuged at 5000 rpm for 10 minutes at room temperature, the precipitate removed afterwards.

Recombinant adenoviruses were purified in Optima XPN-90 (Beckman Coulter Inc.; USA) by double ultracentrifugation in a CsCl gradient (stepwise and equilibrium gradient).

We used PCR and whole genome sequencing to confirm purity and identity of the Ad. The titers of purified viruses were determined using 50% Tissue Culture Infectious Dose (TCID₅₀) assay on HEK293 cells [24]. The results were detected on days 10–12 after cell transduction.

Adenovirus particles quantification

We counted the particles using reagents from the Pico488 dsDNA quantification kit (Lumiprobe; USA). Each well of a 96-well microplate was filled with 10 µl of calibration solutions (in a known concentration) and solutions of the test sample. Next, 10 µl of lysis solution (TE buffer + 0.1% SDS) were added to the wells, mixed there and incubated for 5 minutes at room temperature. Then, we added 80 µl of TE solution and 100 µl of staining solution to the wells and left the mixtures to incubate for 5 minutes. After that, the fluorescence intensity was measured by a spectrofluorimeter at 480 nm excitation and 520 nm emission wavelengths. Next, a graph of the linear dependence of the fluorescence intensity of the calibration solutions (ordinate axis) on the concentration of viral particles (abscissa axis) was plotted.

Adenovirus genomes quantification

We isolated the total DNA using the Wizard Genomic DNA Purification Kit (Promega; USA). The number of genomes was determined by real-time PCR (RT-PCR) using universal primers for all three studied serotypes (F: 5'GGCGGCTGGCGGTAGAG, R: 5'GCAACATCTGGAACCGCG). We used the qPCRmix-HS SYBR mixture (Evrogen; Russia) as prescribed by the manufacturer. Real-time PCR was performed in automatic mode on a CFX 96 Real-Time PCR Detection System (Bio-Rad; USA).

Phylogenetic analysis of the sequences of hexons, fibers and pentons of adenoviruses of various serotypes

Nucleotide sequences of the genomes of various serotypes of human adenoviruses (45 serotypes) and simian adenoviruses (5 serotypes) were taken from the NCBI database (USA).

Using the Geneious Prime program, we aligned the amino acid sequences of the studied proteins of adenoviruses of various serotypes. The Neighbor-Joining method [25] enabled depiction of the evolutionary history [25]. The tree was drawn to scale, with branch lengths in the same units as the evolutionary distances used to build the phylogenetic tree. The evolutionary distances were calculated by the number of differences method and expressed as the number of amino acid differences per sequence. We used the MEGA 11 software to build the tree [26].

RESULTS

Comparison of hexons, pentons and fibers of different serotypes of human and simian adenoviruses

The structural proteins of adenovirus hexon, penton and fiber contain type-specific antigenic determinants that are targets for neutralizing antibodies. For this reason, when choosing an adenovirus serotype for the development of a new vector platform, it is important to take into account how these proteins of this serotype differ from similar proteins of already used recombinant adenoviruses, in particular from Ad5 and Ad26. With this in mind, after obtaining the results of whole genome sequencing of wt-SAd25 we performed a phylogenetic analysis of the amino acid sequences of hexons, pentons, and fibers of various serotypes and compared them to the SAd25 proteins (Fig. 1).

The analysis shows that hexon, penton and fiber of SAd25 are sufficiently distant evolutionarily from the same proteins of adenoviruses Ad5 (subgroup C) and Ad26 (subgroup D), on which the Sputnik V vaccine is based. Therefore, with a high degree of probability, virus-neutralizing antibodies generated by Ad5 or Ad26 vaccination targeting these proteins will not neutralize SAd25, and this vector may be a suitable candidate both for stand-alone use and for priming or boosting.

Construction of the vector based on simian adenovirus type 25

The recombinant SAd25-based replication-defective vector was constructed following the standard viral genome modification pattern used to create vectors based on Ad5 and Ad26 (Fig. 2A). Deletion of the E1 region turns the adenoviral genome into

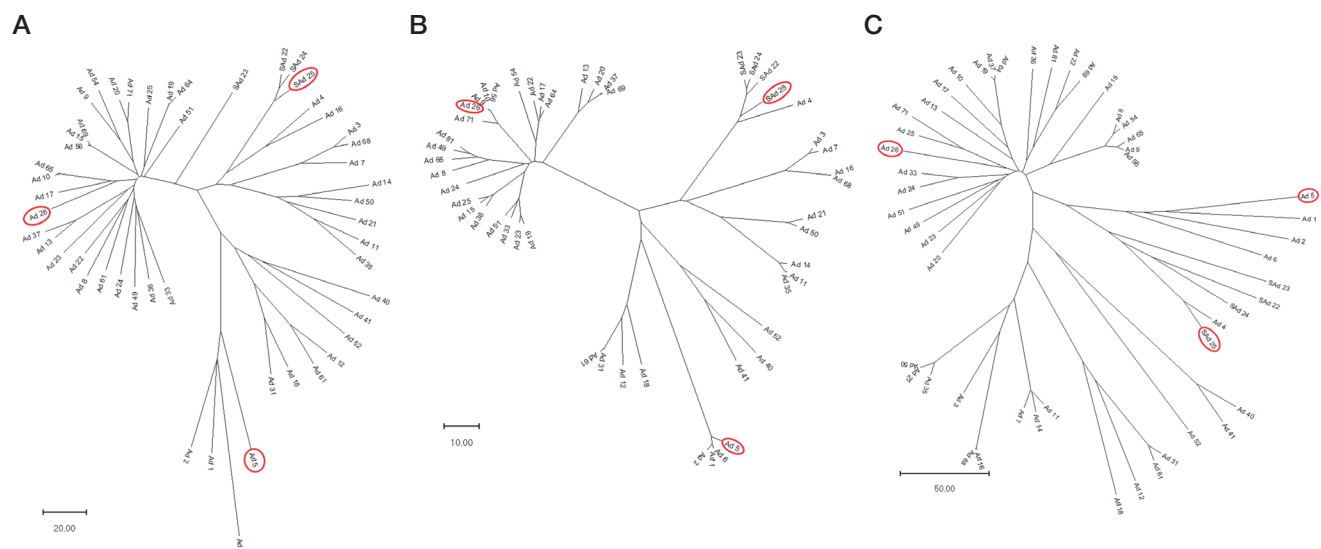


Fig. 1. Phylogenetic tree showing the relatedness of the hexon (A), penton (B) and fiber (C) sequences of adenoviruses of different serotypes. The tree was built based on the amino acid sequences of hexons of 45 human adenovirus serotypes and 5 simian adenovirus serotypes. The evolutionary distances were calculated based on the number of differences; they are given in as amino acid differences per sequence. Ad5, Ad26 and SAd25 are highlighted in red

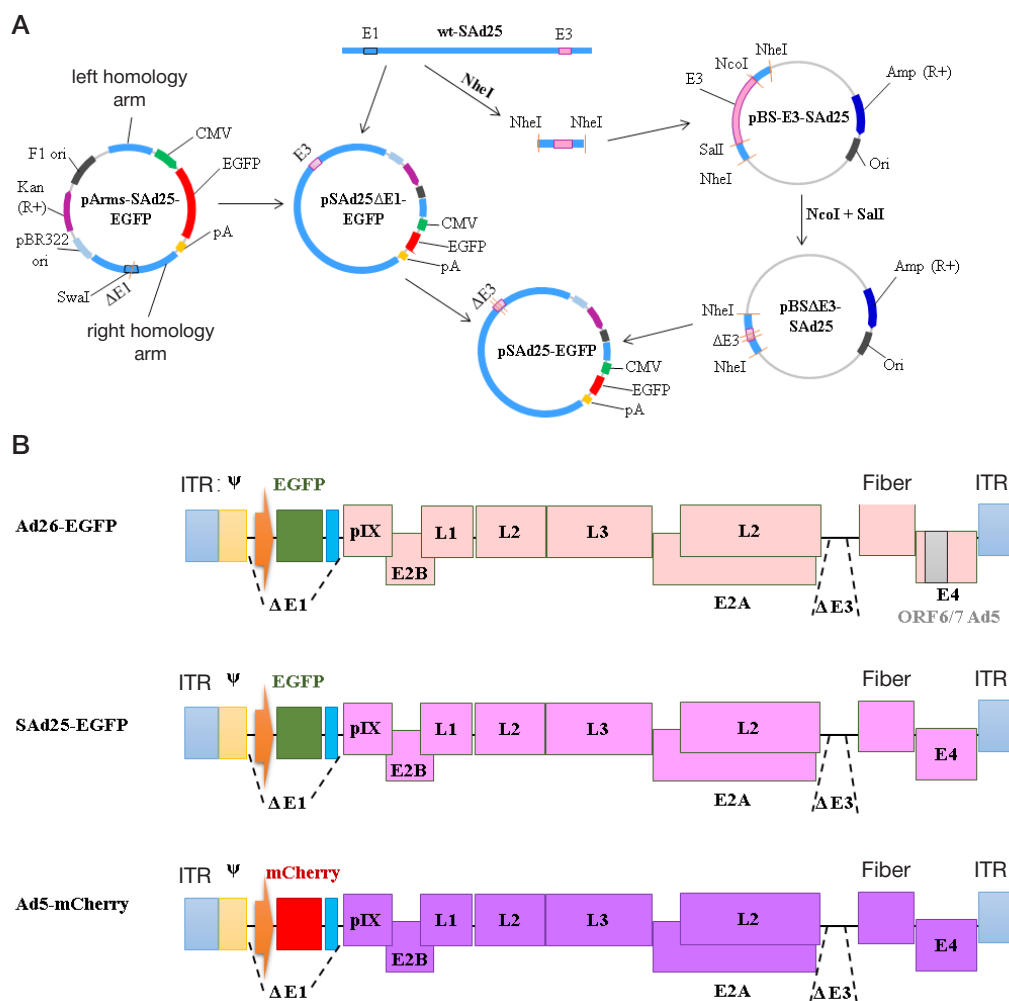


Fig. 2. Patterns of recombinant adenoviral vectors. **A.** Production of a plasmid construct containing the full-length genome of simian adenovirus type 25 and carrying the EGFP gene expression cassette. **B.** Genomes of recombinant replication-defective adenoviruses used in this study

a replication defective (it can only reproduce in a special cell line). The place of the deleted E1 region is occupied with a cassette carrying the reporter gene (CMV promoter, EGFP gene, polyadenylation signal). To increase the packing capacity, we have also deleted the E3 region. The plasmid carrying the recombinant SAd25-EGFP genome was engineered by homologous recombination in bacterial cells.

We used HEK293 cells transfected with pSAd25-EGFP plasmid with the vector part removed (containing the origin of replication (ori) and the kanamycin gene) to produce the infectious progeny of adenovirus. Despite the fact that HEK293 cells express proteins of the E1A region, which have some specificity, especially E1B55K, we have shown that this cell line efficiently assembles recombinant simian adenovirus type 25.

Investigation of biological and physical properties of the new adenoviral vector

One of the important characteristics of a viral vector is the genetic stability of the adenovirus genome. We did a number of passages of the SAd25-EGFP adenovirus on the HEK293 cell line to determine the respective capability of the vector. The genomic DNA was isolated from passages 1, 5 and 10, and then analyzed with the help of whole genome sequencing. The analysis revealed no mutations in the genome; the genome sequences from all three passages had 100% identity. These results allow a conclusion that SAd25-EGFP recombinant adenovirus remains genetically stable after at least 10-fold in vitro passaging.

To compare the replication efficiency of the produced SAd25-EGFP adenovirus and the two recombinant adenoviruses of types Ad5 and Ad26 that were produced earlier at the N.F. Gamaleya National Research Center for Epidemiology and Microbiology, we used vectors expressing the genes for fluorescent proteins EGFP and mCherry (red fluorescent protein). Adenoviruses SAd25-EGFP, Ad5-mCherry, and Ad26-EGFP (Figure 2B shows the genome structures) were transduced into wells of a 96-well plate with HEK293 cells (5×10^4 cells/well) at a dose of 1×10^4 viral particles (v.p.), and incubated for 72 h. Olympus IX73 (Olympus; Japan) inverted microscope with a U-RFL-T fluorescent module (Olympus; Japan) enabled detection of viral plaques in all wells infected with different adenoviruses. Viral plaques found in cells infected with SAd25-EGFP were noticeably larger than those in cells infected with other adenoviruses. In addition, the former had the lysis zone clearly enlarged, which indicates a higher viral cytotoxicity (Fig. 3). These findings are consistent with the results obtained for another simian adenovirus, SAd23 [17].

To perform a more detailed analysis of the replication efficiency of the resulting adenoviral vector, as well as to compare it with other adenoviral vectors, we cultured SAd25-EGFP, Ad5-mCherry and Ad26-EGFP on ten culture dishes (150 mm), purified the cultures by ultracentrifugation and collected them in equal final volumes (2 ml). The final sample could contain virus particles without a genome (unpacked or empty), with a full genome (packed or complete), or various intermediate forms in between. Next, we carried out a physical

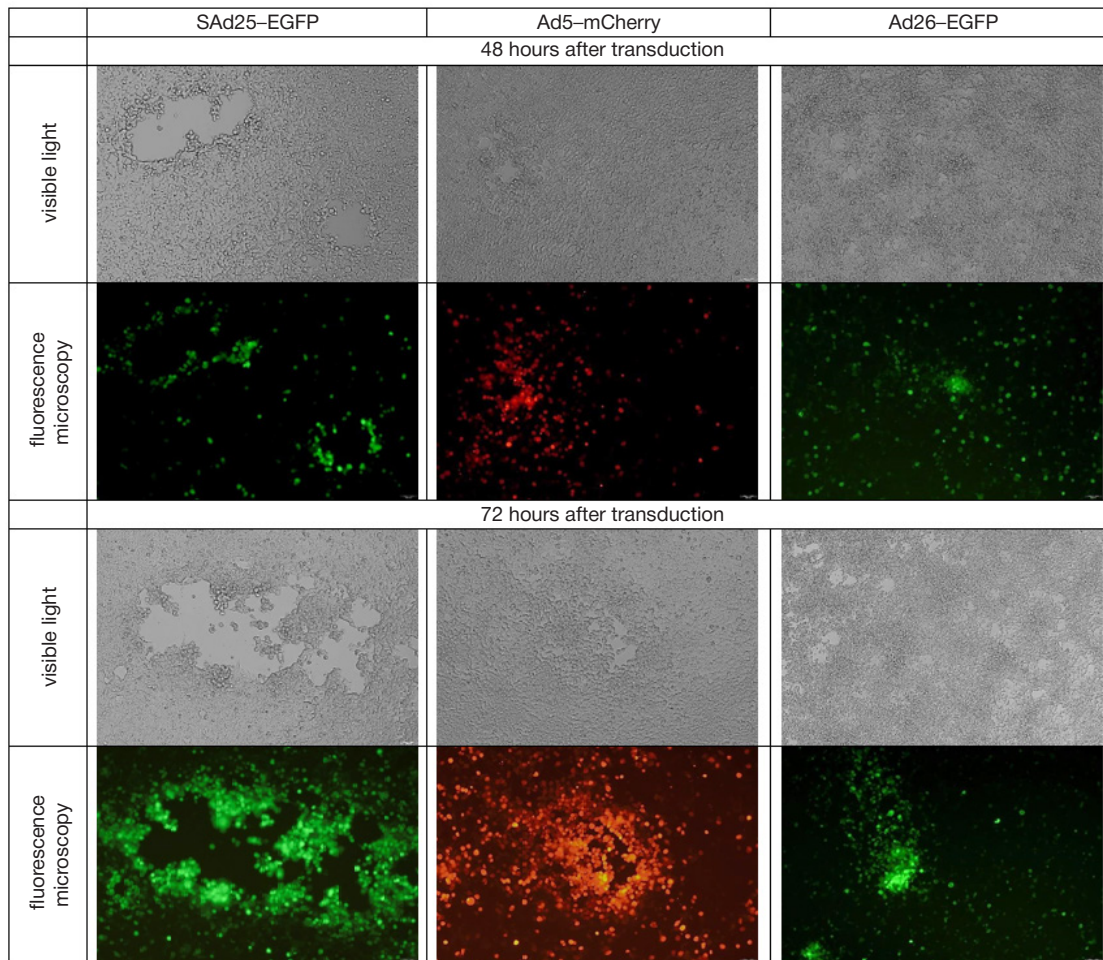


Fig. 3. Cytopathic effect of adenoviruses on HEK293 cells 48 and 72 hours after transduction

and biological characterization of the obtained adenoviruses (see Table).

The amount of SAd25-EGFP v.p. was similar to the amount of Ad5-mCherry and Ad26-EGFP v.p., but the infectious titer of SAd25-EGFP was lower than that of Ad5 and Ad26. The data also indicated that, compared to Ad5 and Ad26, the SAd25-EGFP sample contained more non-infectious viral particles. The yield of recombinant simian adenovirus was lower in comparison with Ad26-EGFP. Detection of more viral genomes for SAd25-EGFP indicates presence of unpackaged viral DNA. Thus, these results show that recombinant SAd25 efficiently accumulates in HEK293 cells. A large number non-infectious viral particles and free viral DNA detected in the SAd25-EGFP samples necessitates the search for optimal conditions of cultivation and purification.

DISCUSSION

Simian adenoviruses have long been subjects of research. They are investigated to understand their capability to act as vectors for delivering target genes into cells. They have an undeniable advantage: human beings almost completely lack antibodies to common serotypes, including CAd63 and CAd68. The first

vector based on a chimpanzee adenovirus was CAd68, which had the E1 region deleted [12]. In preclinical studies of the HIV-1 vaccine, this recombinant adenovirus was shown to be a highly immunogenic vaccine vector [20]. Later, a recombinant adenoviral vector based on simian adenovirus type Y25 was developed; subsequently, it was named ChAdOx1. The vaccine platform based thereon offers a good safety profile, as was shown in phase I-III clinical trials of the ChAdOx1-based vector vaccines designed for prevention of a number of diseases, including influenza, tuberculosis, malaria, prostate cancer, MERS, Zika fever and COVID-19 [27].

The SAd25 adenovirus has a good safety profile and high immunogenicity [27], but there are still no vaccine or gene therapy preparations based thereon that are used in the Russian Federation. Therefore, we have developed a vector platform based on SAd25 with the prospect of its further use as a vaccine platform.

At the first stage of our work, we performed a bioinformatic analysis of the wt-SAd25 genome sequence. We focused on the hexon, penton and fiber adenovirus sequences, i.e. the main proteins of the virion capsid. The epitopes in hexon are targets for neutralizing antibodies in vivo; they are recognized by cytotoxic T cells and serve as one of the parameters in allocation

Table. Biological and physical characteristics of recombinant adenoviruses

Serotype	TCID ₅₀ /ml	number of genomes/ml	number of v.p./ml	number of genomes/TCID ₅₀	number of v.p./ TCID ₅₀
SAd25-EGFP	$2,15 \times 10^9$	$1,79 \times 10^{12}$	$1,15 \times 10^{12}$	833	535
Ad5-mCherry	$4,64 \times 10^9$	$1,01 \times 10^{12}$	$1,02 \times 10^{12}$	218	220
Ad26-EGFP	$6,81 \times 10^9$	$1,88 \times 10^{12}$	$1,91 \times 10^{12}$	276	281

of adenoviruses into various serotypes [28]. Therefore, it was important to establish how far the SAd25 hexon is evolutionarily from other serotypes, including those used in the development of vaccines based on Ad5 and Ad26. As a result, we have shown that hexon, penton, and fiber of SAd25 are quite evolutionarily distant from these proteins of Ad5 and Ad26. Thus, our next task was to create a vector system based on SAd25.

There are several adenoviral vectors construction methods: cloning, obtaining a vector through cosmids, homologous recombination in bacteria and homologous recombination in eukaryotic cells [29]. Among them, the common method is the third one, which was also used in this work. This method includes obtaining a plasmid containing the adenovirus genome by homologous recombination of a shuttle vector carrying regions of homology with the adenovirus genome and genomic adenoviral DNA in *E. coli* BJ5183 cells.

Most of the engineered adenovirus-based vectors investigated as candidate vaccines are considered to be first-generation vectors, in which the E1 and E3 regions of the genome have been deleted. Deletion of the E1 region makes the adenovirus replication-defective, that is, unable to multiply in animal cells. This procedure significantly improves safety and reduces the likelihood of side effects. Deletion E3, another region of the genome, increases the possible insert size to 8 kb, which grants greater flexibility to design of the expression cassette. In addition, this deletion does not affect growth in the complementary cell line. In the recombinant adenoviral vector based on SAd25 that we produced, both of the mentioned regions were removed.

Clinical applicability requires design of a vector that will effectively replicate in a producer cell line. The cell line used in Russia to produce recombinant adenoviral vectors is HEK293, which is complementary and contains the E1 region of the Ad5 genome. But in the case of creating a vector with a deleted E1 region, there is a risk that this vector will form replicatively competent adenoviral particles during growth. However, SAd25 presents no such risk, since the percentage of homology of the

nucleotide sequence of this region is not high enough and there will be no homologous recombination between the SAd25 genome and the E1 region in the HEK293 cell line.

To confirm the stability of the vaccine vector throughout the production process it is necessary to test the genetic stability of the recombinant viral vector. The test involves a number of passages of viral vectors that exceeds the level used in production; the usual amount is 5–10 passages [30]. The frequency of mutations in the genome of a replication-defective adenovirus is considered rare, however, this analysis is important for assessment of unchangeability of the expression cassette and, accordingly, expression of the target gene. We performed 10 passages of the obtained recombinant adenovirus SAd25-EGFP, after which the genomic DNA was analyzed by whole genome sequencing. The SAd25 vector was found to be genetically stable.

Further production and investigation of SAd25-based adenoviral vectors, including safety and immunogenicity studies thereof, and their comparison with the safety profile and immunogenicity of the already existing adenoviral vectors (including Ad5 and Ad26) will expand the panel of recombinant viruses that can be used as basis for development of drugs preventing a wide range of infectious diseases.

CONCLUSIONS

We produced a recombinant adenoviral vector based on simian adenovirus type 25 that has the expression cassette with the target gene (EGFP) inserted into the E1 region and E3 region of the genome removed to increase the potential genetic capacity. This recombinant adenovirus can efficiently replicate in the HEK293 cell line, which is used in production of the adenovirus-based drugs. It was noted that the phenotype of viral plaques in the obtained adenovirus differs from that peculiar to Ad5 and Ad26, since SAd25 plaques are larger and have a larger lysis zone. The data obtained indicate the possibility of further study of the adenoviral vector as a platform for prevention drugs.

References

1. Tatsis N, Ertl HCJ. Adenoviruses as vaccine vectors. *Mol Ther*. 2004; 10 (4): 616–29.
2. Appaiahgari MB, Vrti S. Adenoviruses as gene/vaccine delivery vectors: promises and pitfalls. *Expert Opin Biol Ther*. 2015; 15 (3): 337–51.
3. Lee CS, Bishop ES, Zhang R, Yu X, Farina EM, Yan S, et al. Adenovirus-mediated gene delivery: Potential applications for gene and cell-based therapies in the new era of personalized medicine. *Genes Dis*. 2017; 4 (2): 43–63.
4. Trapnell BC, Gorziglia M. Gene therapy using adenoviral vectors. *Curr Opin Biotechnol*. 1994; 5 (6): 617–25.
5. Dolzhikova IV, Tokarskaya EA, Dzharullaeva AS, Tukhvatulin AI, Shcheblyakov DV, Voronina OL, et al. Virus-Vectored Ebola Vaccines. *Acta Naturae*. 2017; 9 (3): 4–11.
6. Lundstrom K. Viral Vectors for COVID-19 Vaccine Development. *Viruses*. 2021; 13 (2): 317.
7. Henaff D, Salinas S, Kremer EJ. An adenovirus traffic update: From receptor engagement to the nuclear pore. *Future Microbiol*. 2011; 6 (2): 179–92.
8. ICTV. The ICTV report virus taxonomy: the classification and nomenclature of viruses. 2022. Available from: <https://ictv.global/taxonomy/>.
9. Tapia MD, Sow SO, Ndiaye BP, Mbaye KD, Thiongane A, Ndour CT, et al. Safety, reactogenicity, and immunogenicity of a chimpanzee adenovirus vectored Ebola vaccine in adults in Africa: a randomised, observer-blind, placebo-controlled, phase 2 trial. *Lancet Infect Dis*. 2020; 20 (6): 707–18.
10. O'Hara GA, Duncan CJA, Ewer KJ, Collins KA, Elias SC, Halstead FD, et al. Clinical Assessment of a Recombinant Simian Adenovirus ChAd63: A Potent New Vaccine Vector. *J Infect Dis*. 2012; 205 (5): 772–81.
11. Younis BM, Osman M, Khalil EAG, Santoro F, Furini S, Wiggins R, et al. Safety and immunogenicity of ChAd63-KH vaccine in post-kala-azar dermal leishmaniasis patients in Sudan. *Mol Ther*. 2021; 29 (7): 2366–77.
12. Farina SF, Gao GP, Xiang ZQ, Rux JJ, Burnett RM, Alvira MR, et al. Replication-defective vector based on a chimpanzee adenovirus. *J Virol*. 2001; 75 (23): 11603–13.
13. Zhou D, Cun A, Li Y, Xiang Z, Ertl HCJ. A Chimpanzee-Origin Adenovirus Vector Expressing the Rabies Virus Glycoprotein as an Oral Vaccine against Inhalation Infection with Rabies Virus. *Mol Ther*. 2006; 14 (5): 662–72.
14. Napolitano F, Merone R, Abbate A, Ammendola V, Horncastle E, Lanzaro F, et al. A next generation vaccine against human rabies based on a single dose of a chimpanzee adenovirus vector serotype C. *PLoS Negl Trop Dis*. 2020; 14 (7): e0008459.
15. de Jong R, Stockhofe-Zurwieden N, Bonsing J, Wang KF, Vandepaer S, Bouzya B, et al. ChAd155-RSV vaccine is immunogenic and efficacious against bovine RSV infection-induced disease in young calves. *Nat Commun*. 2022; 13 (1): 6142.
16. Roy S, Gao G, Lu Y, Zhou X, Lock M, Calcedo R, et al.

- Characterization of a family of chimpanzee adenoviruses and development of molecular clones for gene transfer vectors. *Hum Gene Ther.* 2004; 15 (5): 519–30.
17. Luo S, Zhang P, Ma X, Wang Q, Lu J, Liu B, et al. A rapid strategy for constructing novel simian adenovirus vectors with high viral titer and expressing highly antigenic proteins applicable for vaccine development. *Virus Res.* 2019; 268: 1–10.
 18. Belousova N, Mikheeva G, Xiong C, Soghomonian S, Young D, Le Roux L, et al. Development of a targeted gene vector platform based on simian adenovirus serotype 24. *J Virol.* 2010; 84 (19): 10087–101.
 19. Bauza K, Malinauskas T, Pfander C, Anar B, Jones EY, Billker O, et al. Efficacy of a plasmodium vivax malaria vaccine using ChAd63 and modified vaccinia Ankara expressing thrombospondin-related anonymous protein as assessed with transgenic plasmodium berghei parasites. *Infect Immun.* 2014; 82 (3): 1277–86.
 20. Fitzgerald JC, Gao GP, Reyes-Sandoval A, Pavlakis GN, Xiang ZQ, Wlazlo AP, et al. A simian replication-defective adenoviral recombinant vaccine to HIV-1 Gag. *J Immunol.* 2003; 170 (3): 1416–22.
 21. Roy S, Medina-Jaszek A, Wilson MJ, Sandhu A, Calcedo R, Lin J, et al. Creation of a panel of vectors based on ape adenovirus isolates. *J Gene Med.* 2011; 13 (1): 17–25.
 22. Davis AR, Wivel NA, Palladino JL, Tao L, Wilson JM. Construction of adenoviral vectors. *Mol Biotechnol.* 2001; 18 (1): 63–70.
 23. Logunov DY, Zubkova OV, Karyagina-Zhulina AS, Shuvalova EA, Karpov AP, Shmarov MM, et al. Identification of HI-Like Loop in CELO adenovirus fiber for incorporation of receptor binding motifs. *J Virol.* 2007; 81 (18): 9641–52.
 24. Kanegae Y, Makimura M, Saito I. A simple and efficient method for purification of infectious recombinant adenovirus. *Jpn J Med Sci Biol.* 1994; 47 (3): 157–66.
 25. N Saitou, M Nei. The neighbor-joining method: a new method for reconstructing phylogenetic trees. *Mol Biol Evol.* 1987; 4 (4): 406–25. DOI: 10.1093/oxfordjournals.molbev.a040454.
 26. Kumar S, Stecher G, Li M, Knyaz C, Tamura K. MEGA X: molecular evolutionary genetics analysis across computing platforms. *Mol Biol Evol.* 2018; 35 (6): 1547–9.
 27. Folegatti PM, Jenkin D, Morris S, Gilbert S, Kim D, Robertson JS, et al. Vaccines based on the replication-deficient simian adenoviral vector ChAdOx1: Standardized template with key considerations for a risk/benefit assessment. *Vaccine.* 2022; 40 (35): 5248–62.
 28. Ebner K, Pinsker W, Lion T. Comparative sequence analysis of the hexon gene in the entire spectrum of human adenovirus serotypes: phylogenetic, taxonomic, and clinical implications. *J Virol.* 2005; 79 (20): 12635–42.
 29. Zhang W, Ehrhardt A. Getting genetic access to natural adenovirus genomes to explore vector diversity. *Virus Genes.* 2017; 53 (5): 675–83.
 30. Fernandes P, Silva AC, Coroadinha AS, Alves PM. Upstream bioprocess for adenovirus vectors. In: *Adenoviral vectors for gene therapy.* Elsevier, 2016; p. 139–61.

Литература

1. Tatsis N, Ertl HCJ. Adenoviruses as vaccine vectors. *Mol Ther.* 2004; 10 (4): 616–29.
2. Appiahgari MB, Vrtati S. Adenoviruses as gene/vaccine delivery vectors: promises and pitfalls. *Expert Opin Biol Ther.* 2015; 15 (3): 337–51.
3. Lee CS, Bishop ES, Zhang R, Yu X, Farina EM, Yan S, et al. Adenovirus-mediated gene delivery: Potential applications for gene and cell-based therapies in the new era of personalized medicine. *Genes Dis.* 2017; 4 (2): 43–63.
4. Trapnell BC, Gorziglia M. Gene therapy using adenoviral vectors. *Curr Opin Biotechnol.* 1994; 5 (6): 617–25.
5. Dolzhikova IV, Tokarskaya EA, Dzharullaeva AS, Tukhvatulin AI, Shcheblyakov DV, Voronina OL, et al. Virus-Vectorized Ebola Vaccines. *Acta Naturae.* 2017; 9 (3): 4–11.
6. Lundstrom K. Viral Vectors for COVID-19 Vaccine Development. *Viruses.* 2021; 13 (2): 317.
7. Henaff D, Salinas S, Kremer EJ. An adenovirus traffic update: From receptor engagement to the nuclear pore. *Future Microbiol.* 2011; 6 (2): 179–92.
8. ICTV. The ICTV report virus taxonomy: the classification and nomenclature of viruses. 2022. Available from: <https://ictv.global/taxonomy/>.
9. Tapia MD, Sow SO, Ndiaye BP, Mbaye KD, Thiongane A, Ndour CT, et al. Safety, reactogenicity, and immunogenicity of a chimpanzee adenovirus vectored Ebola vaccine in adults in Africa: a randomised, observer-blind, placebo-controlled, phase 2 trial. *Lancet Infect Dis.* 2020; 20 (6): 707–18.
10. O'Hara GA, Duncan CJA, Ewer KJ, Collins KA, Elias SC, Halstead FD, et al. Clinical Assessment of a Recombinant Simian Adenovirus ChAd63: A Potent New Vaccine Vector. *J Infect Dis.* 2012; 205 (5): 772–81.
11. Younis BM, Osman M, Khalil EAG, Santoro F, Furini S, Wiggins R, et al. Safety and immunogenicity of ChAd63-KH vaccine in post-kala-azar dermal leishmaniasis patients in Sudan. *Mol Ther.* 2021; 29 (7): 2366–77.
12. Farina SF, Gao GP, Xiang ZQ, Rux JJ, Burnett RM, Alvira MR, et al. Replication-defective vector based on a chimpanzee adenovirus. *J Virol.* 2001; 75 (23): 11603–13.
13. Zhou D, Cun A, Li Y, Xiang Z, Ertl HCJ. A Chimpanzee-Origin Adenovirus Vector Expressing the Rabies Virus Glycoprotein as an Oral Vaccine against Inhalation Infection with Rabies Virus. *Mol Ther.* 2006; 14 (5): 662–72.
14. Napolitano F, Merone R, Abbate A, Ammendola V, Horncastle E, Lanzaro F, et al. A next generation vaccine against human rabies based on a single dose of a chimpanzee adenovirus vector serotype C. *PLoS Negl Trop Dis.* 2020; 14 (7): e0008459.
15. de Jong R, Stockhofe-Zurwieden N, Bonsing J, Wang KF, Vandepaer S, Bouzuya B, et al. ChAd155-RSV vaccine is immunogenic and efficacious against bovine RSV infection-induced disease in young calves. *Nat Commun.* 2022; 13 (1): 6142.
16. Roy S, Gao G, Lu Y, Zhou X, Lock M, Calcedo R, et al. Characterization of a family of chimpanzee adenoviruses and development of molecular clones for gene transfer vectors. *Hum Gene Ther.* 2004; 15 (5): 519–30.
17. Luo S, Zhang P, Ma X, Wang Q, Lu J, Liu B, et al. A rapid strategy for constructing novel simian adenovirus vectors with high viral titer and expressing highly antigenic proteins applicable for vaccine development. *Virus Res.* 2019; 268: 1–10.
18. Belousova N, Mikheeva G, Xiong C, Soghomonian S, Young D, Le Roux L, et al. Development of a targeted gene vector platform based on simian adenovirus serotype 24. *J Virol.* 2010; 84 (19): 10087–101.
19. Bauza K, Malinauskas T, Pfander C, Anar B, Jones EY, Billker O, et al. Efficacy of a plasmodium vivax malaria vaccine using ChAd63 and modified vaccinia Ankara expressing thrombospondin-related anonymous protein as assessed with transgenic plasmodium berghei parasites. *Infect Immun.* 2014; 82 (3): 1277–86.
20. Fitzgerald JC, Gao GP, Reyes-Sandoval A, Pavlakis GN, Xiang ZQ, Wlazlo AP, et al. A simian replication-defective adenoviral recombinant vaccine to HIV-1 Gag. *J Immunol.* 2003; 170 (3): 1416–22.
21. Roy S, Medina-Jaszek A, Wilson MJ, Sandhu A, Calcedo R, Lin J, et al. Creation of a panel of vectors based on ape adenovirus isolates. *J Gene Med.* 2011; 13 (1): 17–25.
22. Davis AR, Wivel NA, Palladino JL, Tao L, Wilson JM. Construction of adenoviral vectors. *Mol Biotechnol.* 2001; 18 (1): 63–70.
23. Logunov DY, Zubkova OV, Karyagina-Zhulina AS, Shuvalova EA, Karpov AP, Shmarov MM, et al. Identification of HI-Like Loop in CELO adenovirus fiber for incorporation of receptor binding motifs. *J Virol.* 2007; 81 (18): 9641–52.
24. Kanegae Y, Makimura M, Saito I. A simple and efficient method for purification of infectious recombinant adenovirus. *Jpn J Med Sci Biol.* 1994; 47 (3): 157–66.

25. N Saitou, M Nei. The neighbor-joining method: a new method for reconstructing phylogenetic trees. *Mol Biol Evol.* 1987; 4 (4): 406–25. DOI: 10.1093/oxfordjournals.molbev.a040454.
26. Kumar S, Stecher G, Li M, Knyaz C, Tamura K. MEGA X: molecular evolutionary genetics analysis across computing platforms. *Mol Biol Evol.* 2018; 35 (6): 1547–9.
27. Folegatti PM, Jenkin D, Morris S, Gilbert S, Kim D, Robertson JS, et al. Vaccines based on the replication-deficient simian adenoviral vector ChAdOx1: Standardized template with key considerations for a risk/benefit assessment. *Vaccine.* 2022; 40 (35): 5248–62.
28. Ebner K, Pinsker W, Lion T. Comparative sequence analysis of the hexon gene in the entire spectrum of human adenovirus serotypes: phylogenetic, taxonomic, and clinical implications. *J Virol.* 2005; 79 (20): 12635–42.
29. Zhang W, Ehrhardt A. Getting genetic access to natural adenovirus genomes to explore vector diversity. *Virus Genes.* 2017; 53 (5): 675–83.
30. Fernandes P, Silva AC, Coroadinha AS, Alves PM. Upstream bioprocess for adenovirus vectors. In: *Adenoviral vectors for gene therapy.* Elsevier, 2016; p. 139–61.

SINGLE-DOMAIN ANTIBODY FOR BINDING THE CONSERVED EPITOPE IN THE SARS-COV-2 SPIKE PROTEIN RECEPTOR-BINDING DOMAIN

Vorobyev PO¹, Tillib SV^{1,2} ✉

¹ Engelhardt Institute of Molecular Biology, Russian Academy of Sciences, Moscow, Russia

² Institute of Gene Biology, Russian Academy of Sciences, Moscow, Russia

Several COVID-19 vaccines have been developed in the last three years using various techniques. Multiple virus-neutralizing antibodies against SARS-CoV-2 have been also obtained to combat the pandemic. However, the use of these medications for prevention and potential treatment faces significant challenges due to the emergence of new mutant virus variants, both more contagious and escaping neutralization by the immune system, that is why it is necessary to continuously renew the vaccines and develop new therapeutic antibodies. The study was aimed to use the technology of generating single-domain antibodies (nanobodies) to target the surface spike (S) protein RBD conserved epitope of the broad spectrum of SARS-CoV-2 variants. Recombinant proteins that corresponded to RBDs of three important SARS-CoV-2 strains and the full-length S protein (Wuhan) were used as antigens for immunization of a camel in order to induce production of appropriate antibodies and/or as immobilized proteins for further cross selection of the nanobody clones with pre-set specificity by the phage display. A nanobody capable of effectively recognizing the conservative region in the S protein RBDs of the broad spectrum of pandemic SARS-CoV-2 variants, including Omicron, was selected from the generated immune library. Along with conventional use in immunoassays and diagnosis, the generated nanobody can be potentially used as a module for target-specific binding used to trap coronavirus in human upper airways during the development of novel combination antiviral drugs.

Keywords: SARS-CoV-2, conserved epitope, single-domain antibody, nanobody, virus retention

Funding: the study was supported by the Ministry of Science and Higher Education of the Russian Federation (agreement № 075-15-2021-1086, contract № RF—193021X0015).

Acknowledgements: the authors thank M.V. Rutovskaya, Severtsov Institute of Ecology and Evolution of the Russian Academy of Sciences, for assistance in immunization of the camel.

Author contribution: Vorobyev PO — molecular cloning and subsequent production of recombinant proteins (antigens for immunization); Tillib SV — developing general conception, carrying out immunization, developing the method for acquisition and primary analysis of the generated single-domain antibodies, manuscript writing.

Compliance with ethical standards: the study was approved by the Ethics Committee of the Severtsov Institute of Ecology and Evolution of the Russian Academy of Sciences (protocol № 17 of 11 February 2018); the animal was handled in strict compliance with the guidelines of the National Standard of the Russian Federation GOST R 53434–2009.

✉ **Correspondence should be addressed:** Sergei V. Tillib
Vavilov str., 34/5, Moscow, 119334, Russia; tillib@genebiology.ru sergei.tillib@gmail.com

Received: 19.12.2022 **Accepted:** 25.01.2023 **Published online:** 24.02.2023

DOI: 10.24075/brsmu.2023.005

ОДНОДОМЕННОЕ АНТИТЕЛО ДЛЯ СВЯЗЫВАНИЯ КОНСЕРВАТИВНОГО ЭПИТОПА РЕЦЕПТОР-СВЯЗЫВАЮЩЕГО ДОМЕНА БЕЛКА SPIKE КОРОНАВИРУСА SARS-COV-2

П. О. Воробьев¹, С. В. Тиллиб^{1,2} ✉

¹ Институт молекулярной биологии имени В. А. Энгельгардта Российской академии наук, Москва, Россия

² Институт биологии гена Российской академии наук, Москва, Россия

В последние три года с помощью разных технологий были разработаны несколько вакцин против COVID-19, а также получено большое число вирус-нейтрализующих антител к коронавирусу SARS-CoV-2 с целью борьбы с пандемией. Однако применение этих препаратов для профилактики и потенциального лечения сталкивается с существенными проблемами из-за появления новых мутантных вариантов вируса, как более контагиозных, так и ускользающих от иммунной нейтрализации, что постоянно требует обновления вакцин и разработки новых терапевтических антител. Целью данного исследования было использовать технологию создания однодоменных антител (нанотел) для таргетирования наиболее консервативных эпитопов рецептор-связывающего домена (RBD) поверхностного S-белка (шипа, Spike) широкого спектра вариантов SARS-CoV-2. Рекombинантные белки, соответствующие RBD трех актуальных штаммов SARS-CoV-2, а также полноразмерному S-белку (Wuhan), были использованы в качестве антигенов для иммунизации верблюда с целью индукции образования соответствующих антител и/или в качестве иммобилизуемых белков для последующих перекрестных процедур селекции клонов нанотел с заданной специфичностью методом фагового дисплея. Из генерированной иммунной библиотеки было отобрано нанотело, обладающее свойством эффективно узнавать консервативный участок RBD S-белка широкого спектра вариантов пандемического коронавируса SARS-CoV-2, включая омикрон. Помимо традиционного использования в иммуноанализе и диагностике, полученное нанотело потенциально может быть использовано в качестве модуля мишень-специфичного связывания для задержки коронавируса в верхних дыхательных путях человека при разработке новых комбинированных противовирусных препаратов.

Ключевые слова: SARS-CoV-2, консервативный эпитоп, однодоменное антитело, нанотело, задержка вируса

Финансирование: работа была поддержана Министерством науки и высшего образования Российской Федерации (договор № 075-15-2021-1086, контракт № RF—193021X0015).

Благодарности: М. В. Рутковской из института Проблем экологии и эволюции им. А. Н. Северцова РАН за помощь в работе по иммунизации верблюда.

Вклад авторов: П. О. Воробьев — проведение молекулярного клонирования и последующей наработки рекомбинантных белков (антигенов для иммунизации); С. В. Тиллиб — разработка общей идеи и реализация этапов иммунизации, способа получения и первичного анализа полученных однодоменных антител, написание статьи.

Соблюдение этических стандартов: исследование одобрено этическим комитетом Института проблем экологии и эволюции им. А. Н. Северцова РАН (протокол № 17 от 11 февраля 2018 г.); работы с животными проводили в строгом соответствии с рекомендациями Национального стандарта Российской Федерации ГОСТ Р 53434–2009.

✉ **Для корреспонденции:** Сергей Владимирович Тиллиб
ул. Вавилова, д. 34/5, г. Москва, 119334, Россия; tillib@genebiology.ru sergei.tillib@gmail.com

Статья получена: 19.12.2022 **Статья принята к печати:** 25.01.2023 **Опубликована онлайн:** 24.02.2023

DOI: 10.24075/vrgmu.2023.005

Most virus neutralizing antibodies against important targets, such as SARS-CoV-2, bind to protein epitopes on the surface of viral particles and prevent the interaction of virus with the cellular receptor that is essential for viral entry. As for SARS-CoV-2, the spike (S) protein (1300 amino acids) displayed on the surface is the main target for neutralizing antibodies. S protein forms a homotrimer on the virion surface. During virus assembly this protein is broken down into N-terminal (S1) region and C-terminal region (S2) that is directly involved in fusion with the host cell membrane. A receptor-binding domain (RBD, 319–541 amino acids or at least 333–527 amino acids) has been identified in the S1 region. In the S protein open conformation, RBD interacts with the angiotensin-converting enzyme 2 (ACE2), the SARS-CoV-2 entry receptor displayed on the host cell surface. The latter triggers S protein rearrangement that results in membrane fusion and viral entry. RBD consists of two core subdomains with the central β -sheet and one external subdomain or the receptor-binding motif (RBM, amino acids 438–506) that is linked to two adjacent β -strands of the core; RBM becomes the region of S protein in its receptor-binding open conformation that is most distant from the viral surface. RBD (and particularly RBM) is the main antigenic region of S protein and the main target for the virus neutralizing antibodies [1–3].

From the beginning of the pandemic the currently circulating SARS-CoV-2 strains have acquired mutations relative to the original Wuhan (WA1) strain. In particular, the B.1.617.2 variant (Delta) [4] and the related B.1.617.1 variant (Kappa) first identified in India carry the RBD L452R-T478K and L452R-E484Q substitutions, respectively, that are probably responsible for enhanced infectiousness [4]. The B.1.1.529 variant (Omicron) identified in South Africa comprises the extension of RBD with 15 substitutions (such as G339D, S371L, S373P, S375F, K417N, N440K, G446S, S477N, T478K, E484A, Q493K, G496S, Q498R, N501Y, Y505H) [5]. RBD mutations found in these variants increase the risk of reducing the effectiveness of modern vaccines and therapeutic human antibodies. These mutations can also contribute to virus evolution and selection of new variants capable of escaping neutralization by human immune system. Thus, generating the broad-spectrum virus neutralizing antibodies against various SARS-CoV-2 strains (existing and future) is extremely challenging [6–8].

The use of antibody-based inhalation medications is a very promising method for targeted interventions and combating respiratory infections at the point of entry into the human body, i.e. in the upper airways [9]. Inhalation is a promising non-invasive strategy for delivery of antibodies used for treatment of respiratory diseases, since this route ensures higher antibody concentrations in the respiratory tract, thereby overcoming the constraints and uncertainty related to the drug levels in the right area after systemic antibody delivery through the bloodstream. The nasal route of drug delivery is one of the well-characterized administration routes. For a number of drugs, the nasal sprays were considered successful and approved for widespread use. Respiratory viruses that infect humans enter the body through the respiratory tract in aerosols produced by the other infected individuals' cough or sneezing. Large aerosol particles are usually retained in the turbinates and sinuses, where these particles may cause upper respiratory infections. The smaller particles can travel to the lower respiratory tract and cause more dangerous infections affecting the alveolar region. The majority of viruses that infect the upper respiratory tract cause acute infections and show seasonality (for example, respiratory syncytial virus (RSV), rhinovirus, parainfluenza and influenza A viruses, adenovirus, human metapneumovirus, human bocavirus, and coronavirus). Mucosal epithelial cells represent

the portal of entry for most respiratory viral infections. The virus would not be able to initiate the infection, if its attachment to the cell is blocked at the point of entry. It has been shown that the influenza virus particles can be trapped in the human respiratory mucus, regardless of haemagglutinin binding sialic acids on mucins [10]. Perhaps the trapping observed is due to the presence of antibodies binding both influenza virus and components of the mucus gel. The link between antibodies and the mucus gel is probably ensured through the antibody Fc fragment multiple low affinity interactions with mucin. It is important to note that adhesive interactions between the antibodies that bind pathogens and the components of respiratory mucus may provide a universal strategy for combating pathogens in the airways. The topical delivery of antibodies that bind the causative agents of respiratory infections can potentially decrease the risk of infection and reduce viral load in the respiratory epithelium.

The format of single-domain antibodies is one of the most promising formats of monoclonal antibodies that gains more attention in recent years, including in the context of developing new means of combating infections.

The recombinant derivatives of the single-domain antigen-binding fragments (VHH) of the specific HCAb antibodies (heavy-chain only antibodies) comprising the truncated heavy chain dimer and no light chains, that are normally found in blood of the Camelidae family members and some species of cartilaginous fishes in addition to conventional immunoglobulin types, are referred to as single-domain antibodies (nanobodies) [11–12]. The main features of nanobodies are as follows: small size (12–15 kDa, 4 × 2.5 nm); high solubility, stability, specificity, and affinity; thermal and chemical resistance; easy realization of various modifications by genetic engineering methods; possibility of using the extremely effective phage display method for selection of optimal nanobody variants. Nanobodies are capable of forming unique paratopes and recognizing unique native antigen epitopes that are unusual for conventional antibodies (mostly conformational epitopes, small grooves, active sites of enzymes). This may result in the extraordinary high specificity of the specified target recognition *in vivo*. The framework regions of the camelid nanobodies (VHH) have high homology (significantly higher compared to the mouse VH) with the framework regions of the variable VH domains of human immunoglobulins (IgG3 subclass). Nanobody production in bacteria or any other expression systems is very cost-effective; nanobodies can be used as building blocks for multi-domain constructs [13–14].

The promising nanobody-based antiviral therapeutic drugs have already been created. For example, several nanobodies have been obtained that specifically bind to the most conserved fragments of haemagglutinin of the influenza viruses of various subtypes [15]. The multi-domain constructs containing four different nanobodies have been inserted in the adeno-associated virus vector.

The mouse model has shown that the expressed multi-domain antibodies targeted at several conserved epitopes at once very effectively prevent infection with influenza A and B viruses. The same strategy can be used for prevention of infection with other viruses/pathogens that show high variability. It is important to note that no such medication has not yet been obtained using conventional monoclonal antibodies.

A number of recently published papers report generating nanobodies against the receptor-binding domain (RBD) of the SARS-CoV-2 spike protein in order to block its interaction with ACE2 and thereby neutralize the virus [16–17]. This was accomplished for many SARS-CoV-2 variants, except for the most heavily mutated Omicron strain.

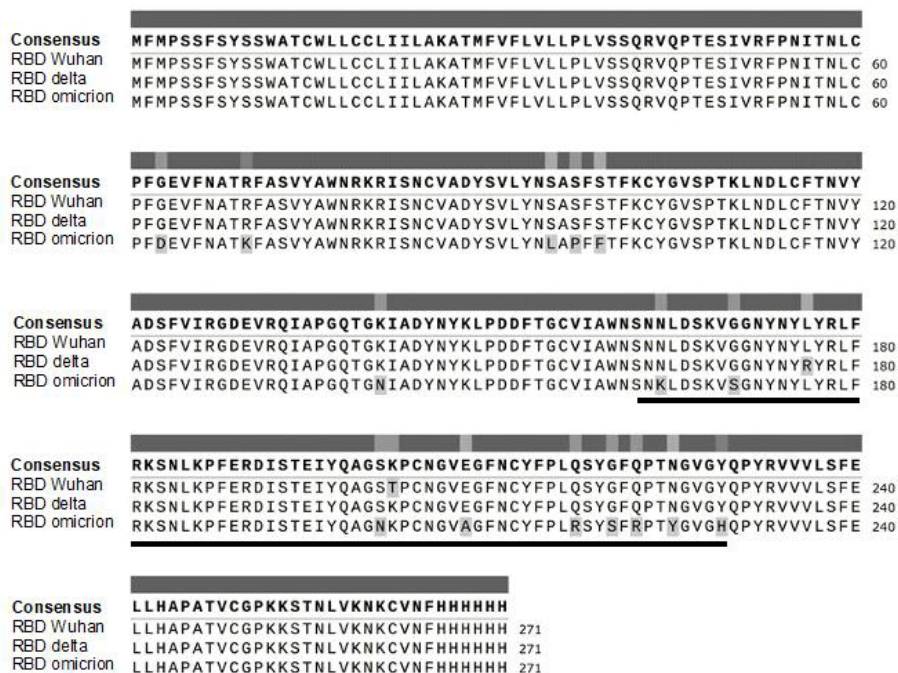


Fig. 1. Scheme of the aligned amino acid sequences of RBDs of three SARS-CoV-2 S protein mutant variants (original RBD Wuhan, RBD Delta, and the most heavily mutated RBD Omicron). Mutations of amino acid residues are highlighted in gray. The bold line represents position of the receptor-binding motif (RBM) that interacts directly with the ACE2 receptor

There is a report of generating the nanobody (Nb6) that binds and blocks S protein in a fully inactive conformation, thus preventing the virus binding to ACE2 [18]. Affinity maturation *in vitro* and trimerization of the high-affinity nanobody derivative have made it possible to obtain a drug against the SARS-CoV-2 infection that shows picomolar neutralization activity. This drug remained stable and retained its function after aerosolization, lyophilization, and heat treatment. The authors assume that

the aerosolized delivery of this potent neutralizer directly to the respiratory epithelium is possible.

The study was aimed to use the antibody-producing technology for selection of nanobody against the S protein RBD conserved epitope of the broad spectrum of SARS-CoV-2 variants, including Omicron. Such a nanobody is considered as a potential virus-binding module of the future aerosol combination virus-trapping drug that would contain an anchor

Table 1. Oligonucleotides (primers) for point mutagenesis

Primer	Nucleotide sequence 5'–3'
<i>For RBD Delta</i>	
RBD delta for 63	atctgaagcccttcgagcgaggacatctccaccgagatctatcaggccggcagcaaaccttg
RBD flank rev 63	tctgctagctcgagtcgcgac
Vector for 59	atcttaagtcgcgactcgagc
Vector rev 59	gtcggccacgcaattgc
RBD new rev 55	gtggagatgtccgctcgaagggtcagattggacttcggaacagccggtatctgtaattg
RBD new flank for 53	gtggagatgtccgctcgaagggtcagattggacttcggaacagccggtatctgtaattg
<i>For RBD Omicron</i>	
LIC ins for II 65	cccttcGACgaggtgttcaatgccaccAAGttgcgctctg
LIC ins omi I for 61	ctgtacaacCTCgccCCGttCTTtacctcaagtgtacggcggtgtcccc
LIC ins omi I for 63	gggctgATGgccacgcccGTAgtgggCCGaaaACTgttaggaTCGcagtGGGAAG
LIC ins omi II rev 65	ttgaagccTGCcacgctgtacaaggAAAGTTgccggcctgatag
LIC vec omi I for 58	CaTACggcggtggcCatcagccc
LIC vec omi I rev 59	AAAgaaCGGggaGAGgtgttacagcacggagtagtcg
LIC vec omi II for 63	ttgtaacggcgtGCAggcttcaactgc
LIC vec omi II rev 65	attgaacacctcGTCgaaggggcacagattg
SDM II omi for 55	gtggcaactacaattacAGAtaccggctgttcc
SDM II omi rev 56	TgactttggagtcagTTTgttgctg
SDM omi for 54	atatcgccgactacaactac
SDM omi for 55	tgcctgtctgtccagg
CAG seq for rbd	tcctgggcaacgtgctgg
CAG seq rev rbd	agatgctcaaggggc

module for binding the major components of the human upper respiratory tract secretions.

METHODS

Production of recombinant proteins corresponding to the S protein receptor-binding domains of three important SARS-CoV-2 strains and the full-length S protein (Wuhan)

The SARS-CoV-2 strain (Wuhan) RBD was produced using the NR-52309 plasmid provided by Krammer et al. [19] (BEI Resources web-site, NIAID, NIH) in the HEK293T eukaryotic cells in accordance with the protocol published on the web-site and as previously reported [20]. The designated vector for the SARS-CoV-2 RBD, Wuhan-Hu-1 (GenBank: MN908947), was generated by fusing the S protein N-terminal signal sequence with RBD (amino acids 319–541) and the C-terminal hexahistidine tag. The target RBD-encoding plasmid was introduced into the HEK293T cells by calcium phosphate transfection. Three days later the RBD protein-containing supernatant was collected and centrifuged at 4 °C and 1500 g for 10 min. The purified supernatant was mixed with 5 mL of Ni-NTA-agarose (Qiagen; USA) equilibrated in phosphate-buffered saline and subsequently incubated with continuous mixing on the orbital shaker (Biosan; Latvia) for an hour at room temperature. Suspension was applied to the column and subsequently washed with the wash buffer (57 mmol NaH₂PO₄·H₂O, 135 mmol NaCl, 20 mmol Imidazol), then RBD was flushed with elution buffer (57 mmol NaH₂PO₄·H₂O, 135 mmol NaCl, 235 mmol Imidazol). The protein obtained was dialyzed against phosphate-buffered saline using a 5 kDa dialysis membrane (Merck; USA). The purified protein was analyzed by polyacrylamide gel electrophoresis. The protein concentration was determined by normalization with the known concentrations of bovine serum albumin (BSA) and by the Pierce BCA protein assay (Thermo Fisher; USA). Absorbance was measured using the CLARIOstar plate reader (BMG Labtech; USA).

To obtain RBDs of the SARS-CoV-2 Delta and Omicron strains, we introduced appropriate nucleotide substitutions (highlighted in Fig. 1) in the original sequence encoding RBD comprised by the above mentioned plasmid. Substitutions were introduced using the specially synthesized oligonucleotides by ligation-free cloning through synthesis of overlapping intermediate PCR products using the T100 Thermal cycler (Bio-Rad; USA). After amplification of appropriate fragments using the PhusionTM high-fidelity DNA polymerase (Thermo Fisher; USA), the amplified fragments were subjected to 1% agarose gel electrophoresis, and the fragments cut were isolated using the Cleanup Standart kit (Evrogen; Russia). The amplified vector and insert were incubated with T4 polymerase at 37 °C for 3 min, then T4 polymerase was inactivated at 75 °C for 15 min followed by incubation on ice for 1 min on ice for 1 min. After that the resulting mixture was used for transformation of the TOP10 competent cells. RBD was expressed and purified as previously described [20].

Oligonucleotides used for mutagenesis are provided in Table 1 (the coordinates correspond to that provided in Fig. 1). As for RBD Delta variant, mutations L176R, T202K were reproduced. To synthesize the sequence encoding the SARS-CoV2 Omicron strain RBD, the nucleotide substitutions that corresponded to mutations G63D, R70K, S95L, S97P, S99F, K141N, N164K, G170S, S201N, T202K, E208A, Q217R, G220S, Q222R, N225Y, Y229H, were introduced in the original plasmid encoding the SARS-CoV-2 strain RBD.

The sequences obtained by cloning were tested by Sanger sequencing using the RBD new flank for 53 or CAG seq oligonucleotides (Table 1).

The full-length SARS-CoV2 S protein was expressed and purified in accordance with the earlier reported protocol [19, 20] as described above, with the difference that the spike protein was expressed instead of RBD (using the pSFHT pCAGGS-wt Spike-Trb-T4-HT plasmid DNA provided by Krammer). Production and purification were performed in the same manner as described for RBD [20].

Immunization and acquisition of the library of cDNA sequences encoding nanobodies

The camel was kept in the spacious enclosure with regular paddock and feeding in the Center for Collective use "Live Collection of Wild Mammals" at the Scientific and Experimental Base "Chernogolovka", Severtsov Institute of Problems of Ecology and Evolution of the Russian Academy of Sciences. Animal work was carried out in accordance with the National Standard of the Russian Federation GOST R 53434–2009. The Bactrian camel (*Camelus bactrianus*) was sequentially immunized with five doses (four weeks after the first injection, then each subsequent injection was performed within 10–14 days) by subcutaneous injection of antigenic material mixed with equal amount of complete (first injection) or incomplete (other injections) Freund's adjuvant. A total of 0.5 mg of the mixture of recombinant proteins corresponding to RBD Wuhan and RBD Delta were used as antigenic material for immunization. Blood (150 mL) was collected five days after the final injection. To prevent blood clotting, 50 mL of the standard phosphate-buffered saline (PBS) containing heparin (100 U/mL) and EDTA (3 mmol) were added. Blood was two-fold diluted with PBS containing 1 mmol EDTA; 35 mL of diluted blood were layered on the 15 mL step of specialized medium (Histopaque-1077; Sigma-Aldrich, USA) with the density of 1.077 g/mL; centrifugation at 800 g was performed for 20 min. Mononuclear cells (lymphocytes and monocytes) were collected from the plasma/Histopaque interphase zone and subsequently washed with PBS containing 1 mmol EDTA. Total RNA was extracted from B cells using TRIzol (Thermo Fisher Scientific; USA). Then poly(A)-containing RNA was purified from total RNA using the Oligo(dT)-cellulose column. RNA concentration was defined with BioPhotometer (Eppendorf; Germany), and the quality of extracted RNA was verified by 1.5% agarose-formaldehyde gel electrophoresis. The reverse transcription reaction was carried out using the Maxima reverse transcriptase (Thermo Fisher Scientific; USA) and the Oligo(dT)18 primer. The reverse transcription products were used as a matrix for two-step polymerase chain reaction, and amplification products were cloned into a phagemid vector with the NcoI(PstI) and NotI sites as previously described [21]. The pHEN4 expression vector [22] kindly provided by Professor S. Muyldermans (Vrije Universiteit Brussel, Belgium) was used for cloning.

Selection of the nanobody clones that bind to RBD; formatting, production, and analysis of anti-RBD nanobodies

The next phage display-based selection procedures involving the use of the M13KO7 bacteriophage (New England Biolabs; USA) as a helper phage were mainly conducted in the same way as the previously described procedures [21].

The Excella E24 and E25 shaker incubators (New Brunswick Scientific; USA) were used to grow the bacterial culture. The 5810R and 5415R refrigerated centrifuges (Eppendorf;

Germany) were used for centrifugation. The recombinant proteins obtained by the above methods were immobilized in the wells of the Maxisorp immuno plate (Nunc; Denmark). The wells were blocked with 1% BSA (bovine serum albumin) in 1× PBS or with the casein blocking buffer (Sigma-Aldrich; USA). Both alternate antigens and blocking proteins were used for sequential selections. The selected clones of the nanobody-encoding sequences were grouped based on the identity of the HMR-fingerprint-like images and the activity of the expressed nanobodies (with the C-terminal HA tag) in periplasmic extracts [21]. The promising clones were re-cloned adding to the C-terminus of the nanobody-encoding sequences additional sequences of the long hinge region (as a linear flexible linker), HA tag and His tag for detection and effective purification of nanobodies, as previously described [23]. All the expression constructs comprised the pelB leader sequence for periplasmic nanobody expression. This made it possible to isolate the nanobody by the osmotic shock method without disrupting bacterial cells. Nanobodies were expressed in the *E. coli* cells (XL1 strain). Protein expression in the exponentially growing cells was induced by adding 0.2-1 mmol IPTG (isopropyl β -D-1-thiogalactopyranoside). The cells were incubated with vigorous agitation for 5 h at 30 °C and overnight at 28 °C. The recombinant proteins were extracted from the periplasmic extract by affinity chromatography with Ni-NTA-Agarose (Qiagen; USA) in accordance with the manufacturer's instructions. The periplasmic extract containing a nanobody with C-terminal HA tag or an affinity purified adapted nanobody were used to assess specificity and efficiency of the nanobody binding to the antigen preparation immobilized in the immune plate well by conventional enzyme-linked immunoassay (ELISA). The horseradish peroxidase-conjugated anti-HA tag monoclonal antibody (H6533, Sigma-Aldrich; USA) was used as a secondary antibody against the HA tag. The horseradish peroxidase activity was defined with the use of 1-Step Ultra TMB-ELISA Substrate Solution (Thermo Fisher Scientific; USA) as a chromogenic substrate. Absorbance was measured at 450 nm with the Multiscan EX photometric microplate absorbance reader (Thermo Labsystems; USA) after adding equal volume of sulfuric acid (2 mol). The control wells contained no antigen, however, these were blocked and processed in parallel with the experimental wells (antigen-containing). Commercially available preparations were used for competitive nanobody assay: XR19 neutralizing mouse monoclonal nanobody (Xema; Russia) that is currently under approval and is manufactured as an experimental batch, and peroxidase conjugated rabbit anti-mouse immunoglobuline antibody (IMTEK; Russia). A measurement was taken three times, and the ELISA results were presented as mean values and standard deviations that did not exceed 10%.

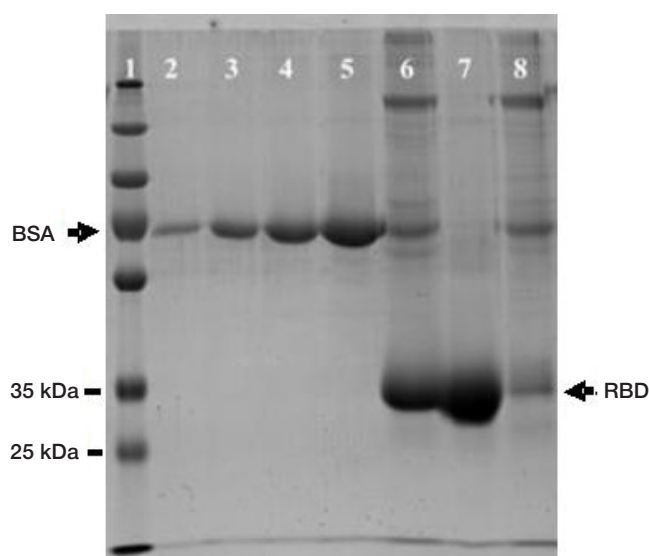


Fig. 2. SDS-polyacrylamide gel electrophoresis showing the produced (using the cloned coding sequence) and subsequently purified recombinant RBDs of three strains (6 — RBD Delta, 7 — RBD Wuhan, 8 — RBD Omicron). Left — lane of marker proteins (Thermo Scientific PageRuler Plus Prestained Protein Ladder, size 10–250 kDa). Different amounts of BSA marker protein have been applied to lanes 2–5 in order to quantify the protein produced (0.25, 0.5, 1.0, and 2.0 mg, respectively)

RESULTS

Initially we cloned and produced recombinant proteins corresponding to the S protein receptor-binding domains of three important SARS-CoV-2 strains (Fig. 2). Yield of produced proteins per 10^8 cells: RBD delta — 2200 ng, RBD Wuhan — 2446 ng, RBD omicron — 300 ng, membrane-associated full-length S-protein Wuhan (Fig. 3) — 75 ng.

Recombinant proteins that corresponded to RBD Delta and RBD Wuhan were produced rather effectively, however, significantly lower reproducible protein output was observed for RBD Omicron. This was probably due to the features of the RBD Omicron protein secondary structure that could be formed harder in this expression system. When we started this study, no information about the RBD Omicron was available, that is why the mixture of RBD Delta and RBD Wuhan proteins was used for immunization of the camel. RBD Omicron was later used at the selection stage.

The recombinant protein produced that corresponded to the full-length SARS-CoV-2 (Wuhan) S protein was used at the same stage of selection and validation ELISA (Fig. 3).

After the Bactrian camel immunization, the titer of IgG binding to RBD Delta and RBD Wuhan in the antiserum

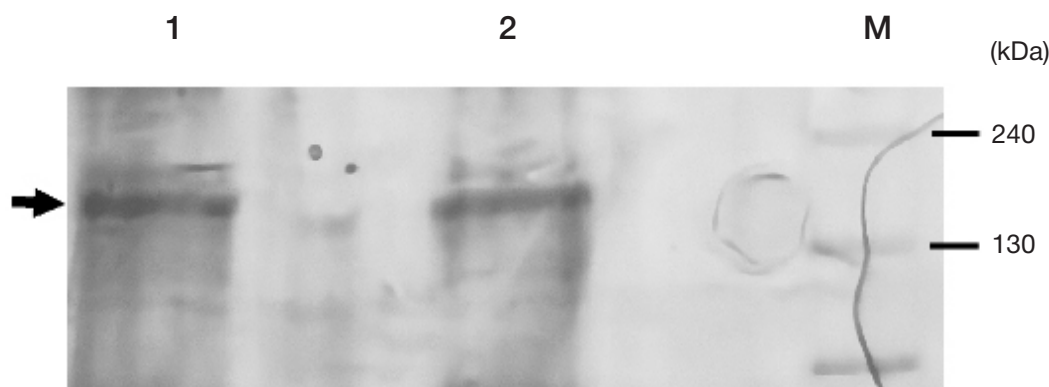


Fig. 3. SDS-polyacrylamide gel electrophoresis showing the produced SARS-CoV-2 (Wuhan) recombinant S (spike) protein. The protein was detected in the cytoplasmic fraction (1) and in the sediment fraction (2). The marker of the polypeptide molecular weight is applied on the right

significantly (about 40 times) increased compared to pre-immune serum. We cloned cDNA sequences encoding the entire repertoire of the single-domain antigen-recognizing sequences (VHH, single-domain antibodies, nanobodies) containing a homodimer of truncated (having no CH1 domain) heavy chains and no light chains in the pHEN4 phagemid expression vector based on mRNA from the immunized camel peripheral blood lymphocytes. The resulting library of the VHH-cDNA sequences was converted into the phage particle format using the M13KO7 helper phage and then used for cross selection with three variants of produced RBD. Selection was performed by sequentially using the immune plate wells showing high sorption capacity (Nunc Maxisorp) that contained recombinant proteins immobilized in PBS with a concentration of 10 µg/100 µL (RBD Wuhan, RBD Delta, and RBD Omicron). The 1% BSA (Sigma-Aldrich; USA) in PBS or the casein blocking buffer (Sigma-Aldrich; USA) were used for blocking. Selection and subsequent amplification of the selected phage particles (containing the gene encoding the single-domain nanobody inside and the expressed single-domain nanobody as a component of the pIII phage surface protein) were usually performed three times in a row using different incubation sequences for all three variants of the immobilized antigens. The first two RBD variants were used for immunization, and it was easy to select nanobodies against these variants. However, it was predictably difficult to select a nanobody capable of effectively binding RBD Omicron as well. The sequences of selected nanobody clones were grouped based on the similarity of fingerprints obtained by electrophoretic separation of the products of hydrolysis of the amplified sequences of single-domain nanobodies using three restriction endonucleases (HinfI, MspI, RsaI) at once. To assess specific activity of the selected nanobodies that represented each group, microinduction of the nanobody synthesis in the bacterial periplasm was performed, and the periplasmic extract containing the generated nanobodies was obtained. Such periplasmic extracts with nanobodies comprising a C-terminal HA tag (antigenic determinant, the YPYDVPDYA fragment of 9 amino acids) were used when performing enzyme-linked immunoassay (ELISA) for detection of the most promising nanobody variants. The horseradish peroxidase-conjugated

anti-HA tag monoclonal antibody (H6533, Sigma-Aldrich; USA) was used as a secondary antibody against the HA tag. We managed to select nine different variants (groups) of the nanobody clones after selection and ELISA. Among those the most promising nanobody referred to as aRBDce1 (anti-RBD conserved epitope 1) that met all the major requirements we had initially set should be highlighted.

The selected cloned nanobody-encoding sequences were adapted for more effective production in the bacterial expression system and subsequent effective nanobody purification, as described earlier [23]. The nanobodies obtained comprise a long C-terminal linker sequence (28 amino acids of the long variant of the non-conventional camelid antibody hinge region) followed by two peptide fragments: HA tag allowing to detect the nanobody using the commercially available antibodies against this peptide and (His)₆ tag, the sequence of six histidine residues, that makes it possible to effectively purify proteins containing the tag by the metal-chelate affinity chromatography on the Ni²⁺-NTA agarose. The selected and adapted nanobodies were tested for functional activity. Initial testing was performed by ELISA in order to test the efficiency of the S protein RBD conserved epitope binding by the nanobodies obtained for three different mutant SARS-CoV-2 variants. Fig. 4 shows the ELISA results suggesting that the aRBDce1 nanobody (1 µg/mL) is highly effective: it binds to the recombinant S proteins, RBD Wuhan (W-RBD), RBD Delta (Δ-RBD), and RBD Omicron immobilized in the plate wells better than other nanobody variants selected alongside, however, it hardly binds to the control well. The wells with immobilized BSA (bovine serum albumin) were used as controls. The signal intensity reflects the nanobody binding efficiency. We can assume higher affinity of the aRBDce1 nanobody binding to RBD (in the low nanomolar range) compared to other earlier generated in one group and characterized nanobodies against other targets; aRBDce1 is so far the only nanobody we have selected that is capable of effectively binding all the RBD variants used, including RBD Omicron and the full-length S protein.

Fig. 5 shows the results of ELISA, during which the immobilized RBD (Wuhan) was first bound/blocked with the increasing concentrations of individual variants of the selected nanobodies (20 µg/mL), then the wells were washed, and a

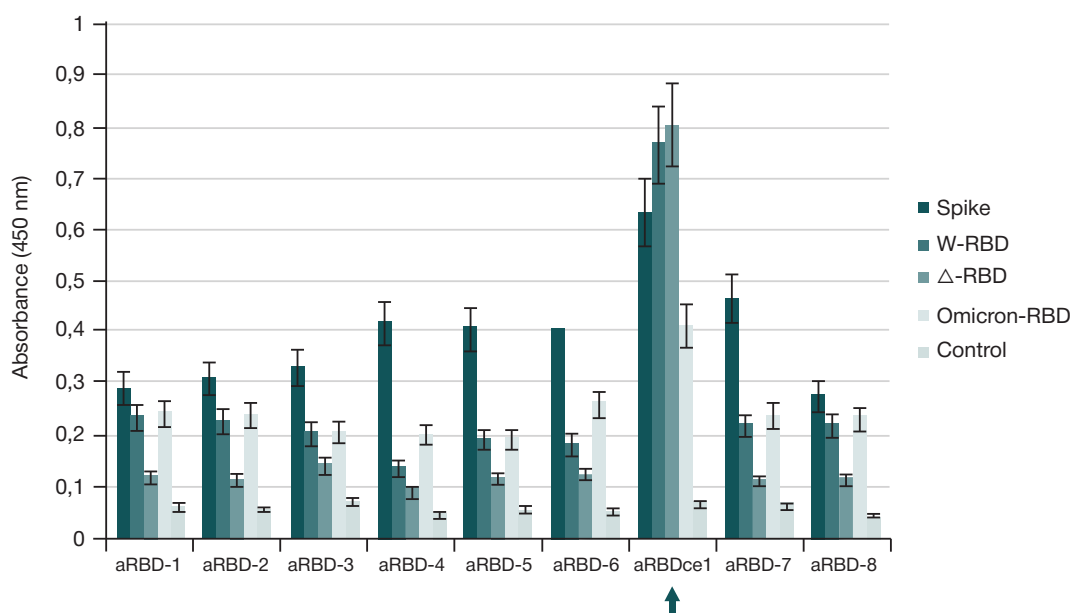
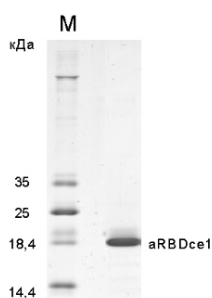


Fig. 4. Results of ELISA of nine selected nanobody variants (aRBD-1–aRBD-8 and aRBDce1) binding to immobilized recombinant proteins that correspond to (left-to-right) spike protein, RBD Wuhan (W-RBD), RBD Delta (Δ-RBD), and RBD Omicron, and to the control well with no antigen blocked with 1% BSA (as in all other wells). The absorbance values reflect the effectiveness of nanobody binding. Mean values for three independent experiments and standard deviations are provided

commercially available XR19 neutralizing mouse monoclonal nanobody (Xema; Russia) at a concentration of 1 $\mu\text{g/mL}$ was added (all antibodies were dissolved in PBS with 0.1% BSA). After washing the peroxidase-conjugated rabbit antibodies against mouse immunoglobulins were added, and the bound peroxidase was determined as described above. It can be seen that the aRBDce1 nanobody does not compete for binding with this virus-neutralizing (according to the manufacturer) antibody. The results obtained allow us to assume with high probability that we have managed to complete the task and generate a single-domain antibody capable of highly effectively binding the SARS-CoV-2 S protein RBD conserved surface (easily accessible) epitope. Fig. 6 shows the amino acid sequence of the generated aRBDce1 nanobody, it also shows how the adapted purified nanobody looks like when sorted in the 14% SDS-polyacrylamide gel. The data obtained provide the basis for the recently submitted patent application (registration number 2022132017).

In the study a nanobody that binds to one of the RBD conserved antigenic epitopes of S protein found in three different SARS-CoV-2 variants, including the most heavily mutated Omicron variant, has been generated according to the task using the technique of generating the nanobodies with pre-set specificity and subsequent effective nanobody selection by phage display. Thus, we have demonstrated an approach allowing to generate such nanobodies. The fundamental difference between our approach and many similar studies (some of the studies are mentioned in the background section [16–18]) is the fact that we are not focused on the virus-neutralizing nanobody variants. We strive to generate nanobodies against the most conserved and the most accessible (displayed on the surface of the virus) epitopes of the viral surface proteins. It is known that the most conserved epitopes of S protein are located in its C-terminal

B



BULLETIN OF RSMU | 1, 2023 | VESTNIKRGMU.RU

region (S2) that is directly involved in fusing with the host cell membrane. However, our unpublished data on the nanobodies against the similar region of the influenza virus haemagglutinin suggest that there could be some spatial constraints that prevent the nanobody from reaching such epitopes *in vivo*. The S protein RBD region comprises the epitopes that are most accessible for binding. Furthermore, it contains regions with the relatively low mutation rate [6–8]. We have chosen this RBD region as the initial target, because this region is potentially the most accessible for binding with the nanobody that is considered as a potential virus-binding module of the future aerosol combination virus-trapping medication that would also contain an anchor module for binding with the major components of human upper respiratory tract secretions. We assume that it is a good idea to have several binding modules against various epitopes to be less dependent on the new mutations. Moreover, in the future we consider the use of inactivated whole virus particle as the

set of antigens most close to native set for immunization and subsequent selection aimed at using the approach similar to that reported in this paper to generate the nanobodies against the conserved surface epitopes of the virus.

CONCLUSIONS

Thus, the paper reports the method to obtain nanobodies (aRBDce1) against the conserved epitope of the receptor-binding domain of the SARS-CoV-2 main surface protein, the spike protein, using the recombinant proteins that correspond to this domain in various most relevant mutant virus variants and the effective technique for generating single-domain antibodies. Along with conventional use in immunoassays and diagnosis, the generated nanobody can be potentially used as a module for target-specific binding of coronavirus during the development of novel combination antiviral drugs.

References

- Hoffmann M, Kleine-Weber H, Schroeder S, Krüger N, Herler T, Erichsen S, et al. SARS-CoV-2 Cell Entry Depends on ACE2 and TMPRSS2 and Is Blocked by a Clinically Proven Protease Inhibitor. *Cell*. 2020; 181 (2): 271–80.
- Walls AC, Park Y-J, Tortorici MA, Wall A, McGuire AT, Veesler D. Structure, Function, and Antigenicity of the SARS-CoV-2 Spike Glycoprotein. *Cell*. 2020; 181 (2): 281–92.
- Zhou T, Tsybovsky Y, Gorman J, Rapp M, Cerutti G, Chuang G-Y, et al. CryoEM Structures of SARS-CoV-2 Spike Without and With ACE2 Reveal a pH Dependent Switch to Mediate Endosomal Positioning of Receptor-Binding Domains. *Cell Host Microbe*. 2020; 28 (6): 867–79.e5.
- Dhawan M, Sharma A, Priyanka S, Thakur N, Rajkhowa TK, Choudhary OP. Delta variant (B.1.617.2) of SARS-CoV-2: Mutations, impact, challenges and possible solutions. *Hum Vaccin Immunother*. 2022; 18 (5): 2068883.
- Mannar D, Saville JW, Zhu X, Srivastava SS, Berezuk AM, Tuttle KS, et al. SARS-CoV-2 Omicron Variant: Antibody Evasion and Cryo-EM Structure of Spike Protein-ACE2 Complex. *Science*. 2022; 375 (6582): eabn7760.
- Harvey WT, Carabelli AM, Jackson B, Gupta RK, Thomson EC, Harrison EM, et al. SARS-CoV-2 Variants, Spike Mutations and Immune Escape. *Nat Rev Microbiol*. 2021; 19 (7): 409–21.
- Starr TN, Greaney AJ, Dingens AS, Bloom JD. Complete Map of SARS-CoV-2 RBD Mutations That Escape the Monoclonal Antibody LY-CoV555 and its Cocktail With LY-Cov016. *Cell Rep. Med*. 2021; 2 (4): 100255.
- Rees-Spear C, Muir L, Griffith SA, Heaney J, Aldon Y, Snitselaar JL, et al. The Effect of Spike Mutations on SARS-CoV-2 Neutralization. *Cell Rep*. 2021; 34 (12): 108890.
- Parray HA, Shukla S, Perween R, Khatri R, Shrivastava T, Singh V, et al. Inhalation monoclonal antibody therapy: a new way to treat and manage respiratory infections. *Appl Microbiol Biotechnol*. 2021; 105 (16–17): 6315–32.
- Wang YY, Harit D, Subramani DB, Arora H, Kumar PA, Lai SK, et al. Influenza-binding antibodies immobilise influenza viruses in fresh human airway mucus. *Eur Respir J*. 2017; 49: 1601709.
- Hamers-Casterman C, Atarhouch T, Muyldermans S, Robinson G, Hammers C, Bajana Songa E, et al. Naturally occurring antibodies devoid of light chains. *Nature*. 1993; 363: 446–8.
- Flajnik MF, Kasahara M. Origin and evolution of the adaptive immune system: genetic events and selective pressures. *Nat Rev Genet*. 2010; 11: 47–59.
- Harmsen MM, De Haard HJ. Properties, production, and applications of camelid single-domain antibody fragments. *Appl Microbiol Biotechnol*. 2007; 77: 13–22.
- Muyldermans S. Nanobodies: natural single-domain antibodies. *Annu Rev Biochem*. 2013; 82: 775–97.
- Laursen NS, Friesen RHE, Zhu X, Jongeneelen M, Blokland S, Vermond J, et al. Universal protection against influenza infection by a multidomain antibody to influenza hemagglutinin. *Science*. 2018; 362 (6414): 598–602.
- Güttler T, Aksu M, Dickmanns A, Stegmann KM, Gregor K, Rees R, et al. Neutralization of SARS-CoV-2 by highly potent, hyperthermostable, and mutation-tolerant nanobodies. *The EMBO Journal*. 2021; 40: e107985. DOI: 10.15252/embj.2021107985.
- Casasnovas JM, Margolles Y, Noriega MA, Guzmán M, Arranz R, Melero R, et al. Nanobodies protecting from lethal SARS-CoV-2 infection target receptor binding epitopes preserved in virus variants other than omicron. *Front Immunol*. 2022; 13: 863831.
- Schoof M, Faust B, Saunders RA, Sangwan S, Rezelj V, Hoppe N, et al. An ultrapotent synthetic nanobody neutralizes SARS-CoV-2 by stabilizing inactive Spike. *Science*. 2020; 370 (6523): 1473–9.
- Krammer F, F Amanat F, Strohmeier S. Vector pCAGGS Containing the SARS-Related Coronavirus 2, Wuhan-Hu-1 Spike Glycoprotein Receptor Binding Domain (RBD), NR-52309. Available from: <https://www.beiresources.org/Catalog/BEIPlasmidVectors/NR-52309.aspx>.
- Stadlbauer D, Amanat F, Chromikova V, Jiang K, Strohmeier S, Arunkumar GA, et al. SARS-CoV-2 Seroconversion in Humans: a detailed protocol for a serological assay, antigen production, and test setup. *Curr Protoc Microbiol*. 2020; 57 (1): e100.
- Tillib SV, Ivanova TI, Vasilev LA. Fingerprinyj analiz selekcii «nanotel» metodom fagovogo displeya s ispol'zovaniem dvux variantov fagov-pomoshchnikov. *Acta Naturae*. 2010; 2 (3): 100–8. Russian.
- Arbabi Ghahroudi M, Desmyter A, Wyns L, Hamers R, Muyldermans S. Selection and identification of single domain antibody fragments from camel heavy-chain antibodies. *FEBS Lett*. 1997; 414 (3): 521–6. DOI: 10.1016/S0014-5793(97)01062-4. PMID: 9323027.
- Tillib S, Ivanova TI, Vasilev LA, Rutovskaya MV, Saakyan SA, Gribova IY, et al. Formatted single-domain antibodies can protect mice against infection with influenza virus (H5N2). *Antiviral Research*. 2013; 97: 245–54.

Литература

- Hoffmann M, Kleine-Weber H, Schroeder S, Krüger N, Herrler T, Erichsen S, et al. SARS-CoV-2 Cell Entry Depends on ACE2 and TMPRSS2 and Is Blocked by a Clinically Proven Protease Inhibitor. *Cell*. 2020; 181 (2): 271–80.
- Walls AC, Park Y-J, Tortorici MA, Wall A, McGuire AT, Veesler D. Structure, Function, and Antigenicity of the SARS-CoV-2 Spike Glycoprotein. *Cell*. 2020; 181 (2): 281–92.
- Zhou T, Tsybovsky Y, Gorman J, Rapp M, Cerutti G, Chuang G-Y, et al. CryoEM Structures of SARS-CoV-2 Spike Without and With ACE2 Reveal a pH Dependent Switch to Mediate Endosomal Positioning of Receptor-Binding Domains. *Cell Host Microbe*. 2020; 28 (6): 867–79.e5.
- Dhawan M, Sharma A, Priyanka S, Thakur N, Rajkhowa TK, Choudhary OP. Delta variant (B.1.617.2) of SARS-CoV-2: Mutations, impact, challenges and possible solutions. *Hum Vaccin Immunother*. 2022; 18 (5): 2068883.
- Mannar D, Saville JW, Zhu X, Srivastava SS, Berezhuk AM, Tuttle KS, et al. SARS-CoV-2 Omicron Variant: Antibody Evasion and Cryo-EM Structure of Spike Protein-ACE2 Complex. *Science*. 2022; 375 (6582): eabn7760.
- Harvey WT, Carabelli AM, Jackson B, Gupta RK, Thomson EC, Harrison EM, et al. SARS-CoV-2 Variants, Spike Mutations and Immune Escape. *Nat Rev Microbiol*. 2021; 19 (7): 409–21.
- Starr TN, Greaney AJ, Dingens AS, Bloom JD. Complete Map of SARS-CoV-2 RBD Mutations That Escape the Monoclonal Antibody LY-CoV555 and its Cocktail With LY-Cov016. *Cell Rep. Med*. 2021; 2 (4): 100255.
- Rees-Spear C, Muir L, Griffith SA, Heaney J, Aldon Y, Snitselaar JL, et al. The Effect of Spike Mutations on SARS-CoV-2 Neutralization. *Cell Rep*. 2021; 34 (12): 108890.
- Parray HA, Shukla S, Perween R, Khatri R, Shrivastava T, Singh V, et al. Inhalation monoclonal antibody therapy: a new way to treat and manage respiratory infections. *Appl Microbiol Biotechnol*. 2021; 105 (16–17): 6315–32.
- Wang YY, Harit D, Subramani DB, Arora H, Kumar PA, Lai SK, et al. Influenza-binding antibodies immobilise influenza viruses in fresh human airway mucus. *Eur Respir J*. 2017; 49: 1601709.
- Hamers-Casterman C, Atarhouch T, Muyldermans S, Robinson G, Hammers C, Bajjaya Songa E, et al. Naturally occurring antibodies devoid of light chains. *Nature*. 1993; 363: 446–8.
- Flajnik MF, Kasahara M. Origin and evolution of the adaptive immune system: genetic events and selective pressures. *Nat Rev Genet*. 2010; 11: 47–59.
- Harmsen MM, De Haard HJ. Properties, production, and applications of camelid single-domain antibody fragments. *Appl Microbiol Biotechnol*. 2007; 77: 13–22.
- Muyldermans S. Nanobodies: natural single-domain antibodies. *Annu Rev Biochem*. 2013; 82: 775–97.
- Laursen NS, Friesen RHE, Zhu X, Jongeneelen M, Blokland S, Vermond J, et al. Universal protection against influenza infection by a multidomain antibody to influenza hemagglutinin. *Science*. 2018; 362 (6414): 598–602.
- Güttler T, Aksu M, Dickmanns A, Stegmann KM, Gregor K, Rees R, et al. Neutralization of SARS-CoV-2 by highly potent, hyperthermostable, and mutation-tolerant nanobodies. *The EMBO Journal*. 2021; 40: e107985. DOI: 10.15252/emboj.2021107985.
- Casasnovas JM, Margolles Y, Noriega MA, Guzmán M, Arranz R, Melero R, et al. Nanobodies protecting from lethal SARS-CoV-2 infection target receptor binding epitopes preserved in virus variants other than omicron. *Front Immunol*. 2022; 13: 863831.
- Schoof M, Faust B, Saunders RA, Sangwan S, Rezelj V, Hoppe N, et al. An ultrapotent synthetic nanobody neutralizes SARS-CoV-2 by stabilizing inactive Spike. *Science*. 2020; 370 (6523): 1473–9.
- Krammer F, Amanat F, Strohmeier S. Vector pCAGGS Containing the SARS-Related Coronavirus 2, Wuhan-Hu-1 Spike Glycoprotein Receptor Binding Domain (RBD), NR-52309. Available from: <https://www.beiresources.org/Catalog/BEIPlasmidVectors/NR-52309.aspx>.
- Stadlbauer D, Amanat F, Chromikova V, Jiang K, Strohmeier S, Arunkumar GA, et al. SARS-CoV-2 Seroconversion in Humans: a detailed protocol for a serological assay, antigen production, and test setup. *Curr Protoc Microbiol*. 2020; 57 (1): e100.
- Тиллиб С. В., Иванова Т. И., Васильев Л. А. Фингерпринтный анализ селекции «нанотел» методом фагового дисплея с использованием двух вариантов фагов-помощников. *Acta Naturae*. 2010; 2 (3): 100–8.
- Arbabi Ghahroudi M, Desmyter A, Wyns L, Hamers R, Muyldermans S. Selection and identification of single domain antibody fragments from camel heavy-chain antibodies. *FEBS Lett*. 1997; 414 (3): 521–6. DOI: 10.1016/S0014-5793(97)01062-4. PMID: 9323027.
- Tillib S, Ivanova TI, Vasilev LA, Rutovskaya MV, Saakyan SA, Gribova IY, et al. Formatted single-domain antibodies can protect mice against infection with influenza virus (H5N2). *Antiviral Research*. 2013; 97: 245–54.

THE APPROACH TO PATIENT CLUSTERING BASED ON THE MICROCHIP DATA CONFINED TO DISTINCT LOCI USING THE COMBINATIONS OF VARIANTS

Iulmetova LN, Kulemin NA, Sharova EI[✉]

Lopukhin Federal Research and Clinical Center of Physical-Chemical Medicine of the Federal Medical Biological Agency, Moscow, Russia

Fuchs' endothelial corneal dystrophy is a socially significant hereditary disease. More than a half of cases in the European population are caused by the increased number of trinucleotide repeats in the *TCF4* gene. The study was aimed to develop and test the approach of dividing patients into groups based on the chip-based genotyping and genome-wide association study (GWAS) results. The analysis was conducted using FECD Genetics Multi-center Study and AREDS project datasets containing the data of 1721 clinical cases and 2408 control patients. When analyzing the GWAS results, the patients and the control group were divided into two groups by means of hierarchical clustering suggesting that patients with the increased number of repeats in the *TCF4* gene are carriers of specific combinations of genomic variants (haplotypes). It was shown that individual variants cannot be used for the molecular genetic stratification of patients with the increased number of repeats in *TCF4* due to inconsistent results obtained for the variants. Furthermore, the haplotype-based approach outperformed the SNPs in terms of odds ratio. The paper proposes a method that enables further search for the biologically relevant combinations of genomic variants.

Keywords: genome wide association study, Fuchs endothelial corneal dystrophy, trinucleotide repeat expansion, patient stratification, locus

Funding: the study was supported by the President of the Russian Federation (grant for young postdocs MK-2951.2022.1.4)

Acknowledgements: the authors thank dbGaP for providing access to the phs000421.v1.p1 and phs000001.v3.p1 datasets. The dataset with the dbGaP registration number phs000421.v1.p1 was obtained from the genetic study of Fuchs' endothelial corneal dystrophy (FECD) available from https://www.ncbi.nlm.nih.gov/projects/gap/cgi-bin/study.cgi?study_id=phs000421.v1.p1. The authors recognize the grants that have been used to support registration of cases and controls and would be used in this GWAS: R01EY016514 (DUEC, PI: Gordon Klintworth), R01EY016482 (CWRU, PI: Sudha Iyengar) and 1X01HG006619-01 (PI: Sudha Iyengar, Natalie Afshari). The authors express their gratitude to the FECD study participants and the FECD research team for their valuable contribution to this study. The dataset with the dbGaP registration number phs000001.v3.p1 was obtained from the Age-Related Eye Disease Study (AREDS) database available from https://www.ncbi.nlm.nih.gov/projects/gap/cgi-bin/study.cgi?study_id=phs000001.v3.p1. AREDS was funded by the National Eye Institute (N01-EY-0-2127). The authors thank the AREDS participants and research team for their valuable contribution to this study. The authors express their gratitude to L.O. Skorodumova, research fellow at the Lopukhin Federal Research and Clinical Center of Physical-Chemical Medicine, for valuable suggestions, comments, and support.

Author contribution: Sharova EI — concept and selection of data; Sharova EI, Iulmetova LN — planning and selection of methods; Kulemin NA — project funding and management; Iulmetova LN — design and computation; Sharova EI, Iulmetova LN, Kulemin NA — discussion, manuscript writing and editing.

Compliance with ethical standards: the study was performed according to the principles of the Declaration of Helsinki using the data of the phs000421.v1.p1 and phs000001.v3.p1 projects, the access to which was approved and provided by dbGaP in accordance with the policy of approval and access to specific datasets.

✉ **Correspondence should be addressed:** Elena I. Sharova
Malaya Pirogovskaya, 1, str. 3, Moscow, 119435, Russia; sharova78@gmail.com

Received: 12.12.2022 **Accepted:** 20.01.2023 **Published online:** 12.02.2023

DOI: 10.24075/brsmu.2023.001

ПОДХОД К КЛАСТЕРИЗАЦИИ ПАЦИЕНТОВ ПО МИКРОЧИПОВЫМ ДАННЫМ ВНУТРИ ОТДЕЛЬНЫХ ЛОКУСОВ С ИСПОЛЬЗОВАНИЕМ КОМБИНАЦИЙ ВАРИАНТОВ

Л. Н. Юльметова, Н. А. Кулемин, Е. И. Шарова[✉]

Федеральный научно-клинический центр физико-химической медицины имени Ю. М. Лопухина Федерального медико-биологического агентства, Москва, Россия

Дистрофия роговицы Фукса является социально значимым наследственным заболеванием. Более половины случаев в европейской популяции вызваны увеличением числа тринуклеотидных повторов в гене *TCF4*. Целью исследования было разработать и проверить подход разделения пациентов на группы на основе результатов чип-генотипирования и полногеномного ассоциативного исследования (GWAS). В качестве исходных данных использовали датасеты FECD Genetics Multi-center Study и проекта AREDS в количестве 1721 клинических случаев и 2408 контрольных пациентов. При анализе результатов GWAS было проведено разделение пациентов и группы контроля на две группы методом иерархической кластеризации с учетом предположения, что пациенты с увеличенным числом повторов в гене *TCF4* имеют определенные сочетания геномных вариантов (гаплотипов). Показано, что одиночные варианты не могут быть использованы для молекулярно-генетической классификации пациентов с увеличенным числом повторов в гене *TCF4* из-за рассогласованности результатов по вариантам. При этом гаплотипный подход превзошел анализируемые варианты по параметру отношения шансов, перекрывая 95%-й доверительный интервал выборки двух экспериментальных исследований. Предложенный метод позволяет продолжать поиск биологически обоснованных сочетаний геномных вариантов.

Ключевые слова: полногеномное ассоциативное исследование, эндотелиальная дистрофия роговицы, экспансия тринуклеотидных повторов, классификация пациентов, локус

Финансирование: работа выполнена в рамках гранта Президента РФ для молодых ученых-кандидатов наук MK-2951.2022.1.4.

Благодарности: авторы благодарят dbGaP за предоставление доступа к наборам данных phs000421.v1.p1 и phs000001.v3.p1. Набор данных с регистрационным номером dbGaP phs000421.v1.p1 получен из исследования генетики эндотелиальной дистрофии роговицы Фукса (FECD) https://www.ncbi.nlm.nih.gov/projects/gap/cgi-bin/study.cgi?study_id=phs000421.v1.p1. Авторы признают гранты, финансировавшие регистрацию случаев и контролей, которые будут использоваться в этом GWAS: R01EY016514 (DUEC, PI: Gordon Klintworth), R01EY016482 (CWRU, PI: Sudha Iyengar) и 1X01HG006619-01 (PI: Sudha Iyengar, Натали Афшари). Авторы благодарят участников FECD и исследовательскую группу FECD за их ценный вклад в это исследование. Набор данных с регистрационным номером dbGaP phs000001.v3.p1 получен из базы данных исследования возрастных заболеваний глаз (AREDS) по адресу https://www.ncbi.nlm.nih.gov/projects/gap/cgi-bin/study.cgi?study_id=phs000001.v3.p1. Финансовая поддержка AREDS была предоставлена Национальным глазным институтом (N01-EY-0-2127). Авторы благодарят участников AREDS и исследовательскую группу AREDS за их ценный вклад в это исследование. Авторы благодарят научного сотрудника ФГБУ ФНКЦ ФХМ имени Ю. М. Лопухина Л. О. Скородумову за ценные предложения, замечания и поддержку.

Вклад авторов: Е. И. Шарова — идея и подбор данных; Е. И. Шарова, Л. Н. Юльметова — планирование и выбор методов; Н. А. Кулемин — финансирование и администрирование проекта; Л. Н. Юльметова — разработка и вычисления; Е. И. Шарова, Л. Н. Юльметова, Н. А. Кулемин — обсуждение результатов, написание и редактирование статьи.

Соблюдение этических стандартов: исследование проведено с соблюдением принципов Хельсинкской декларации, с использованием наборов данных проектов phs000421.v1.p1 и phs000001.v3.p1., доступ к которым одобрен и получен через dbGaP в соответствии с их политикой одобрения и доступа к конкретным сетам данных.

✉ **Для корреспонденции:** Елена Ивановна Шарова
ул. Малая Пироговская, д. 1с3, г. Москва, 119435, Россия; sharova78@gmail.com

Статья получена: 12.12.2022 **Статья принята к печати:** 20.01.2023 **Опубликована онлайн:** 12.02.2023

DOI: 10.24075/vrgmu.2023.001

Finding a biological basis for the inheritability of phenotypes is one of the main tasks of modern medical genetics. Generally, approaches aimed at the detection of pathogenic genomic variants can be divided into two categories: biological and mathematical. Biological methods include the approaches that explain phenotypes based on the studied biochemical processes. When it is impossible to directly trace the biochemical pathway underlying phenotype formation, but the disease shows a familial tendency, various statistical approaches are applied: genome-wide association studies (GWAS) [1], polygenic risk score (PRS) [2], haplotype identification approaches [3], and other methods. Basic GWAS methodology performs single nucleotide polymorphism (SNP) association testing to identify SNP loci exceeding a genome-wide significance p -value threshold. Thus, the GWAS results for any disorder representing a combination of rare inherited mutations could be inaccurate, since the number of rare polymorphisms don't meet the significance criteria. The PRS approach might be considered as an extension of GWAS, however, it also evaluates the effect of each SNP independently. For some disorders the genetic basis can't be explained by biological or popular statistical methods. The inheritance of such phenotypes is based on the haplotype architectures. We define a haplotype as a linear combination of a certain number (up to several hundred) of the linked variable variants that together form a small number (less than 100, 10–20 on average) of allele variants. The approach involving identification of specific haplotype variants is actively used in pharmacogenetics for analysis of P450 cytochromes. For example, there are more than 120 haplotype variants for *CYP2D6* resulting from more than 500 polymorphisms [4]. However, this approach is extremely rarely discussed with reference to the majority of loci of polygenic diseases.

GWAS is commonly applied to the nervous system disorders, polygenic developmental disorders and neurodegenerative diseases, such as amyotrophic lateral sclerosis, Parkinson's disease, schizophrenia, autism spectrum disorders. GWAS method allows to identify genome regions, the alterations of which are overrepresented in affected individuals relative to the general (control) population. GWAS also handles the structural variations that can't be detected directly by the chip SNPs but are in linkage disequilibrium with those ones. In particular, the amyotrophic lateral sclerosis GWAS detects the *C9orf72* gene locus comprising the G4C2 expanded six-nucleotide repeat (GGGGCC) [5], however, the repeat variants are not detected directly with the chip. The Huntington's disease GWAS reveals the chromosome 15 *HTT* gene locus comprising trinucleotide repeats [6], but there are no probes matching the repeat region in the chip.

Fuchs Endothelial Corneal Dystrophy (FECD) is a hereditary eye disease characterized by a decrease in the number of corneal endothelial cells that maintain the corneal stroma water balance. FECD is a polygenic disease that is of considerable interest for genetic research [7]. There are two FECD forms: early onset and late onset FECD. These forms have different genetic bases. Early onset FECD is diagnosed at the age below 50 and is a very rare disorder associated with the *COL8A2* gene pathogenic variants [8]. The late onset FECD manifests at the age greater than 50 and it is the most common form of FECD. It was shown that late onset FECD is associated with the intronic CTG18.1 trinucleotide repeat expansion in *TCF4* [9]. According to our data and the data provided by foreign authors, the CTG18.1 intronic trinucleotide repeat expansion in *TCF4* is the most common FECD-associated variant among Caucasoid populations. The expansion of at least one allele of CTG18.1 trinucleotide repeat was detected in approximately

two thirds of the FECD patients in European descent cohorts. Later Afshari et al. [10] made an attempt to find other variants associated with FECD in a bigger cohort also using GWAS. They confirmed the association of the *TCF4* locus and identified three new loci in the genes *KANK4*, *LAMC1* genes and near the *ATP1B1* gene, however, their independence from trinucleotide repeat expansion was not tested [10]. The role of mutations in *ZEB1* [11], *SLC4A11* [12], *AGBL1* [13], and *LOXHD1* [14] in the development of FECD is also discussed. The question, whether FECD is a set of phenocopies or a polygenic disease, still remains open. The reported asymptomatic carriers of the repeat expansion [9, 15] and the disputable nature of the clear monogenic link of FECD to some other genes suggest that late onset FECD is a set of polygenic phenocopies. This makes it similar to other late onset repeat expansion diseases.

Thus it leads to the question if it's possible to split the patients into groups within the loci using GWAS results and what accuracy can be achieved. And is it possible to stratify late onset FECD patients by expansion/no expansion based on the microchip-based data? Are the haplotype stratification results and simple patient grouping based on the minor allele of SNPs comparable for these purposes? The study was aimed to develop and test the approach of dividing patients into groups based on the chip-based genotyping and genome-wide association study (GWAS) results.

METHODS

The analysis was carried on dbGaP datasets corresponding to two studies: the FECD Genetics Multi-center Study [16] and the Age-Related Eye Disease Study (AREDS, Refractive Error Substudy) [17–18]. All samples were genotyped on Illumina HumanOmni2.5-4v1 arrays. Clinical manifestations of the disease were classified using a modified Krachmer grading scale based on the slit lamp biomicroscopy data [19].

Both sample-level and variant-level quality control (QC) was performed. The genotyping data were preprocessed using the PLINK 1.9 software [20], GRAF 2.4 [21–22], and code written in R version 4.1.0.

First genotypes with GenCall (GC) scores below 0.3 were removed. Subsequent QC selected markers met the following criteria: missing genotype rate < 10%, minor allele frequency > 1%, number of Mendel errors, a Hardy-Weinberg Equilibrium p -value > 1×10^{-10} for control samples and p -value > 1×10^{-15} for FECD patients. Duplicate markers, i.e. markers with different IDs but identical genetic positions and allele coding, were detected and analyzed separately. Both markers of each pair of duplicates were excluded from consideration. One marker with the lowest missing genotype rate was excluded from each pair of duplicates showing 10 differences or more. A total of 1,580,746 SNP markers were included in the analysis after applying all the filters.

The following inclusion criteria were defined for the group of FECD patients: age 47 or older; keratoplasty in at least one eye or grade 2 or above disease (according to the modified Krachmer grading scale) in at least one eye.

Inclusion criteria for the control group: age 60 or older; normal cornea with no epithelial, endothelial, or stromal abnormalities except corneal injuries.

Exclusion criteria: samples with Mendel errors, samples with mismatch between annotated and genetic sex (determined based on the X chromosome heterozygosity rate and Y chromosome genotype counts); samples with genotype missingness above 5%; relatives up to the second degree of relationship (according to GRAF-rel).

Table 1. Characteristics of the study participants

	Patients with FECD	Control samples	
Sample	According to Afshari et al, 2017	According to Afshari et al, 2017	According to ARED
Number of participants	1287	2373	
		562	1811
Males	408	989	
		245	744
Females	879	1384	
		317	1067
Median age	71	72	68
		69	

The population structure was estimated using GRAF-pop in order to obtain a genetically homogenous sample. The samples identified as outliers in the genetic distance coordinates were filtered out. The patients were divided into groups according to the potential carrier state of repeat expansion in three stages:

Stage 1: selection of significant variants;

Stage 2: clustering the study participants based on the haplotypes/combinations of the selected variants, calculation of the repeat expansion rate;

Stage 3: evaluation of the concordance between the obtained repeat expansion rate and the percentage of the repeat expansion carriage according to the experimental data reported in previous studies. The repeat allele was considered as expanded if the number of the repeats was ≥ 40 and as unexpanded if the number of the repeats was < 40 .

In the first stage, variants were tested for association with FECD using logistic regression with sex and the first six principal components as covariates. p -values were adjusted for multiple testing using the Benjamini–Hochberg method. The chromosome 18 (carrying the locus with the repeats) variants were first filtered by p -value $< 1 \times 10^{-15}$. For comparison with the haplotype-based approach, three SNPs showing the lowest p -values in the resulting set of variants were considered as the potential markers of the increased number of repeats. Additionally marker pruning based on LD ($r^2 > 0.6$) was performed. The genotype matrix was encoded according to the dominant inheritance model.

In the second stage, we used the assumption that the patients with the repeat expansion in the *TCF4* gene carried the certain combinations of SNPs. We expected that the FECD samples would cluster within the *TCF4* locus based on the haplotypes and the combinations of individual variants. However,

individuals with phenocopy due to expansion would fall into common clusters based on the similarity of the combinations of minor variants. Asymptomatic control repeat carriers from the control sample (2–10%) and a fraction of the control sample carrying minor haplotypes with no repeats would fall into the same clusters. Furthermore, the combinations of major variants and haplotypes showing predominance of major alleles would form clusters mostly of the control sample representatives. However, these clusters would also include some FECD patients with phenocopy and some patients with the expansion no longer linked to minor haplotypes (in 7% of FECD patients, linked haplotypes and repeats sometimes break apart, which has been earlier demonstrated for the rs613872 variant [23]). That is why the percentage of FECD patients and subjects with no FECD can be used as a surrogate marker of the carriage of the repeats in specific clusters.

Agglomerative hierarchical clustering implemented in the hclust function of the stats R package was used for clustering. The algorithm arranges the data into a tree representation by merging the pairs of clusters with the minimum distance into a new cluster. The algorithm takes the matrix of pairwise distances between the points (samples) as input; initially each point represents a distinct cluster. Since the haplotypes are not identical, we expected that there would be more than two clusters, while the optimal number of clusters was defined by the Silhouette metrics.

For each cluster we calculated the percentage of patients and controls. Clusters with a patient predominance we considered associated with FECD. For the selected three SNPs, carriage of the minor allele was considered as a marker of the repeat expansion carriage.

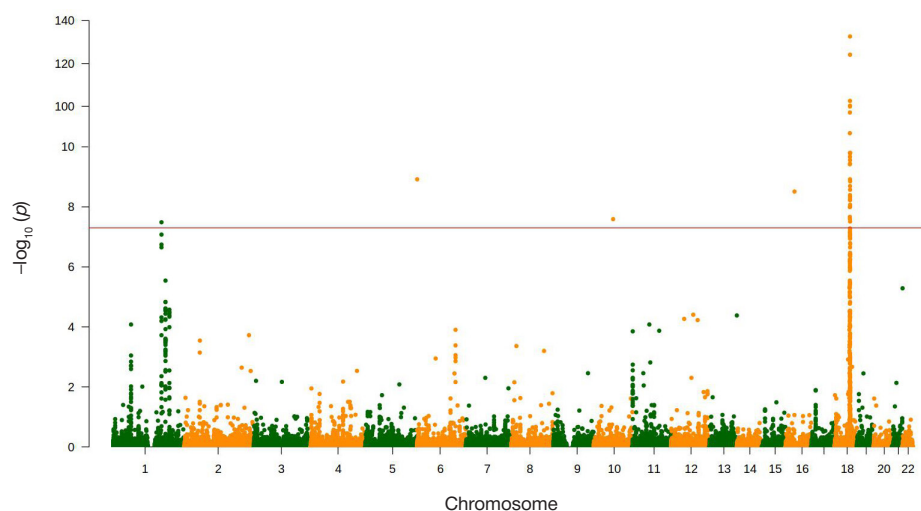


Fig. 1. Genome-wide association study results presented through a Manhattan plot. Points represent the assessed variants. Their positions on the x axis are determined by positions of the variants in the genome, while positions on the y axis represent the degree of the disease association ($-\log_{10}$ of the p -value)

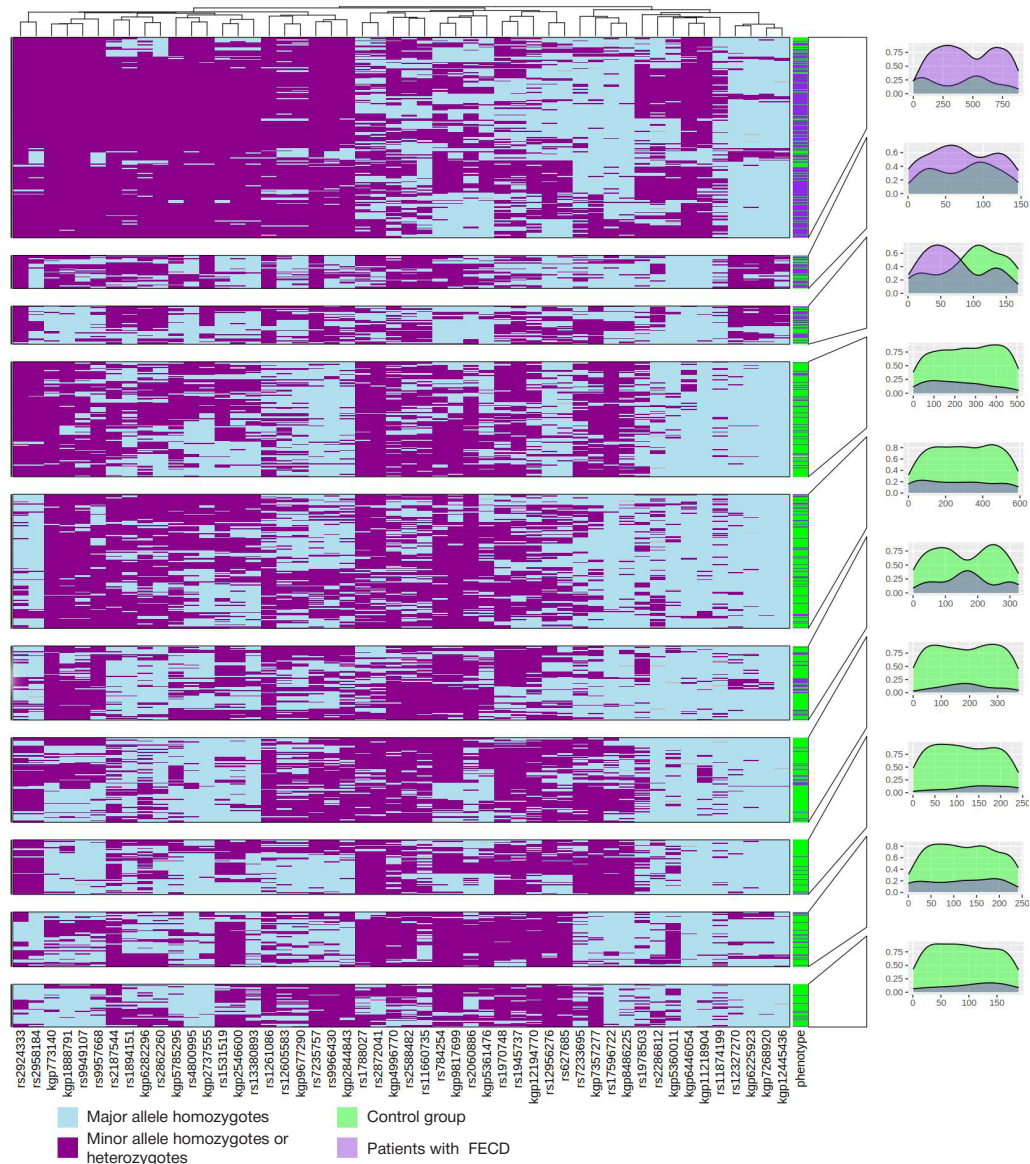


Fig. 2. Heatmap visualization of clustering output. Columns represent variants patients, and rows represent patients various genomic variants. Annotations on the right show the distribution of the FECD samples and the control samples within each cluster

To evaluate the resulting partition, we calculated the odds ratio from the estimates of the expansion status in each group.

The last step was to compare the results obtained by the proposed approach with the experimental data reported in the previous studies. We selected studies based on the following conditions:

1. The number of repeats in *TCF4* was determined by means of fragment analysis or triplet repeat primed PCR.
2. The study participants were individuals of European ancestry.
3. The sample size was at least 50 people for each comparison group.

RESULTS

After the quality control procedure, the discovery dataset consists of 3,660 samples of European ancestry (Table 1) and 1,580,746 SNP markers.

Since GWAS was performed on the same cohort of samples that were studied in the Afshari et al [10], its results (Fig. 1) are comparable to those described in the article. The genomic inflation factor was 1.05, which indicated slight population stratification.

For further analysis, only the locus of chromosome 18 was considered. Filtering by p -values resulted in 134 SNPs,

Table 2. Distribution of probable repeat expansion carriers across the comparison groups

Marker of increased repeat count	Patients with FECD			Control sample		
	Predicted repeat expansion	Predicted no repeat expansion	Predicted repeat expansion carriers, %	Predicted repeat expansion	Predicted no repeat expansion	Predicted repeat expansion carriers, %
Group of clusters	764	523	59.4	264	2109	11.1
rs784257	1046	237	81.5	765	1602	32.3
rs72932578	698	583	54.5	286	2082	12.1
rs618869	852	431	66.4	588	1780	24.8

Table 3. Results of experimental studies of the percentage of people with the repeat expansion in *TCF4* among patients with FECD and control samples of European ancestry

	Country	FECD		Total	
		Total	Repeat expansion	Total	Repeat expansion
Skorodumova et al, 2018 [15]	Russia	100	72	100	5
Viberg et al., 2022 [24]	Sweden	85	76	102	4
Foja et al., 2017 [25]	Germany	61	47	113	13
Kuot et al., 2017 [26]	Australia	189	107	183	9

three of which with the lowest p -values were rs784257, rs72932578, and rs618869 (and according to gnomAD v3.1.2, the frequencies of the C, T, and C minor alleles in the European population are 0.17932, 0.05649, and 0.13451, respectively). These variants were further tested in terms of dividing patients into groups.

The haplotype block size was 50 variants left after pruning. After clustering the samples were divided into 10 subgroups (Fig. 2).

Clustering has shown that clusters with a predominance of control group participants are homogeneous in terms of their representation. However, three clusters with the potentially increased repeat counts (in which FECD patients prevail) are heterogeneous in terms of haplotypes. This is reflected by the uneven distribution of patients with various phenotypes within each cluster. This may be due to both asymptomatic carriers of the increased repeat number in this locus and the resolution of the population-variable chip SNPs that is not enough for accurate division of samples based on the repeats of varying length.

Our analysis has shown that the proportion of people from clusters with a presumptive carriage of expanded repeats in the group of samples with FECD is significantly higher than in the control group (Table 2). Furthermore, the calculated rate of probable repeat expansion carriers varies significantly depending on the selected method (prediction of expansion based on the haplotypes/combinations of variants or based on the genotypes of certain variants with low p -values).

To verify the results obtained we have selected the studies involving experimental determination of the repeat expansion. The number of repeats is routinely defined by conventional fragment analysis or triplet repeat primed PCR with subsequent

fragment analysis. A total of five papers with appropriate samples have been found (Table 3).

To compare the predicted and reported frequencies of the expansion carriers we have merged the samples from the papers. Comparative analysis has shown that markers reproduce the frequency of the expansion carriers in the comparison groups to a different extent (Fig. 3).

None of the applied approaches represent the repeat frequency in the group of patients and the control group accurately enough compared to the results of direct typing reported in the papers (Table 4). However, the haplotype-based approach outperformed the SNPs in terms of odds ratio by covering the 95% confidence intervals of the samples used in two studies.

It is interesting to note that the individual variants we have considered produce extremely discordant results (Fig. 4), i.e. quite different people are carriers of minor allele in these variants, which makes the applied metrics volatile. rs784257 differs most from the haplotype-based approach in terms of the allele carrier state, it is also the most significant variant according to the GWAS results. At the same time, it shows the maximum discrepancy in the proportions of potential expansion carriers in the control group and no better correspondence with the FECD group. This allele is most likely to show weaker linkage to the repeat carrier state than the other two alleles.

DISCUSSION

Molecular genetic stratification of patients with polygenic diseases is a useful tool for studying the disease genetics. Furthermore, there could be patients with the groups of causal variants linked to various haplotypes within one phenotype.

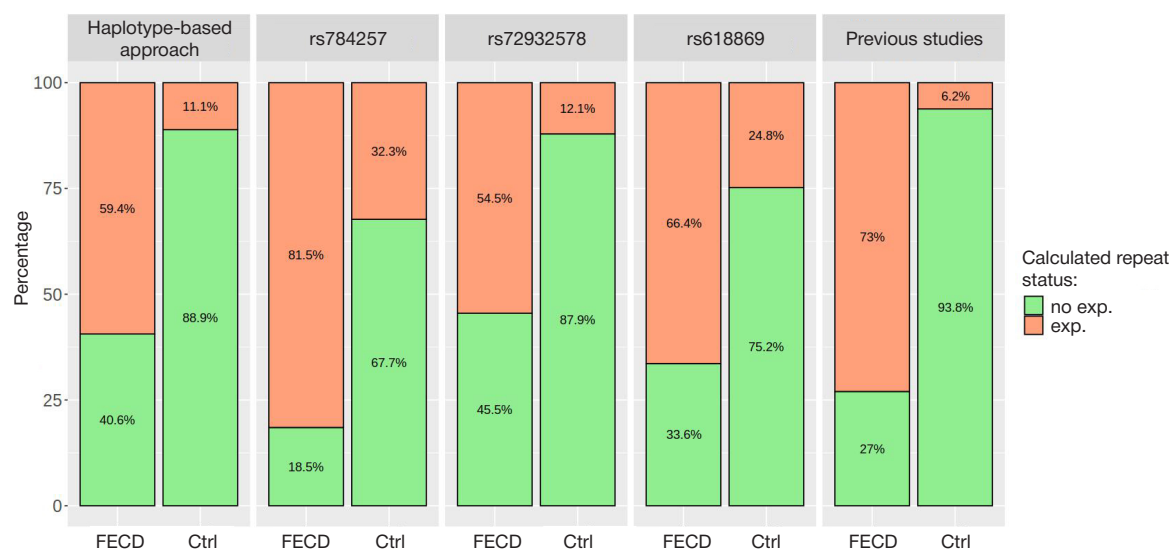
**Fig. 3.** Percentage of people with the repeat expansion and no repeat expansion in the *TCF4* gene intron based on the data of our study (haplotype-based approach, carriers of minor alleles of the rs784257, rs72932578, rs618869 variants) and other studies. FECD — individuals with Fuchs' endothelial corneal dystrophy, Ctrl — control group

Table 4. Odds ratio of finding the expansion in the group of patients with FECD compared to the control group

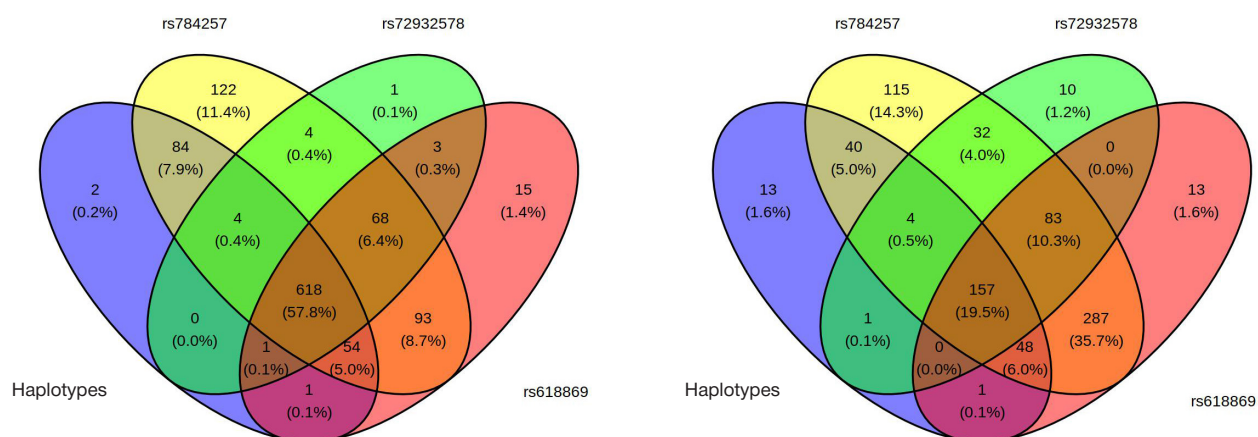
	Odds ratio	95% confidence interval
Haplotype-based approach (h-clust)	11.67	9.85–13.83
rs784257	9.24	7.83–10.90
rs72932578	8.72	7.39–10.28
rs618869	5.98	5.16–6.94
Skorodumova et al, 2018 [15]	48.86	17.98–132.76
Viberg et al., 2022 [24]	206.89	61.37–697.50
Foja et al., 2017 [25]	25.82	11.25–59.26
Kuot et al., 2017 [26]	25.23	12.17–52.31

Despite the fact that the gene is definitely associated with the disease, p -values of the variants would be higher due to the large number of the groups of linked variants, i.e. the variants that are significant for every group do not surpass the generally accepted significance threshold (p -value $< 5 \times 10^{-8}$) due to the features of the disease genetic basis. Moreover, many loci, the significance of which is close to the generally accepted threshold, are characterized by the marked sparseness of the significant variants, under which only a few variants are strongly associated with the disease. Thus, it is impossible to choose between genomic variants as the population outliers (the significance of which results from random population frequency shift) or assigning these variants to the potentially significant group of variants. That is why the genetic data structuring methods that involve assessing interactions between both variants within haplotype blocks and haplotype blocks are a promising tool for the disease genetic basis clarification.

GWAS makes it possible to obtain more information about the disease genetic basis than exclusion of variants based on p -values and loci formation with reference to the nearest gene that represents the transition from the "variant" level to the "gene" level. However, questions remain about unequal contribution of various loci to the genetic basis of the disease in specific groups of people with the same phenotype. This is due, among other things, to the lack of advanced approaches to formation of the combinations of variants, i.e. to working at the intermediate level between the "variant" level and "gene" level. Since the variants show incomplete linkage, it would be reasonable to consider the sets of haplotypes/combinations of variants that define the differentiated disease risk instead of the specific risk haplotypes or protective haplotypes. This means that the variant with the highest population attributable risk (combination of allele frequency and relative risk) is likely to be the most significant one in the locus.

Assessment of the groups of haplotypes linked to the causal variants is still a challenging task, however, it more and more often outperforms GWAS, even despite the lack of the high throughput standard approaches. The GWAS performed in 2005 showed that the *CFH* gene was associated with age-related macular degeneration [27]. Later it was reported that this association was not confined to individual variants and was also observed in the groups of patients with structural alterations, such as partial deletions of the *CFHR1-5* genes [27]. Furthermore, it was found that most of the variation attributed to individual variants was in fact the marker of haplotypes showing large-scale structural alterations in this region. And these are haplotype variants of the locus structure, including those with different population abundance, that show much stronger correlation with the risk of retinal degeneration than the majority of individual variants in this locus [28].

In this study we have implemented sample clustering by variants of the region containing the expansion based on the data on the association of individual variants with the repeats [14, 23, 29], particularly, allele G of the rs613872 variant, and haplotype blocks [29]. After clustering the samples of the group of patients with FECD turned out to be distributed unevenly across the clusters, which was indirect evidence of clustering by haplotypes linked to the expansion. All clusters except one (cluster 3) had a clear status of the repeats. Uncertainty in defining the status was due to parity between patients and controls in the cluster. In the future we have to decide what to do with such clusters: re-cluster people in these clusters in the case-by-case manner or leave them with uncertain status. It is also necessary to select another clustering metrics. This requires additional data that include both sample genotyping results and information about the repeat length. Regardless of these limitations, the results obtained using the haplotype-based approach were better than the results shown by

**Fig. 4.** Consistency of the repeat status determination results obtained by different approaches: based on the genotypes of the rs784257, rs72932578, rs618869 variants and haplotype-based. Left — for the repeat expansion carriers in the FECD group, right — for the repeat expansion carriers in the control group

individual variants. However, these results turned out to be not precise enough to consider our method optimal.

This work accomplished two goals.

1. Initial testing of an approach that allows stratification of patients and control groups at the intermediate level (not the level of a single variant and not the level of the gene closest to the locus) without first understanding the haplotype structure of the locus. The proportion of patients with FECD and control samples in clusters is used as a measure, allowing this approach to be used for diseases in which the approximate proportion of individuals with a phenotype closely related to or due to changes in a given locus is not known in advance.

2. Obtaining a subsample of patients with FECD and no expansion carrier state for precision re-analysis of GWAS in order to refine genetic structure in this particular category of patients.

In the future, patient clustering will make it possible not only to allocate groups within the phenotype showing a strong contribution from distinct genetic variants, including structural variants, but also to propose the basis and approaches to predicting the patients' responses to various types of therapy.

CONCLUSIONS

The study has shown the possibility of using the haplotype-based approach for genetic stratification of patients based on the cause of the genetic disorder, namely the presence of the repeat expansion. The findings have made it possible to draw the following conclusions: 1) the haplotype-based approach is better suited for detection of the association of loci with certain groups of patients than individual variants; 2) for a more accurate picture we should reconsider the approach to defining the haplotype composition and modeling the data matrix for clustering. In particular, it is planned to analyze some methods of computing the genetic similarities (genetic distances (genetic distances) among samples and apply more specific methods for initial selection of variants; 3) the results obtained show that clustering splits the patients with FECD and the control group based on the groups of haplotypes/combinations of variants associated with the repeat expansion. Further testing of the approach requires additional evidence base that demands the use of more validation data.

References

- Uffelmann E, Huang QQ, Munung NS, De Vries J, Okada Y, Martin AR, et al. Genome-wide association studies. *Nature Reviews Methods Primers*. 2021; 1 (1): 59. Available from: <https://doi.org/10.1038/s43586-021-00056-9>.
- Lewis CM, Vassos E. Polygenic risk scores: from research tools to clinical instruments. *Genome medicine*. 2020; 12 (1): 1–1. Available from: <https://doi.org/10.1186/s13073-020-00742-5>.
- Stram DO. Multi-SNP haplotype analysis methods for association analysis. *Statistical Human Genetics: Methods and Protocols*. 2017: 485–504. Available from: https://doi.org/10.1007/978-1-4939-7274-6_24.
- Twesigomwe D, Wright GE, Drögemöller BI, da Rocha J, Lombard Z, Hazelhurst S. A systematic comparison of pharmacogene star allele calling bioinformatics algorithms: a focus on CYP2D6 genotyping. *NPJ genomic medicine*. 2020; 5 (1): 30. Available from: <https://doi.org/10.1038/s41525-020-0135-2>.
- Van Rheenen W, Van Der Spek RA, Bakker MK, Van Vugt JJ, Hop PJ, Zwamborn RA, et al. Common and rare variant association analyses in amyotrophic lateral sclerosis identify 15 risk loci with distinct genetic architectures and neuron-specific biology. *Nature genetics*. 2021; 53 (12): 1636–48.
- Lee JM, Wheeler VC, Chao MJ, Vonsattel JP, Pinto RM, Lucente D, et al. Identification of genetic factors that modify clinical onset of Huntington's disease. *Cell*. 2015; 162 (3): 516–26.
- Fautsch MP, Wieben ED, Baratz KH, Bhattacharyya N, Sadan AN, Hafford-Tear NJ, et al. TCF4-mediated Fuchs endothelial corneal dystrophy: Insights into a common trinucleotide repeat-associated disease. *Progress in retinal and eye research*. 2021; 81: 100883.
- Biswas S, Munier FL, Yardley J, Hart-Holden N, Perveen R, Cousin P, et al. Missense mutations in COL8A2, the gene encoding the $\alpha 2$ chain of type VIII collagen, cause two forms of corneal endothelial dystrophy. *Human molecular genetics*. 2001; 10 (21): 2415–23.
- Wieben ED, Aleff RA, Tosakulwong N, Butz ML, Highsmith WE, Edwards AO, et al. A common trinucleotide repeat expansion within the transcription factor 4 (TCF4, E2-2) gene predicts Fuchs corneal dystrophy. *PLoS One*. 2012; 7 (11): e49083.
- Afshari NA, Igo Jr RP, Morris NJ, Stambolian D, Sharma S, Pulagam VL, et al. Genome-wide association study identifies three novel loci in Fuchs endothelial corneal dystrophy. *Nature communications*. 2017; 8 (1): 14898.
- Chung DW, Frausto RF, Ann LB, Jang MS, Aldave AJ. Functional impact of ZEB1 mutations associated with posterior polymorphous and Fuchs' endothelial corneal dystrophies. *Investigative Ophthalmology & Visual Science*. 2014; 55 (10): 6159–66.
- Chaurasia S, Ramappa M, Annapurna M, Kannabiran C. Coexistence of congenital hereditary endothelial dystrophy and Fuchs endothelial corneal dystrophy associated with SLC4A11 mutations in affected families. *Cornea*. 2020; 39 (3): 354–7.
- Riazuddin SA, Vasanth S, Katsanis N, Gottsch JD. Mutations in AGL1 cause dominant late-onset Fuchs corneal dystrophy and alter protein-protein interaction with TCF4. *The American Journal of Human Genetics*. 2013; 93 (4): 758–64.
- Riazuddin SA, Parker DS, McGlumphy EJ, Oh EC, Iliff BW, Schmedt T, et al. Mutations in LOXHD1, a recessive-deafness locus, cause dominant late-onset Fuchs corneal dystrophy. *The American Journal of Human Genetics*. 2012; 90 (3): 533–9.
- Skorodumova LO, Belodedova AV, Antonova OP, Sharova EI, Akopian TA, Selezneva OV, et al. CTG18. 1 expansion is the best classifier of late-onset Fuchs' corneal dystrophy among 10 biomarkers in a cohort from the European part of Russia. *Investigative Ophthalmology & Visual Science*. 2018; 59 (11): 4748–54.
- Louttit MD, Kopplin LJ, Igo Jr RP, Fondran JR, Tagliaferri A, Bardenstein D, et al. A multi-center study to map genes for Fuchs' endothelial corneal dystrophy: baseline characteristics and heritability. *Cornea*. 2012; 31 (1): 26.
- Age-Related Eye Disease Study Research Group. The age-related eye disease study (AREDS): design implications AREDS report no. 1. *Controlled clinical trials*. 1999; 20 (6): 573.
- Stambolian D, Wojciechowski R, Oexle K, Pirastu M, Li X, Raffel LJ, et al. Meta-analysis of genome-wide association studies in five cohorts reveals common variants in RBFOX1, a regulator of tissue-specific splicing, associated with refractive error. *Human molecular genetics*. 2013; 22 (13): 2754–64.
- Krachmer JH, Purcell JJ Jr, Young CW, Bucher KD. Corneal endothelial dystrophy. A study of 64 families. *Arch Ophthalmol*. 1978; 96 (11): 2036–9. DOI: 10.1001/archophth.1978.03910060424004.
- Chang CC, Chow CC, Tellier LC, Vattikuti S, Purcell SM, Lee JJ. Second-generation PLINK: rising to the challenge of larger and richer datasets. *Gigascience*. 2015; 4: 7. DOI: 10.1186/s13742-015-0047-8.
- Jin Y, Schäffer AA, Sherry ST, Feolo M. Quickly identifying identical and closely related subjects in large databases using genotype data. *PLoS One*. 2017; 12 (6): e0179106. DOI: 10.1371/journal.pone.0179106.

22. Jin Y, Schaffer AA, Feolo M, Holmes JB, Kattman BL. GRAF-pop: A Fast Distance-Based Method To Infer Subject Ancestry from Multiple Genotype Datasets Without Principal Components Analysis. *G3 (Bethesda)*. 2019; 9 (8): 2447–61. DOI: 10.1534/g3.118.200925.
23. Okumura N, Hayashi R, Nakano M, Tashiro K, Yoshii K, Aleff R. et al. Association of rs613872 and Trinucleotide Repeat Expansion in the TCF4 Gene of German Patients With Fuchs Endothelial Corneal Dystrophy. *Cornea*. 2019; 38 (7): 799–805. DOI: 10.1097/ICO.0000000000001952.
24. Viberg A, Westin IM, Golovleva I, Byström B. TCF4 trinucleotide repeat expansion in Swedish cases with Fuchs' endothelial corneal dystrophy. *Acta Ophthalmol*. 2022; 100 (5): 541–8. DOI: 10.1111/aos.15032. Epub 2021 Oct 13.
25. Foja S, Luther M, Hoffmann K, Rupprecht A, Gruenauer-Kloevekom C. CTG18.1 repeat expansion may reduce TCF4 gene expression in corneal endothelial cells of German patients with Fuchs' dystrophy. *Graefes Arch Clin Exp Ophthalmol*. 2017; 255 (8): 1621–31. DOI: 10.1007/s00417-017-3697-7. Epub 2017 Jun 12.
26. Kuot A, Hewitt AW, Snibson GR, Souzeau E, Mills R, Craig JE, et al. TGC repeat expansion in the TCF4 gene increases the risk of Fuchs' endothelial corneal dystrophy in Australian cases. *PLoS One*. 2017; 12 (8): e0183719. DOI: 10.1371/journal.pone.0183719.
27. Klein RJ, Zeiss C, Chew EY, Tsai JY, Sackler RS, Haynes C, et al. Complement factor H polymorphism in age-related macular degeneration. *Science*. 2005; 308 (5720): 385–9. DOI: 10.1126/science.1109557. Epub 2005 Mar 10.
28. Spencer KL, Hauser MA, Olson LM, Schmidt S, Scott WK, Gallins P, et al. Deletion of CFHR3 and CFHR1 genes in age-related macular degeneration. *Hum Mol Genet*. 2008; 17 (7): 971–7. DOI: 10.1093/hmg/ddm369. Epub 2007 Dec 15.
29. Baratz KH, Tosakulwong N, Ryu E, Brown WL, Branham K, Chen W, et al. E2-2 protein and Fuchs's corneal dystrophy. *N Engl J Med*. 2010; 363 (11): 1016–24. DOI: 10.1056/NEJMoa1007064. Epub 2010 Aug 25.

Литература

1. Uffelmann E, Huang QQ, Munung NS, De Vries J, Okada Y, Martin AR, et al. Genome-wide association studies. *Nature Reviews Methods Primers*. 2021; 1 (1): 59. Available from: <https://doi.org/10.1038/s43586-021-00056-9>.
2. Lewis CM, Vassos E. Polygenic risk scores: from research tools to clinical instruments. *Genome medicine*. 2020; 12 (1): 1–1. Available from: <https://doi.org/10.1186/s13073-020-00742-5>.
3. Stram DO. Multi-SNP haplotype analysis methods for association analysis. *Statistical Human Genetics: Methods and Protocols*. 2017: 485–504. Available from: https://doi.org/10.1007/978-1-4939-7274-6_24.
4. Twesigomwe D, Wright GE, Drögemöller BI, da Rocha J, Lombard Z, Hazelhurst S. A systematic comparison of pharmacogene star allele calling bioinformatics algorithms: a focus on CYP2D6 genotyping. *NPJ genomic medicine*. 2020; 5 (1): 30. Available from: <https://doi.org/10.1038/s41525-020-0135-2>.
5. Van Rheenen W, Van Der Spek RA, Bakker MK, Van Vugt JJ, Hop PJ, Zwamborn RA, et al. Common and rare variant association analyses in amyotrophic lateral sclerosis identify 15 risk loci with distinct genetic architectures and neuron-specific biology. *Nature genetics*. 2021; 53 (12): 1636–48.
6. Lee JM, Wheeler VC, Chao MJ, Vonsattel JP, Pinto RM, Lucente D, et al. Identification of genetic factors that modify clinical onset of Huntington's disease. *Cell*. 2015; 162 (3): 516–26.
7. Fautsch MP, Wieben ED, Baratz KH, Bhattacharyya N, Sadan AN, Hafford-Tear NJ, et al. TCF4-mediated Fuchs endothelial corneal dystrophy: Insights into a common trinucleotide repeat-associated disease. *Progress in retinal and eye research*. 2021; 81: 100883.
8. Biswas S, Munier FL, Yardley J, Hart-Holden N, Perveen R, Cousin P, et al. Missense mutations in COL8A2, the gene encoding the $\alpha 2$ chain of type VIII collagen, cause two forms of corneal endothelial dystrophy. *Human molecular genetics*. 2001; 10 (21): 2415–23.
9. Wieben ED, Aleff RA, Tosakulwong N, Butz ML, Highsmith WE, Edwards AO, et al. A common trinucleotide repeat expansion within the transcription factor 4 (TCF4, E2-2) gene predicts Fuchs corneal dystrophy. *PLoS One*. 2012; 7 (11): e49083.
10. Afshari NA, Igo Jr RP, Morris NJ, Stambolian D, Sharma S, Pulagam VL, et al. Genome-wide association study identifies three novel loci in Fuchs endothelial corneal dystrophy. *Nature communications*. 2017; 8 (1): 14898.
11. Chung DW, Frausto RF, Ann LB, Jang MS, Aldave AJ. Functional impact of ZEB1 mutations associated with posterior polymorphous and Fuchs' endothelial corneal dystrophies. *Investigative Ophthalmology & Visual Science*. 2014; 55 (10): 6159–66.
12. Chaurasia S, Ramappa M, Annapurna M, Kannabiran C. Coexistence of congenital hereditary endothelial dystrophy and Fuchs endothelial corneal dystrophy associated with SLC4A11 mutations in affected families. *Cornea*. 2020; 39 (3): 354–7.
13. Riazuddin SA, Vasanth S, Katsanis N, Gottsch JD. Mutations in AGBL1 cause dominant late-onset Fuchs corneal dystrophy and alter protein-protein interaction with TCF4. *The American Journal of Human Genetics*. 2013; 93 (4): 758–64.
14. Riazuddin SA, Parker DS, McGlumphy EJ, Oh EC, Iliff BW, Schmedt T, et al. Mutations in LOXHD1, a recessive-deafness locus, cause dominant late-onset Fuchs corneal dystrophy. *The American Journal of Human Genetics*. 2012; 90 (3): 533–9.
15. Skorodumova LO, Belodedova AV, Antonova OP, Sharova EI, Akopian TA, Selezneva OV, et al. CTG18.1 expansion is the best classifier of late-onset Fuchs' corneal dystrophy among 10 biomarkers in a cohort from the European part of Russia. *Investigative Ophthalmology & Visual Science*. 2018; 59 (11): 4748–54.
16. Louttit MD, Kopplin LJ, Igo Jr RP, Fondran JR, Tagliaferri A, Bardenstein D, et al. A multi-center study to map genes for Fuchs' endothelial corneal dystrophy: baseline characteristics and heritability. *Cornea*. 2012; 31 (1): 26.
17. Age-Related Eye Disease Study Research Group. The age-related eye disease study (AREDS): design implications AREDS report no. 1. *Controlled clinical trials*. 1999; 20 (6): 573.
18. Stambolian D, Wojciechowski R, Oexle K, Pirastu M, Li X, Raffel LJ, et al. Meta-analysis of genome-wide association studies in five cohorts reveals common variants in RBFOX1, a regulator of tissue-specific splicing, associated with refractive error. *Human molecular genetics*. 2013; 22 (13): 2754–64.
19. Krachmer JH, Purcell JJ Jr, Young CW, Bucher KD. Corneal endothelial dystrophy. A study of 64 families. *Arch Ophthalmol*. 1978; 96 (11): 2036–9. DOI: 10.1001/archophth.1978.03910060424004.
20. Chang CC, Chow CC, Tellier LC, Vattikuti S, Purcell SM, Lee JJ. Second-generation PLINK: rising to the challenge of larger and richer datasets. *Gigascience*. 2015; 4: 7. DOI: 10.1186/s13742-015-0047-8.
21. Jin Y, Schäffer AA, Sherry ST, Feolo M. Quickly identifying identical and closely related subjects in large databases using genotype data. *PLoS One*. 2017; 12 (6): e0179106. DOI: 10.1371/journal.pone.0179106.
22. Jin Y, Schaffer AA, Feolo M, Holmes JB, Kattman BL. GRAF-pop: A Fast Distance-Based Method To Infer Subject Ancestry from Multiple Genotype Datasets Without Principal Components Analysis. *G3 (Bethesda)*. 2019; 9 (8): 2447–61. DOI: 10.1534/g3.118.200925.
23. Okumura N, Hayashi R, Nakano M, Tashiro K, Yoshii K, Aleff R. et al. Association of rs613872 and Trinucleotide Repeat Expansion in the TCF4 Gene of German Patients With Fuchs Endothelial Corneal Dystrophy. *Cornea*. 2019; 38 (7): 799–805. DOI: 10.1097/ICO.0000000000001952.
24. Viberg A, Westin IM, Golovleva I, Byström B. TCF4 trinucleotide repeat expansion in Swedish cases with Fuchs' endothelial corneal dystrophy. *Acta Ophthalmol*. 2022; 100 (5): 541–8. DOI: 10.1111/aos.15032. Epub 2021 Oct 13.
25. Foja S, Luther M, Hoffmann K, Rupprecht A, Gruenauer-

- Kloevekorn C. CTG18.1 repeat expansion may reduce TCF4 gene expression in corneal endothelial cells of German patients with Fuchs' dystrophy. *Graefes Arch Clin Exp Ophthalmol*. 2017; 255 (8): 1621–31. DOI: 10.1007/s00417-017-3697-7. Epub 2017 Jun 12.
26. Kuot A, Hewitt AW, Snibson GR, Souzeau E, Mills R, Craig JE, et al. TGC repeat expansion in the TCF4 gene increases the risk of Fuchs' endothelial corneal dystrophy in Australian cases. *PLoS One*. 2017; 12 (8): e0183719. DOI: 10.1371/journal.pone.0183719.
 27. Klein RJ, Zeiss C, Chew EY, Tsai JY, Sackler RS, Haynes C, et al. Complement factor H polymorphism in age-related macular degeneration. *Science*. 2005; 308 (5720): 385–9. DOI: 10.1126/science.1109557. Epub 2005 Mar 10.
 28. Spencer KL, Hauser MA, Olson LM, Schmidt S, Scott WK, Gallins P, et al. Deletion of CFHR3 and CFHR1 genes in age-related macular degeneration. *Hum Mol Genet*. 2008; 17 (7): 971–7. DOI: 10.1093/hmg/ddm369. Epub 2007 Dec 15.
 29. Baratz KH, Tosakulwong N, Ryu E, Brown WL, Branham K, Chen W, et al. E2-2 protein and Fuchs's corneal dystrophy. *N Engl J Med*. 2010; 363 (11): 1016–24. DOI: 10.1056/NEJMoa1007064. Epub 2010 Aug 25.

SURVIVAL OF HUMAN CELLS IN TISSUE-ENGINEERED CONSTRUCTS STORED AT ROOM TEMPERATURE

Rogovaya OS¹✉, Alpeeva EV¹, Ruchko ES¹, Ereemeev AV^{1,2}, Vorotelyak EA¹¹ Koltzov Institute of Developmental Biology, Russian Academy of Sciences, Moscow, Russia² Lopukhin Federal Research and Clinical Center of Physical-Chemical Medicine of Federal Medical Biological Agency, Moscow, Russia

Tissue-engineered constructs (TECs), the dermal equivalent (DE) and the skin equivalent (SE), are allogenic equivalents of the skin and derm used to treat critical skin loss. Selection of storage conditions that contribute to longer shelf life, thereby expanding the possibilities of logistics and use, is one of the major issues related to the TECs development. The study was aimed to determine the shelf life of the DE and SE TECs stored in normal saline at room temperature by assessing morphology and viability of the cells on their surface, along with the levels of endothelial growth factor (VEGF) secreted by these cells. Using the MTT assay and staining with vital dye, we discovered the following: when TECs of both types were stored in normal saline, the cells viability and metabolic activity decreased by more than 50% by days 3–4 of storage. Furthermore, these decreased faster in DEs than in SEs. Morphology of the cells isolated from DEs and SEs after the 3-day storage remained unchanged. Mesenchymal stem cells on the surface of TECs kept producing VEGF after TECs culture medium was changed for saline solution (confirmed by immunofluorescence assay), which could indicate that the cells retained essential secretory activity.

Keywords: tissue-engineered construct, TEC, skin equivalent, mild hypothermia, keratinocytes, MSCs**Funding:** the study was supported by the Ministry of Science and Higher Education of the Russian Federation, Agreement № 075-15-2021-1063 of 28.09.2021.**Author contribution:** Rogovaya OS, Ereemeev AV — experimental procedure, data analysis; Alpeeva EV — data interpretation, literature review; Ruchko ES — experimental procedure; Vorotelyak EA — study planning.**Compliance with ethical standards:** the study was approved by the Ethics Committee of the Koltzov Institute of Developmental Biology, RAS (protocol № 51 of 09 September 2021) and conducted in accordance with the principles of the WMA Declaration of Helsinki and its subsequent revisions.✉ **Correspondence should be addressed:** Olga S. Rogovaya
Vavilova, 26, Moscow, 119334, Russia; rogovaya26f@yandex.ru**Received:** 16.12.2022 **Accepted:** 15.01.2023 **Published online:** 30.01.2023**DOI:** 10.24075/brsmu.2023.003

ВЫЖИВАЕМОСТЬ КЛЕТОК ЧЕЛОВЕКА В БИМЕДИЦИНСКИХ КЛЕТОЧНЫХ ПРОДУКТАХ ПРИ ХРАНЕНИИ ПРИ КОМНАТНОЙ ТЕМПЕРАТУРЕ

О. С. Роговая¹✉, Е. В. Алпеева¹, Е. С. Ручко¹, А. В. Еремеев^{1,2}, Е. А. Воротеяк¹¹ Институт биологии развития имени Н. К. Кольцова Российской академии наук, Москва, Россия² Федеральный научно-клинический центр физико-химической медицины имени Ю. М. Лопухина Федерального медико-биологического агентства, Москва, Россия

Биомедицинские клеточные продукты (БМКП) — дермальный эквивалент кожи (ДЭК) и биологический эквивалент кожи (БЭК) — это аллогенные эквиваленты дермы и кожи человека, применяемые для лечения в случаях критической потери кожи. Одним из важных вопросов разработки БМКП является подбор условий хранения, способствующих увеличению срока их годности для расширения возможностей логистики и использования. Целью исследования было определить срок годности ДЭК и БЭК путем оценки морфологии и жизнеспособности клеток в их составе и уровней секреции ими фактора роста эндотелия сосудов (VEGF) в процессе хранения в физиологическом растворе при комнатной температуре. Используя МТТ-тест и окраску витальным красителем, мы установили, что при хранении обоих видов БМКП в физиологическом растворе снижение жизнеспособности и метаболической активности клеток более чем на 50% происходило к 3–4 суткам хранения, причем в ДЭК быстрее, чем в БЭК. Морфология клеток, выделенных из ДЭК и БЭК после 3 суток хранения, оставалась неизменной. После помещения БМКП в физиологический раствор мезенхимные стволовые клетки в их составе продолжали синтезировать VEGF (показано методом ИФА), что может свидетельствовать о сохранении ими необходимой секреторной активности.

Ключевые слова: биомедицинский клеточный продукт, БМКП, эквивалент кожи, умеренная гипотермия, кератиноциты, МСК**Финансирование:** исследование поддержано Министерством науки и высшего образования Российской Федерации, Соглашение № 075-15-2021-1063 от 28.09.2021.**Вклад авторов:** О. С. Роговая, А. В. Еремеев — проведение экспериментов, анализ данных; Е. В. Алпеева — интерпретация данных, анализ литературы; Е. С. Ручко — проведение экспериментов; Е. А. Воротеяк — планирование исследования.**Соблюдение этических стандартов:** исследование одобрено этическим комитетом ИБР РАН (протокол № 51 от 09 сентября 2021 г.), проведено с соблюдением принципов Хельсинкской декларации ВМА и ее последующих пересмотров.✉ **Для корреспонденции:** Ольга Сергеевна Роговая
ул. Вавилова, д. 26, г. Москва, 119334, Россия; rogovaya26f@yandex.ru**Статья получена:** 16.12.2022 **Статья принята к печати:** 15.01.2023 **Опубликована онлайн:** 30.01.2023**DOI:** 10.24075/vrgmu.2023.003

Tissue-engineered constructs (TECs) assessed in this study, the dermal equivalent (DE) and the skin equivalent (SE), are three-dimensional equivalents of the skin and derm that comprise living cells cultured on the surface of biocompatible matrices. One of the TEC disadvantages is the low survival rate of the cellular component when frozen and its short shelf life at positive temperatures, which limit TEC logistics and use. To introduce TECs into a wide clinical practice, it is necessary

to find a balance when the cell-based product would not require storage conditions that are difficult to maintain but simultaneously would meet such criteria as functional activity and sufficiently high viability of the cellular component by the moment of transplantation. Developing the reliable method for TEC storage without using xenobiotics would facilitate their widespread integration into clinical practice. Furthermore, an adequate shelf life of the ready-to-use cell-based products

would provide enhanced capabilities for quality control before usage [1].

While successful preservation of the frozen plain TECs has been reported, viability of the cellular component of the cell- and matrix-based 3D systems after thawing usually does not exceed 50% [2–4]. Such viability scores are insufficient to achieve optimal therapeutic outcome. At the same time, there is evidence of successful full-thickness skin graft storage in simple saline solutions at low positive temperatures [5, 6].

These data combined with the need to use complex freezing/thawing modes, specialized equipment, and methods for TEC cleaning of cryopreservation media before usage suggest that the development of the protocol for TEC storage at positive temperatures by the moment of transplantation is promising.

It is known that the range of positive temperatures enabling preservation of cells without significant loss of vitality is +4–+37 °C, while the viability rates at +5 and +25 °C are different. Thus, the cold-induced injury occurs in rat hepatocytes at a temperature below +16 °C, and the injury reaches its maximum at +4–+8 °C [7]. As has been previously demonstrated, human cells can retain 90% viability when stored in isotonic solutions at low positive temperatures for 30 h [8]. There is evidence that adipose tissue-derived mesenchymal stem cells (AT-MSCs) retain all their properties when stored in saline solutions at room temperature [9]. The method for the MSC-based transplant storage under mild hypothermic conditions being an alternative strategy for short-term graft preservation has also been proposed. The authors have earlier shown that the viability of MSCs as a component of TECs is significantly higher at +25 °C than at +4 °C [10].

In view of the above, the sample storage temperature of +22 °C was chosen for this study. The TECs (DE and SE) stability was assessed throughout three-day storage based on the following properties: sample integrity and color; volume, color, and clarity of the liquid in the dish containing the sample; sterility of the sample; the number of viable cells in the sample, metabolic and secretory activity of these cells. The DE TEC was constructed using the biocompatible matrix containing hyaluronic acid and type I collagen and the cellular component (AT-MSCs). The SE TEC was constructed using the biocompatible matrix containing hyaluronic acid and type I collagen and the cellular component (AT-MSCs and skin keratinocytes). The study was aimed to determine the shelf life of the ready-to-use DE and SE TECs stored at room temperature consistent with the criterion of preserving secretory activity and high viability of their cell component.

METHODS

The study was performed in the laboratory conditions. All the procedures involving cell growth and cell culture transfer to biopolymer matrices were performed under aseptic conditions.

TEC engineering and storage

TECs were constructed using human cells obtained from the Cell Culture Collections for Biotechnological and Biomedical Research (Koltzov Institute of Developmental Biology, RAS, Moscow, Russia). AT-MSCs and keratinocytes had been isolated from the skin biopsies of healthy adult donors (40–70 years of age).

The G-DERM, histoequivalent-bioplasmic material (G-Group; Russia) made of hyaluronic acid and type I collagen, was used as a matrix for cell growth when culturing TECs.

Thawing and culturing cells

The cryotubes containing cells (1×10^6 cells per a tube) were retrieved from the cryogenic storage tanks, thawed at +37 °C, and centrifuged at 200 g. After that the supernatant was removed, and the cellular precipitate was resuspended in the culture medium and transferred to the T25 culture flasks (SPL; Korea).

The α -MEM culture medium (PanEco; Russia) supplemented with 10% fetal bovine serum (FBS)(Hyclon; USA), 1% Glutamax (Gibco; USA), and 1% PenStrep (Gibco; USA) was used for AT-MSCs. Cells were incubated in the CO₂ incubator set to +37 °C, 5% CO₂, and high humidity. The culture medium was changed completely every two days. The cells were passaged after reaching 80% confluence. Passaging was performed in accordance with the following scheme: the culture medium was withdrawn, the cells were washed once with the Versene solution (PanEco; Russia), then 800 μ L of the 0.05% trypsin solution (Gibco; USA) were added to the flask and incubated at +37 °C for 5–10 min until the cells became round and detached from the bottom. Trypsin was inhibited by the culture medium. The acquired cell suspension was pipetted and subcultured into new flasks at a 1 : 3 ratio.

The DMEM/F12 culture medium (PanEco; Russia) supplemented with 10% FBS (Hyclon; USA), 10 ng/mL of epidermal growth factor (EGF) (Sigma; USA), 1% Glutamax (Gibco; USA), 1% PenStrep (Gibco; USA), and 1% ITS (Gibco; USA) was used for keratinocytes. The cells were cultured the same way as AT-MSCs.

Construction of the DE and SE TECs

Biocompatible matrix for TECs was prepared as follows: a piece of the G-DERM dry sheet sized 6 × 6 cm was cut and placed into a Petri dish with a diameter of 10 cm, then 10 mL of culture medium was added to the Petri dish, and the sheet was left in the medium for 2 h to swell.

For DEs fabrication AT-MSCs were passaged 6–8 times. The cells were removed from the culture flasks using the Versene solution and trypsin as described above and centrifuged at 300 g. The cellular precipitate was resuspended in the culture medium for AT-MSCs to obtain a concentration of 3×10^5 cells/mL. The suspension containing AT-MSCs was applied on the well-prepared biocompatible matrix, 3 mL of cellular suspension per one DE. Two hours after cell seeding the volume of the medium in the dish containing the matrix was adjusted to 10 mL, and the equivalent obtained was incubated in the CO₂ incubator for three days.

Cells of two types were used to prepare SEs: AT-MSCs were passaged 6–8 times, and keratinocytes were passaged 1–2 times before the procedure. At the first stage, AT-MSCs were plated on the matrix as described above. Two hours after seeding AT-MSCs, the second layer of cells (keratinocytes) was applied on the matrix. To do this, keratinocytes were removed from the culture flask and centrifuged at 300 g. The cellular precipitate was resuspended in the culture medium for keratinocytes. The cellular suspension was poured into the Petri dish containing the previously prepared matrix with AT-MSCs based on the ratio of 1×10^5 cells/cm². After that the TEC was incubated in the CO₂ incubator for three days.

TEC storage

The culture medium was removed from the Petri dishes containing DEs and SEs, and they were washed twice with

DPBS (PanEco; Russia). After that, 10 mL of sterile saline were added to each dish containing TEC, and the dishes were packed in vacuum bags. The ready-to-use TECs obtained by this method were stored in a thermostat at a temperature of +22 °C for five days. Several samples were withdrawn for analysis every day.

Visual assessment of sample quality after storage

Sample integrity and color change, volume, color, and clarity of the liquid in the dish containing the sample, and the sample sterility were assessed after the sample withdrawal from storage prior to further analysis of the cellular component in the following way. After the packages containing samples were transferred to the laminar flow hood, where the secondary packaging (vacuum bag) was removed, the Petri dish was opened, the saline used for sample storage was collected, the liquid volume was measured, and liquid was transferred to the new dish. The saline was inspected using the IX73 inverted microscope equipped with the DP74 camera (Olympus; Japan) at 200× and 400× magnification to reveal the traces of contamination. The sample was examined and tested for integrity using tweezers. Then assessment of the cellular component viability and functional activity was performed.

Assessment of the cells ability to adhere and form cell cultures after being part of a TEC

After storage, cells were isolated from TECs in the following way. The samples were washed with the Versene solution (PanEco; Russia), then treated with 3 mL of the 0.25% trypsin solution (PanEco; Russia) and left for 10 min at +37 °C with intense shaking for fermentation. After that trypsin was inhibited by the equal volume of culture medium supplemented with 10% FBS and pipetted in order to wash as much cells away from the matrix surface as possible. Then the obtained suspension was centrifuged for 5 min at 200 g. Supernatant was removed, while the precipitate was resuspended in the culture medium and plated on the cell culture Petri dishes. A day later, the cells were examined and imaged using the IX73 inverted microscope equipped with the DP74 camera (Olympus; Japan).

Assessment of metabolic activity of the cells on the surface of TECs using MTT assay

To estimate metabolic activity at every time point of storage, TECs were taken out of the packages, cut into fragments sized 1 × 1 cm, and put into separate wells of the 24-well plate. Then MTT reagent (Sigma-Aldrich; USA) was added to the wells to reach the final concentration of 30 µg/mL and incubated for 2.5 h. After incubation, the medium was collected, and 180 µL of DMSO (PanEco; Russia) were added to each well. The plate was placed on the shaker. After 1 min the stained solution was collected and put into the wells of the 96-well plate (60 µL per well) for optical density measurement. Optical density of the solution was measured using the Stat Fax 2100 photometer (Awareness Technology; USA) at the wavelength of 530 nm.

Identification of viable cells on the surface of TECs

To identify viable and dead cells on the surface of TECs withdrawn from storage, the samples were stained using the Calcein AM vital intercalating dye (1 µM) (Sigma; USA) in accordance with the manufacturer's guidelines. TECs were

stained in the CO₂ incubator (+37 °C, 5% CO₂) for 30 min. The staining method is based on the activity of intracellular esterases present in living cells only. These esterases cleave the dye, thereby making it emit fluorescence in the green spectral region. No fluorescence is detected in the dead cells. The stained samples were examined and imaged using the IX73 inverted microscope equipped with the DP74 camera (Olympus; Japan). The protocol of the Image J software (LOCI, University of Wisconsin; USA) with the open-source plugin [11], which calculated the share of regions stained with calcein in the field of view, was used to define the percentage of living cells in TECs. The values were obtained via three repetitions of the experiment, and the data calculated by assessing original TEC samples cultured in the CO₂ incubator for three days were taken as 100%.

Assessment of the TEC secretory activity by determination of VEGF levels in the conditioned medium by immunofluorescence assay

The samples of normal saline used for TEC sample storage were collected daily throughout the three-day storage in the following way. Packages containing samples were transferred to the laminar flow hood, where the secondary packaging (vacuum bag) was opened, and 100 µL of the liquid were collected from each dish containing TEC under sterile conditions. After sample collection, the dishes were sealed again and moved into the thermostat for further storage. Original TEC samples in the culture medium and AT-MSCs (of the same cell line and passage as the cells of the studied TECs), which were seeded in the wells of the 24-well plate and cultured utilizing standard method, were used as a control. To provide the control, the growth medium samples were collected before the beginning of the study along with the samples of the medium used for incubation of the matrix alone during the same period. The VEGF-EIA-BEST (A-8784) kit (Vector-Best; Russia) was used for the assessment.

The analysis was performed in accordance with the manufacturer's instructions. Spectrophotometric analysis of the samples was performed at the wavelength of 450 nm using the xMark Microplate Absorbance Spectrophotometer (Bio-Rad; USA).

We calculated mean optical density (OD) values for the well pairs and plotted a calibration curve of OD as a function of VEGF concentration (IU/mL) using linear coordinates. The curve was used to define the concentrations of the control and test samples in IU/mL in accordance with the guidelines issued by the manufacturer of the kit. The results were taken into account when the value for the control sample calculated based on the calibration curve matched the value specified on the label of the flask in the kit.

Statistical analysis

All the experiments with TECs were performed in three biological replicates; each individual experiment — at least in three technical replicates. After obtaining the values in the experiments involving calculation of the share of viable cells and when assessing the MTT assay results, the values were normalized to the data obtained when assessing intact samples before the beginning of the experiment. The mean and mean standard deviation were calculated in Microsoft Excel (Microsoft Corporation; USA).

Significance of differences in the groups was tested by ANOVA using the Prism 8 (GraphPad Software).

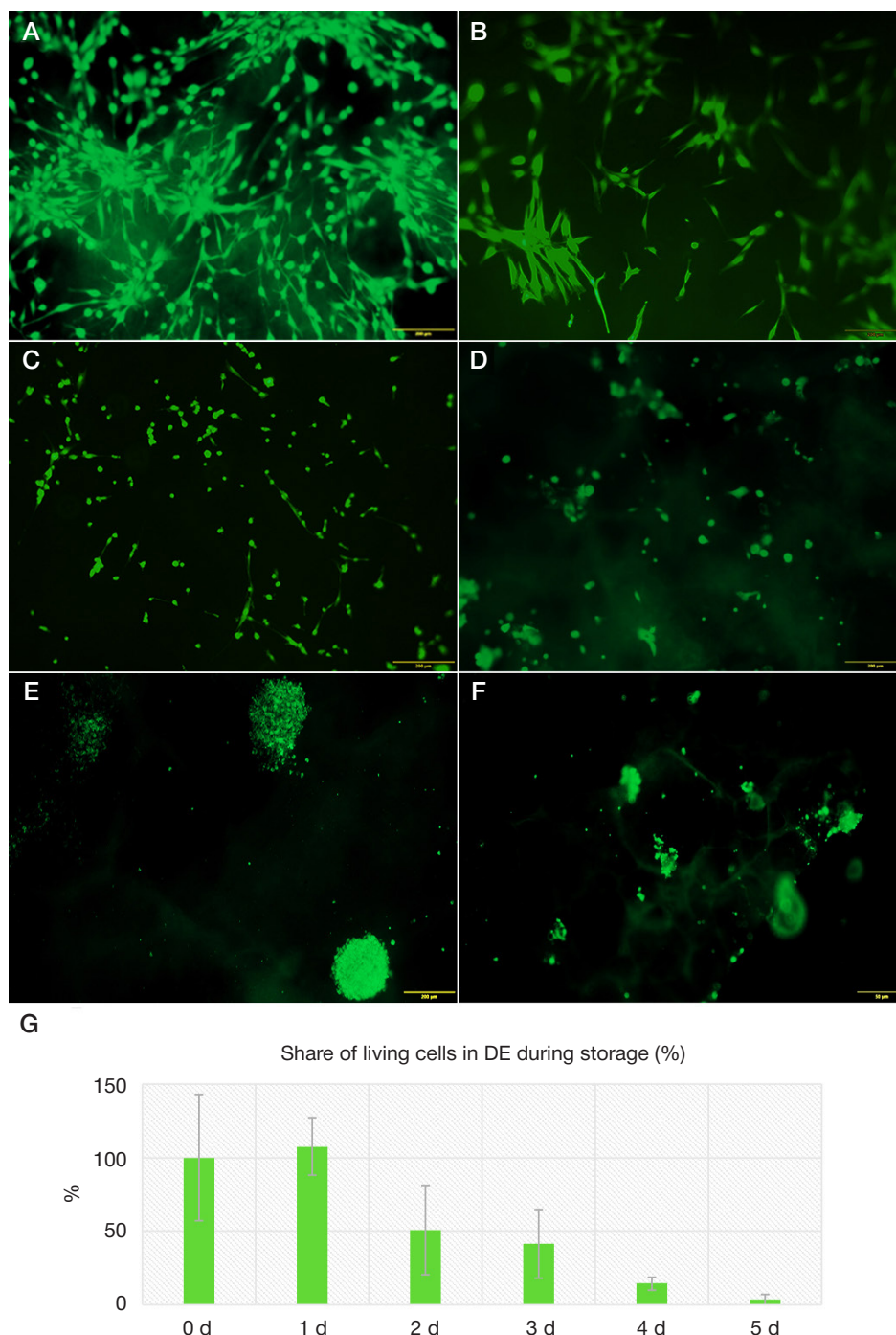


Fig. 1. Identification of living cells stained with the calcein vital dye (green stain) on the matrix surface in the DE TEC at various stages of storage at a temperature of +22 °C (A–F): at the beginning of the experiment (no storage, zero day) (A), day one (B), day two (C), day three (D), day four (E), and day five (F) of storage. G. The graph showing the percentage of living cells in the DE TEC as a function of the sample condition on the zero day of storage. The data are presented as the mean share of green pixels in three fields of view for three technical repetitions, error bars \pm SD (%)

RESULTS

All the samples seemed to be preserved after removing the secondary packaging when withdrawing from storage: the normal saline in which the TECs had been stored remained clear, no volume reduction or contamination by microorganisms was revealed. The samples remained unimpaired and retained their original pinkish-beige color throughout the study.

Viability of the cells in the cultured and packed ready-to-use TECs that were stored at +22 °C was assessed by two methods: by staining with the calcein vital dye and by MTT assay.

The results of the experiment showed that the number of living cells decreased faster in the DE TECs. By the second

day, a two-fold decrease in the number of calcein-positive cells was observed in the DE (Fig. 1), while in the SE no decrease was revealed (Fig. 2). Furthermore, the AT-MSC morphology alterations were observed in equivalents of both types on day three: the cells that were normally spindle-shaped became less elongated, several cells started to detach from the surface of the matrix. The critical decrease in the number of living cells in both TECs, to 14% in DE and to 22.3% in SE (the confirmed significance for both TEC types (p -value) ≤ 0.005), was detected on day four of storage (Fig. 1, 2).

The second method we had selected to assess the state of the TEC cellular component involved measuring the intensity of the formazan crystal formation in the cell environment when

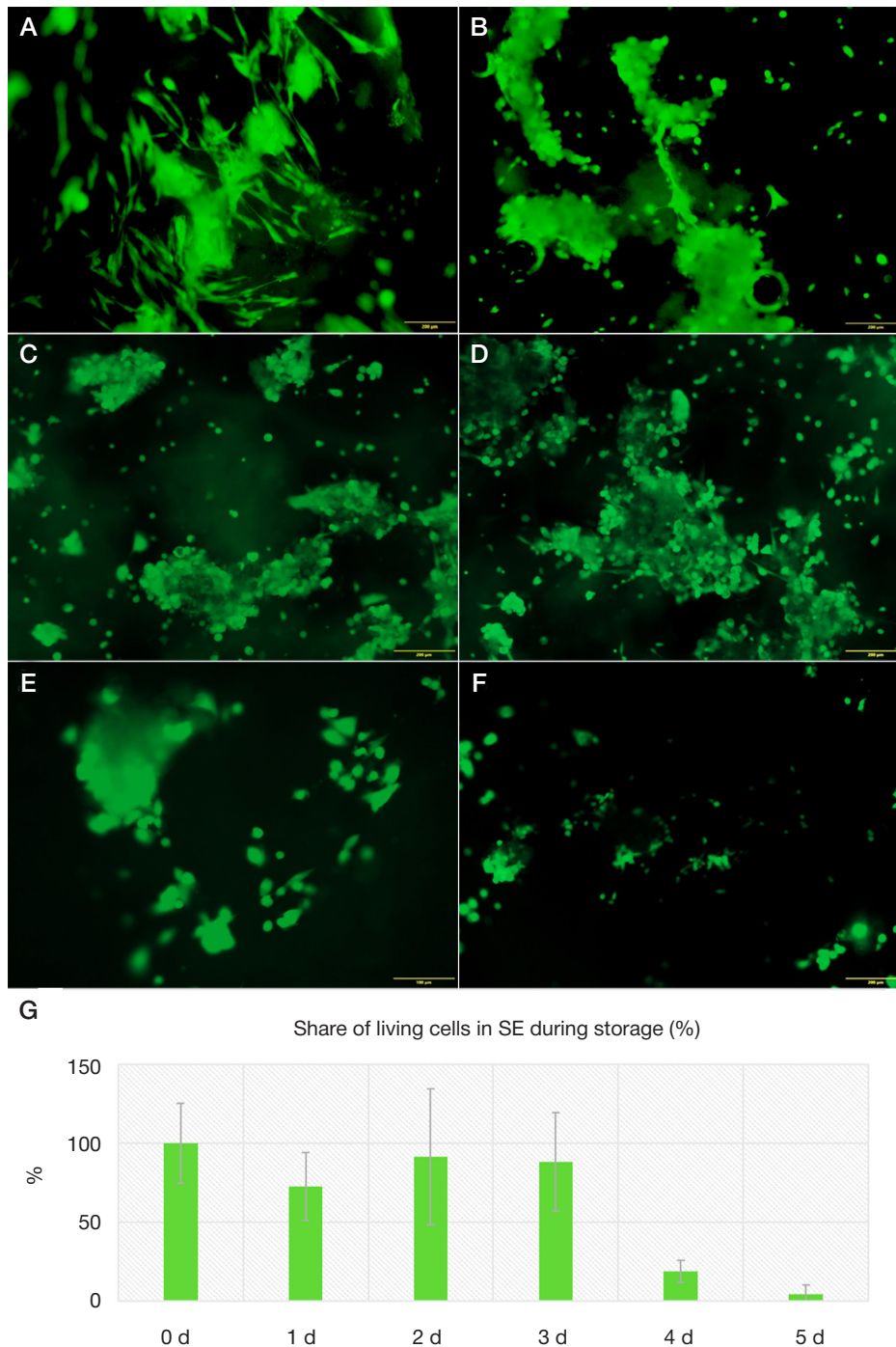


Fig. 2. Identification of living cells stained with the calcein vital dye (green stain) on the matrix surface in the SE TEC at various stages of storage at a temperature of +22 °C (A–F): at the beginning of the experiment (no storage, zero day) (A), day one (B), day two (C), day three (D), day four (E), and day five (F) of storage. G. The graph showing the percentage of living cells in the SE TEC as a function of the sample condition on the zero day of storage. The data are presented as the mean share of green pixels in three fields of view for three technical repetitions, error bars \pm SD (%)

exposed to the cell metabolites that correlated with the metabolic rate of the cells, which was considered reflecting cell viability. This test has shown that cell metabolic activity decreases faster in DE than in SE, since metabolic activity reduction to 44.6% compared to the beginning of the storage has been revealed in DE ($p \leq 0.005$), while in SE it has been still at 79.1% by day three (the difference from the baseline value at this stage was non-significant). Only 18% of the cell baseline metabolic activity was observed in DE by day five, while in SE metabolic activity significantly decreased to 33.7% ($p \leq 0.005$) (Fig. 3A, B).

When assessing concentration of VEGF secreted by cells into the normal saline used for sample storage, VEGF was

revealed in all samples. The levels of this factor in the storage solution decreased slightly by day three (Fig. 3C, D). Thus, about 506 ± 136 IU/mL of VEGF were revealed in the samples of the solution used for storage of DEs in the first day, while there were 493 ± 136 IU/mL by day three (the difference was non-significant); 1583.333 ± 189 IU/mL and 1733 ± 208 IU/mL were revealed in the samples of the solution used for storage of SEs at the same stages, respectively (the difference was non-significant).

The cellular component was isolated from TEC on day three. As previously described, cells of only one type, AT-MSCs, were used to create DEs, while cells of two types, AT-MSCs

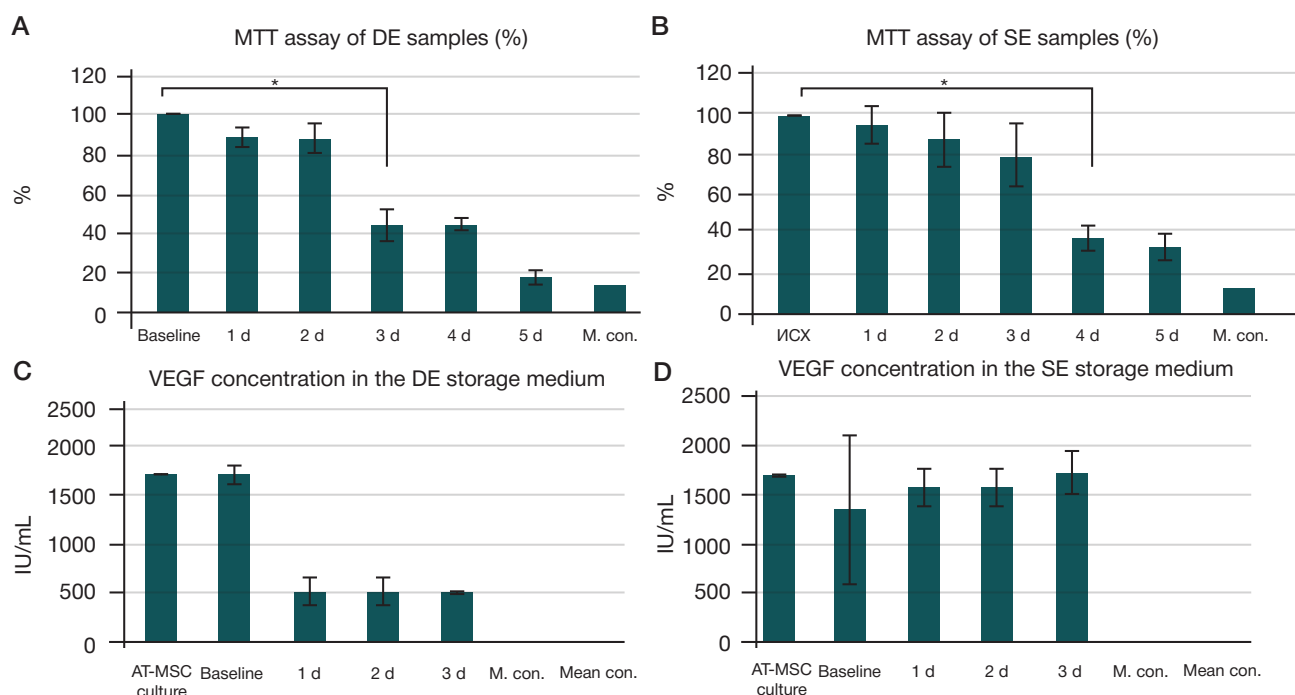


Fig. 3. The changes in the cells' mitochondrial activity assessed by MTT assay in the DE (A) and SE (B) TECs and presented as mean optical density values obtained at various stages of storage vs. data obtained before storage (zero day), percentage obtained in three technical repetitions, error bars \pm SD (%). Significance of the metabolic activity decline observed on day three in DEs and day four in SEs is calculated by ANOVA ($p \leq 0.005$). The data on the VEGF levels in the normal saline used for the DE (C) and SE (D) TEC sample storage measured by enzyme immunoassay are presented as mean optical density for nine repetitions, error bars \pm SD (%). Matrix with no cells, culture medium, and original AT-MSC culture used to construct TECs were used as controls. There were no significant differences between the normal saline samples in the storage groups within three days

and keratinocytes, were used to create SEs, that is why the cells isolated from DEs and SEs were different in morphology and number. All the isolated cells showed normal ability to adhere. These cells quickly attached to the bottom of the cell culture dish, spread, acquired standard morphology (Fig. 4A, C), and retained it throughout the observation period (up to four days) (Fig. 4B, D). Visual inspection showed that the number of attaching AT-MSCs isolated from SEs was significantly higher than that of AT-MSCs isolated from DEs (Fig. 4).

DISCUSSION

The study was focused on the defining the storage duration at room temperature of the DEs and SEs created in our library, when their cellular components retain functioning and viability. Our previous studies (unpublished data) showed that TEC freezing at -70°C and -20°C using various cryoprotectants (DMSO, glycerol), specialized freezing media for sensitive cell lines, such as Bambanker (Lymphotec; Japan), and for multicellular objects, such as Cryoderm (PanEco; Russia), resulted in the loss of cell viability after thawing. A significant decrease in the TEC cell viability within 24 h was also reported at a temperature of $+4^\circ\text{C}$. According to the literature, specialized commercially available culture media (such as Synth-a-Freeze) are often used to freeze TECs, and the freezing/thawing protocols are carefully developed [4, 12, 13]. This complicates and increases the cost of TEC storage and logistics. As noted by our colleagues from the Privolzhsky Research Medical University in their review focused on cryopreservation of MSCs and TECs, there is little research on cryopreservation of the cell-based 3D structures and TECs, and there is no the whole picture of the mechanisms underlying freezing of such products [14]. The conditions are developed specifically for each product, and TEC cryopreservation method was designed initially for longer storage. According to global practice, bioengineered tissue

constructs are delivered on ice "just-in-time". The exceptions include the FDA-approved commercially available tissue-engineered Dermagraft and Apligraf, which are stored and shipped at -75°C and $+20$ – $+23^\circ\text{C}$, respectively [15]. Thus, the task of developing the conditions for the short-term storage of tissue-engineered constructs is quite important. The literature analysis has shown that the solution is usually found out for each variant of the product.

Our study was aimed to determine the possibility of the DE and SE TEC storage under the most technically feasible conditions: without the use of any expensive imported reagents, accessory equipment or specific thermal modes. Furthermore, storage in the sterile saline, which represents an approved medicinal product, simplifies TEC preparation for use, since there is no need to wash TECs from saline before transplantation to a patient.

We managed to show that DEs and SEs generally retained their main quality parameters after three days of storage under most simple conditions (room temperature and normal saline). Furthermore, SEs showed better results compared to DEs. The higher cell survival rate in SEs is probably due to the presence of two cell types that have a beneficial effect on the viability of each other. After assessing the rate of viability decline in the studied samples we concluded that storage for more than three days under the current conditions resulted in the reduction of the viable cell number by more than 50% in TECs of both types. Consequently, we did not examine the samples stored for more than 72 h in further research.

As the expected therapeutic effects of the DE and SE TECs include not only mechanical skin wound closure, but also the wound healing regenerative effect, the cellular component secretory activity is an important indicator of the TEC quality. Mesenchymal cells, such as MSCs, are known to play a key role in regulation of the cell-cell interaction and maintaining tissue homeostasis [16]. The AT-MSCs can stimulate angiogenesis

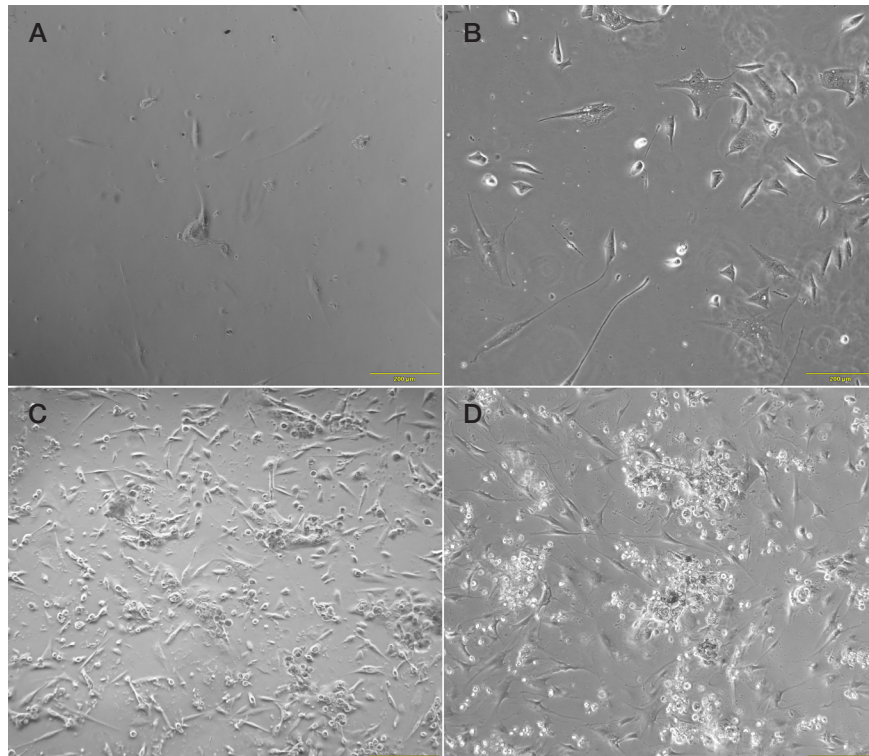


Fig. 4. The culture of cells extracted from DE (A, B) and SE (C, D) TECs after 72 h of storage. Cells after one day (A, C) and three days (B, D) after extraction (light microscopy, phase contrast)

via activation of blood vessel growth and stabilization of the growing vessels [17]. Growth factors of the VEGF family produced by these cells can induce directed cell migration, proliferation, and differentiation of endothelial cells in the region of the defect via interaction with their VEGF-R receptors, which is reflected in the reduced defect area, the increased number of blood vessels, and higher blood vessel density [9]. Normally, the cultured cells of TECs actively secrete growth factors, such as VEGF. In our experiment, VEGF levels in the culture medium were 1600–2000 IU/mL or higher. Furthermore, we showed that AT-MSCs in TECs we had constructed kept producing VEGF in the normal saline, and the VEGF secretion levels were comparable with its levels in the culture medium used for incubation of TECs before packaging and storage.

The results of the experiment that involved measuring VEGF concentrations for SE and DE suggest that keratinocytes contribute to the AT-MSCs survival and promote VEGF secretion by them.

CONCLUSIONS

When the SE TEC is stored under mild hypothermia conditions at room temperature (+22 °C), its cellular component viability remains at the level over 50% of the value obtained at the beginning of the three-day storage. Viability of the DE TEC cellular component decreases faster: the values that do not exceed 50% of the baseline value are observed by day three. The demonstrated ability of AT-MSCs on the surface of TECs to secrete VEGF when stored under selected conditions can be an indicator of paracrine activity exerted by these TECs that can play a therapeutic role in treatment of skin wounds of different etiology and can be considered an indirect sign of the cell functional activity in the ready-to-use product. The SE cellular component viability and metabolic activity during storage are significantly higher than that of DE. These findings are essential to accelerate implementation of the tissue engineering and regenerative medicine methods into clinical practice.

References

1. Utheim TP, Raeder S, Utheim OA, de la Paz M, Roald B, et al. Sterility control and long-term eye-bank storage of cultured human limbal epithelial cells for transplantation. *Br J Ophthalmol*. 2003; 93: 980–3. DOI: 10.1136/bjo.2008.149591.
2. Mutsenko VV, Rogulska OY, Petrenko YA, Ehrlich H, Mazur SP, et al. Cryosensitivity of Mesenchymal Stromal Cells Cryopreserved Within Marine Sponge Ianthella basta Skeleton-Based Carriers. *Probl Cryobiol Cryomedicine*. 2016; 26: 13–23. DOI: 10.15407/cryo26.01.013.
3. Petrenko Y, Petrenko A, Martin I, Wendt D. Perfusion bioreactor-based cryopreservation of 3D human mesenchymal stromal cell tissue grafts. *Cryobiology*. 2017; 76: 150–3. DOI: 10.1016/j.cryobiol.2017.04.001.
4. Arutyunyan I, Elchaninov A, Sukhikh G, Fatkhudinov T. Cryopreservation of Tissue-Engineered Scaffold-Based Constructs: From Concept to Reality. *Stem Cell Rev Rep*. 2022; 18: 1234–52. DOI: 10.1007/s12015-021-10299-4.
5. Knapik A, Kornmann K, Kerl K, Calcagni M, Contaldo C, et al. Practice of split-thickness skin graft storage and histological assessment of tissue quality. *J Plast Reconstr Aesthet Surg*. 2013; 66: 827–34. DOI: 10.1016/j.bjps.2013.02.003.
6. Ge L, Sun L, Chen J, Mao X, Kong Y, et al. The viability change of pigskin in vitro. *Burns*. 2010; 36: 533–8. DOI: 10.1016/j.burns.2009.08.001.
7. Rauen U, Kerkweg U, de Groot H. Iron-dependent vs. iron-independent cold-induced injury to cultured rat hepatocytes: a comparative study in physiological media and organ preservation solutions. *Cryobiology*. 2007; 54 (1): 77–86. DOI: 10.1016/j.

- cryobiol.2006.11.008.
8. Rogovaya OS, Petrakova OS, Gvazava IG, Borisov MA, Vasil'ev AV. Issledovanie zhiznesposobnosti kul'tiviruemykh kletok cheloveka v suspenzii. Vestnik Moskovskogo universiteta. Seriya 16: biologiya. 2016; 3: 44–48.
 9. Fujita Ya, Nishimura M, Komori NW, Wada T, Shirakawa Ch, et al. A pair of cell preservation solutions for therapy with human adipose tissue-derived mesenchymal stromal cells. Regen Ther. 2020; 14: 95–102. DOI: 10.1016/j.reth.2019.10.004.
 10. Vackova I, Vavrinova E, Musilkova J, Havlas V, Petrenko Y. Hypothermic Storage of 3D Cultured Multipotent Mesenchymal Stromal Cells for Regenerative Medicine Applications. Polymers (Basel). 2022; 14 (13): 2553. DOI: 10.3390/polym14132553.
 11. Schulze K, López DA, Tillich UM, Frohme M. A simple viability analysis for unicellular cyanobacteria using a new autofluorescence assay, automated microscopy, and Image J. BMC Biotechnol. 2011; 11: 118. DOI: 10.1186/1472-6750-11-118.
 12. Tam E, McGrath M, Sladkova M, AlManaie A, Alostaad A, de Peppo GM. Hypothermic and cryogenic preservation of tissue-engineered human bone. Ann NY Acad Sci. 2020; 1460 (1): 77–87. DOI: 10.1111/nyas.14264.
 13. Sampaio-Pinto V, Janssen J, Chirico N, Serra M, Alves PM, et al. Roadmap to Cardiac Tissue-Engineered Construct Preservation: Insights from Cells, Tissues, and Organs. Adv Mater. 2021; 33 (27): e2008517. DOI: 10.1002/adma.202008517.
 14. Linkova DD, Rubtsova YP, Egorikhina MN. Cryostorage of Mesenchymal Stem Cells and Biomedical Cell-Based Products. Cells. 2022; 11 (17): 2691. DOI: 10.3390/cells11172691.
 15. Criswell T, Swart C, Stoudemire J, Brockbank K, Floren M, Eaker S, Hunsberger J. Shipping and Logistics Considerations for Regenerative Medicine Therapies. Stem Cells Transl Med. 2022; 11 (2): 107–13. DOI: 10.1093/stcltm/szab025.
 16. Jing D, Li C, Yao K, Xie X, Wang P, et al. The vital role of Gli1+ mesenchymal stem cells in tissue development and homeostasis. J Cell Physiol. 2021; 236 (9): 6077–89. DOI: 10.1002/jcp.30310.
 17. Krawczenko A, Klimczak A. Adipose Tissue-Derived Mesenchymal Stem/Stromal Cells and Their Contribution to Angiogenic Processes in Tissue Regeneration. Int J Mol Sci. 2022; 23 (5): 2425. DOI: 10.3390/ijms23052425.

Литература

1. Utheim TP, Raeder S, Utheim OA, de la Paz M, Roald B, et al. Sterility control and long-term eye-bank storage of cultured human limbal epithelial cells for transplantation. Br J Ophthalmol. 2003; 93: 980–3. DOI: 10.1136/bjo.2008.149591.
2. Mutsenko VV, Rogulska OY, Petrenko YA, Ehrlich H, Mazur SP, et al. Cryosensitivity of Mesenchymal Stromal Cells Cryopreserved Within Marine Sponge Ianthella basta Skeleton-Based Carriers. Probl Cryobiol Cryomedicine. 2016; 26: 13–23. DOI: 10.15407/cryo26.01.013.
3. Petrenko Y, Petrenko A, Martin I, Wendt D. Perfusion bioreactor-based cryopreservation of 3D human mesenchymal stromal cell tissue grafts. Cryobiology. 2017; 76: 150–3. DOI: 10.1016/j.cryobiol.2017.04.001.
4. Arutyunyan I, Elchaninov A, Sukhikh G, Fatkhudinov T. Cryopreservation of Tissue-Engineered Scaffold-Based Constructs: From Concept to Reality. Stem Cell Rev Rep. 2022; 18: 1234–52. DOI: 10.1007/s12015-021-10299-4.
5. Knapik A, Kornmann K, Kerl K, Calcagni M, Contaldo C, et al. Practice of split-thickness skin graft storage and histological assessment of tissue quality. J Plast Reconstr Aesthet Surg. 2013; 66: 827–34. DOI: 10.1016/j.bjps.2013.02.003.
6. Ge L, Sun L, Chen J, Mao X, Kong Y, et al. The viability change of pigskin in vitro. Burns. 2010; 36: 533–8. DOI: 10.1016/j.burns.2009.08.001.
7. Rauen U, Kerkweg U, de Groot H. Iron-dependent vs. iron-independent cold-induced injury to cultured rat hepatocytes: a comparative study in physiological media and organ preservation solutions. Cryobiology. 2007; 54 (1): 77–86. DOI: 10.1016/j.cryobiol.2006.11.008.
8. Роговая О. С., Петракова О. С., Гвазава И. Г., Борисов М. А., Васильев А. В. Исследование жизнеспособности культивируемых клеток человека в суспензии. Вестник Московского университета. Серия 16: биология. 2016; 3: 44–48.
9. Fujita Ya, Nishimura M, Komori NW, Wada T, Shirakawa Ch, et al. A pair of cell preservation solutions for therapy with human adipose tissue-derived mesenchymal stromal cells. Regen Ther. 2020; 14: 95–102. DOI: 10.1016/j.reth.2019.10.004.
10. Vackova I, Vavrinova E, Musilkova J, Havlas V, Petrenko Y. Hypothermic Storage of 3D Cultured Multipotent Mesenchymal Stromal Cells for Regenerative Medicine Applications. Polymers (Basel). 2022; 14 (13): 2553. DOI: 10.3390/polym14132553.
11. Schulze K, López DA, Tillich UM, Frohme M. A simple viability analysis for unicellular cyanobacteria using a new autofluorescence assay, automated microscopy, and Image J. BMC Biotechnol. 2011; 11: 118. DOI: 10.1186/1472-6750-11-118.
12. Tam E, McGrath M, Sladkova M, AlManaie A, Alostaad A, de Peppo GM. Hypothermic and cryogenic preservation of tissue-engineered human bone. Ann NY Acad Sci. 2020; 1460 (1): 77–87. DOI: 10.1111/nyas.14264.
13. Sampaio-Pinto V, Janssen J, Chirico N, Serra M, Alves PM, et al. Roadmap to Cardiac Tissue-Engineered Construct Preservation: Insights from Cells, Tissues, and Organs. Adv Mater. 2021; 33 (27): e2008517. DOI: 10.1002/adma.202008517.
14. Linkova DD, Rubtsova YP, Egorikhina MN. Cryostorage of Mesenchymal Stem Cells and Biomedical Cell-Based Products. Cells. 2022; 11 (17): 2691. DOI: 10.3390/cells11172691.
15. Criswell T, Swart C, Stoudemire J, Brockbank K, Floren M, Eaker S, Hunsberger J. Shipping and Logistics Considerations for Regenerative Medicine Therapies. Stem Cells Transl Med. 2022; 11 (2): 107–13. DOI: 10.1093/stcltm/szab025.
16. Jing D, Li C, Yao K, Xie X, Wang P, et al. The vital role of Gli1+ mesenchymal stem cells in tissue development and homeostasis. J Cell Physiol. 2021; 236 (9): 6077–89. DOI: 10.1002/jcp.30310.
17. Krawczenko A, Klimczak A. Adipose Tissue-Derived Mesenchymal Stem/Stromal Cells and Their Contribution to Angiogenic Processes in Tissue Regeneration. Int J Mol Sci. 2022; 23 (5): 2425. DOI: 10.3390/ijms23052425.

ASSESSMENT OF THE ZONA PELLUCIDA MICRODISSECTION ON ITS THICKNESS IN MAMMALIAN EMBRYOS

Sitnikov DS¹ ✉, Ilina IV¹, Filatov MA², Silaeva YuYu²

¹ Joint Institute for High Temperatures of the Russian Academy of Sciences, Moscow, Russia

² Institute of Gene Biology of the Russian Academy of Sciences, Moscow, Russia

The zona pellucida (ZP) is a dynamically changing object that plays an important role during the preimplantation stage of embryogenesis. The ZP thickness may affect the implantation success and pregnancy rate, it is considered as a prognostic factor in a number of studies. The study was aimed to assess the dynamic changes in the mouse embryonic ZP thickness after laser assisted hatching (LAH) that involved breaching the ZP integrity at the blastocyst stage. Femtosecond laser pulses were used to perform the zona microsurgery. The zona thickness was measured both at the stage of blastocyst microsurgery (~E3.5, i.e. 3.5 days of embryogenesis) and at the hatching stage (~E5). Significant differences in the ZP thickness were revealed in the control group of embryos: from 6.21 μm (E3.5) to 5.4 μm (E5). The changes in thickness from 6.6 μm (E3.5) to 6.2 μm (E5) observed in the group subjected to LAH were non-significant. Tracing the ZP thickness of a particular embryo from the blastocyst stage to the hatching stage made it possible to estimate the thinning coefficients in the experimental and control groups. The findings that indicate lower tensile strength of the zona in case of LAH can provide the basis for further research on the ZP properties in case of using the embryo cryopreservation protocols.

Keywords: blastocyst, zona pellucida thickness, thinning, laser assisted hatching, femtosecond laser pulses

Funding: experimental studies of laser assisted hatching were performed using the unique scientific facility "Terawatt Femtosecond Laser Complex" in the Center for Collective Usage "Femtosecond Laser Complex" of JIHT RAS and were funded by the Ministry of Science and Higher Education of the Russian Federation (State Assignment № 075-01129-23-00). Embryos were obtained using the unique scientific facility Transgenebank and supported by the Ministry of Science and Higher Education of the Russian Federation (grant № 075-15-2021-668 of 29.07.2021).

Author contribution: Sitnikov DS — laser microsurgery, data processing, manuscript writing; Ilina IV — study concept, manuscript writing; Filatov MA — handling embryos, statistical processing, manuscript writing; Silaeva YuYu — management; discussion and manuscript editing — all authors.

Compliance with ethical standards: animals were handled in accordance with the Declaration of Helsinki and the guidelines issued by the Bioethics Commission at the Institute of Gene Biology of the Russian Academy of Sciences.

✉ **Correspondence should be addressed:** Dmitry S. Sitnikov
Krasnokazarmennaya, 17a, Moscow, 111116, Russia; sitnik.ds@gmail.com

Received: 09.11.2022 **Accepted:** 30.12.2022 **Published online:** 27.01.2023

DOI: 10.24075/brsmu.2023.002

ИССЛЕДОВАНИЕ ВЛИЯНИЯ МИКРОДИССЕКЦИИ БЛЕСТЯЩЕЙ ОБОЛОЧКИ ЭМБРИОНОВ МЛЕКОПИТАЮЩИХ НА ЕЕ ТОЛЩИНУ

Д. С. Ситников¹ ✉, И. В. Ильина¹, М. А. Филатов², Ю. Ю. Силаева²

¹ Объединенный институт высоких температур Российской академии наук, Москва, Россия

² Институт биологии гена Российской академии наук, Москва, Россия

Блестящая оболочка (*zona pellucida*, ZP) — динамически меняющийся объект, играющий важную роль на преимплантационной стадии развития эмбриона. Ее толщина может оказывать влияние на успешность имплантации и частоту наступления беременности, в ряде исследований ее рассматривают как прогностический критерий. Целью работы было исследовать динамику толщины блестящей оболочки эмбриона мыши в результате процедуры вспомогательного лазерного хетчинга (ВЛХ), когда нарушение целостности ZP проводят на стадии бластоцисты. Для микрохирургии оболочки использовали импульсы излучения фемтосекундной длительности. Измерение толщины оболочки проводили как на стадии микрохирургии бластоцисты (~E3.5, т. е. 3,5 дня эмбрионального развития), так и на стадии вылупления (~E5). Обнаружены статистически значимые различия толщины ZP эмбрионов в контрольной группе — с 6,21 мкм (E3.5) до 5,4 мкм (E5). В группе, подвергавшейся ВЛХ, изменения толщины с 6,6 мкм (E3.5) до 6,2 мкм (E5) оказались статистически не значимыми. Отслеживание толщины ZP индивидуального эмбриона от стадии бластоцисты до стадии вылупления позволило оценить коэффициент истончения для контрольной и экспериментальной групп. Полученные данные свидетельствуют о снижении предела прочности оболочки при проведении ВЛХ и могут служить базисом для последующих исследований ее свойств в случае применения протоколов криоконсервации эмбрионов.

Ключевые слова: бластоциста, толщина блестящей оболочки, истончение, вспомогательный лазерный хетчинг, фемтосекундные лазерные импульсы

Финансирование: экспериментальные исследования по ВЛХ были выполнены с использованием УНУ «Лазерный тераваттный фемтосекундный комплекс», входящим в состав ЦКП «Лазерный фемтосекундный комплекс» ОИВТ РАН при финансовой поддержке Министерства образования и науки РФ в рамках Государственного задания № 075-01129-23-00. Эмбрионы были получены с использованием Уникальной научной установки «Трансгенбанк» при финансовой поддержке Министерства образования и науки РФ в рамках проекта (Соглашение № 075-15-2021-668 от 29.07.2021).

Вклад авторов: Д. С. Ситников — проведение лазерной микрохирургии, обработка результатов, написание статьи; И. В. Ильина — идея исследования, написание статьи; М. А. Филатов — работа с эмбрионами, статистическая обработка, написание статьи; Ю. Ю. Силаева — руководство; обсуждение и редактирование статьи — все авторы.

Соблюдение этических стандартов: все манипуляции с животными производили в соответствии с требованиями Хельсинкской декларации и рекомендациями комиссии по биоэтике Института биологии гена РАН.

✉ **Для корреспонденции:** Дмитрий Сергеевич Ситников
ул. Краснаязаременная, д. 17а, г. Москва, 111116, Россия; sitnik.ds@gmail.com

Статья получена: 09.11.2022 **Статья принята к печати:** 30.12.2022 **Опубликована онлайн:** 27.01.2023

DOI: 10.24075/vrgmu.2023.002

The zona pellucida (ZP) is an extracellular matrix that surrounds the oocyte at the early stages of development and performs a number of important functions during oogenesis, fertilization, and preimplantation development. The ZP plays a role of physical barrier protecting the embryo from microorganisms, viruses, and immune cells, which could be present in the oviduct [1]. It allows the oocyte to move freely in the fallopian tube after ovulation, prevents embryo implantation in the oviduct wall [2], enables species-specific fertilization, induction of acrosome reaction in sperm, and blocks polyspermic fertilization [3]. Limitation of volume of the embryo surrounded by the ZP ensures a close contact between blastomeres that is essential for compaction at the stage of cleavage [4] and later maintains integrity of the inner cell mass (ICM) [5]. The ZP thickness of the embryo is crucial: it affects the embryo's implantation in the endometrium.

There are certain factors, the effects of which make it difficult for the embryo to hatch from its shell on its own and then to implant: for example, in case of thicker (more than 17 μm thick) [6, 7] or dense ZP, or in case of impaired production of enzymes responsible for the ZP lysis [8]. In the last decade, laser assisted hatching (LAH) has become increasingly used in the clinics. This procedure is based on the ZP exposure to laser pulses aimed at the zona thinning/dissecting and facilitation of subsequent embryo hatching. Millisecond infrared laser dissectors are usually used for this purpose. Laser pulse absorption by the shell results in the local ZP protein disruption due to heating to several hundred degrees [9]. The size of the dissection site of 5–20 μm is determined by the laser pulse energy and thermophysical properties of the object. There is a possibility of thermal damage to embryonic cells adjacent to the ZP, that is why it is recommended to perform laser microdissection in strict compliance with the regulations at the early stages of preimplantation development characterized by wider perivitelline space (i.e. the space between the ZP and the cell membrane of oocyte or zygote) compared to the later stages of preimplantation development.

The laser microsurgery technique involving the use of femtosecond laser pulses can be an alternative to the applied commercial solutions. The physics of the femtosecond pulse interaction with the biological objects is based on the multiphoton absorption processes, and the local breaching of the ZP integrity is of non-thermal nature [10]. This fact makes it possible to precisely define the area of laser exposure confined to the focal spot size of $\sim 1.5\text{--}2\ \mu\text{m}$. The benefits of using femtosecond laser pulses that include minimum ZP dissection width and minimization of the radiation thermal effects on adjacent embryonic cells were earlier implemented in the technologies for controlled laser assisted hatching [11] and embryo tagging during preimplantation development [12, 13].

The interest in studying the ZP properties is increased due to the desire to discover reliable indicators of oocyte quality. It is oocyte quality that is considered one of the major factors of female fertility, since it determines the original potential of embryogenesis [14]. Thus, there is a number of studies of the correlation of the ZP thickness (as one of the indicators) [15, 16] and its variability in embryos with the pregnancy and implantation rates [6, 15, 17, 18]. The ZP mechanical characteristics were also considered as predictors of successful oocyte development after fertilization [19], embryo quality [20], and successful implantation [21].

Despite the fact that LAH has been used in clinical practice for several decades, there are just a few studies focused on the impact of this procedure on the ZP structure and morphology. The relevance of such studies is beyond doubt,

since comparison of the ZP dynamic changes associated with experimental breaching of its integrity with the natural cycle makes it possible to acquire additional data on the mechanisms underlying the ZP disruption/thinning and the factors that determine successful hatching and subsequent embryo implantation. Furthermore, effective approaches to embryo cryopreservation by vitrification at any stage of preimplantation development have been introduced into clinical practice. At the same time, there are data on alteration of the ZP physical and chemical properties in such embryos, as well as on the ZP thickening (the so called zona hardening) [22]. In this regard it is essential to study the effects of LAH on alterations of the ZP properties, since the findings can provide the basis for comparative analysis of hatching peculiarities in the embryos subjected to vitrification.

The study was aimed to assess the effects of LAH performed using femtosecond laser on the ZP characteristics of the house mouse (*Mus musculus*) embryos at the blastocyst stage. This stage of embryogenesis represents the beginning of embryo hatching, during which the ZP is subjected to substantial strain. The fundamental possibility of the ZP microsurgery at the blastocyst stage (i.e. on the later stage of preimplantation development) is ensured by using femtosecond laser pulses. As shown earlier [11, 23], the ZP microsurgery involving such pulses has no adverse effect on embryogenesis.

METHODS

Experimental apparatus

Microsurgical experiments involving embryos were performed using the femtosecond laser scalpel set-up (Fig. 1) created by the Joint Institute for High Temperatures of the Russian Academy of Sciences [24]. The beam generated by the TETA femtosecond laser source (Avesta; Troitsk) was used as a laser scalpel. After conversion to the second harmonic in the DKDP crystal, the laser pulse parameters were as follows: pulse duration 280 fs, energy 50 μJ , wavelength 514 nm, pulse repetition rate 2.5 kHz. The laser beam was fed through the right side port of the Olympus IX-71 inverted microscope and focused into the spot with a diameter of about 2 μm (FWHM) with the 20 \times UPlanFL objective lens (Olympus; Japan) having a 0.5 numerical aperture (NA). Attenuator was mounted on the laser beam path before entering the microscope for the laser pulse energy adjustment, and the telescope was used to align the laser beam diameter with the objective lens aperture. When performing microsurgical procedures, the laser pulse energy was 20 nJ, which corresponded to the intensity of 2.5 TW/cm². The embryos were distributed into droplets of growth medium in Petri dishes with the glass bottom thickness of 170 μm . A Petri dish was placed on the motorized microscope stage (Märzhäuser Wetzlar; Germany) to move the embryo relative to the stationary laser beam. The beam was focused in the plane of maximum embryo cross-section, i.e. in the equatorial plane. Imaging of the embryos was performed using the DFK 72AUC02 camera (The Imaging Source; Germany). Software allowing the operator to set the trajectory of the laser beam motion over the image of the embryo was used to automate the microsurgical procedure.

Animals

Embryos were collected from the C57Bl/6JxCBA F1 hybrid mice purchased from the animal house of the Federal Medical Biological Agency of Russia (Stolbovaya branch; Russia).

Animals were kept in the controlled environment (22–24 °C, 14 : 10 h light/dark cycle (day : night)) with *ad libitum* access to food (special extruded diet for mouse breeding) and water.

Hormonal stimulation of ovulation

The widely accepted protocol for ovulation induction was used to collect a large number of embryos at once. Immature females about 3 weeks of age with body weight of 10–12 g were used as donors. Hormonal stimulation was performed in accordance with the two-step protocol: the pregnant mare serum gonadotropin (PMSG) was administered intraperitoneally at 13:00 of day one, 5 IU per animal. HCG (Chorulon, Merck Animal Health, USA), 10 IU per animal were administered 48 h later. After that the females were housed with males for mating.

Obtaining embryos

Animals were euthanized by cervical dislocation. The zygote stage embryos were collected on the day of the copulation plug detection. Oviducts were cut out from the animal's body with scissors and placed in the HEPES-containing Ooclean medium (PanEco; Russia) heated to 37 °C. Then the oviduct ampullae were dissected with the syringe needles under stereomicroscope to extract the cumulus-oocyte complexes. Then about 0.03 g of hyaluronidase (Lydase; Microgen, Russia) were added to this droplet to provide zygote purification from the cumulus cells. The zygotes obtained were serially washed in four droplets of Ooclean medium and transferred to the culture medium.

Transportation of embryos

To be transferred from the Institute of Gene Biology of the Russian Academy of Sciences to the Joint Institute for High Temperatures of the Russian Academy of Sciences for LAH, the embryos were placed in the HEPES-containing Ooclean medium (PanEco; Russia) previously heated to 37 °C. The embryos were transported in the 2 ml eppendorf tubes. The temperature of +37 °C was maintained during transfer of the tube containing embryos. After transportation the embryos were washed in the culture medium. For that these were transferred from one droplet to another three times.

Embryo culture

The embryos were cultured to the morula stage (about 2.5 days of embryogenesis, E2.5) in the four-well plates (Thermo Fisher Scientific Nunc; USA) using the CSCM-C culture medium for gametes and embryos (Fujifilm Irvine Scientific; USA). During the morula and blastocyst stages (E3.5), the embryos were cultured in the 20 µL droplets of the CSCM-C medium (Fujifilm Irvine Scientific; USA) covered with mineral oil, 2–3 embryos per droplet.

Experiment

Three droplets containing culture medium were previously formed in each glass bottom Petri dish (catalogue number № 200350; SPL Lifesciences, Korea), then the droplets were covered with mineral oil. A day before the experiment, the morula stage embryos were distributed into well-prepared Petri dishes and transferred to the incubator. Three embryos were placed in each droplet. Microsurgery of the embryos' ZP was performed at the blastocyst stage (~E3.5).

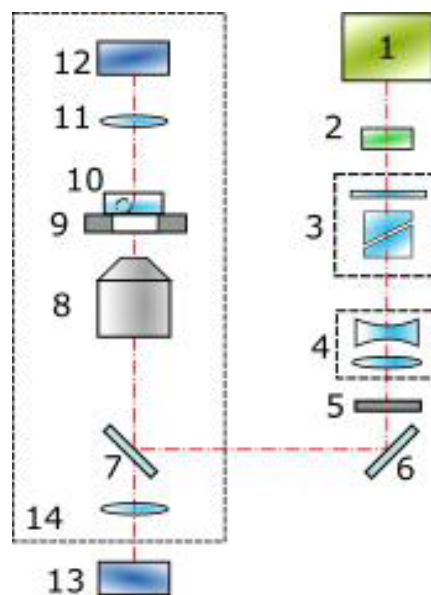


Fig. 1. Scheme of femtosecond laser scalpel. 1 — femtosecond laser; 2 — converter to second harmonic; 3 — attenuator; 4 — telescope; 5 — mechanical laser interrupter; 6, 7 — mirrors for the laser beam wavelength; 8 — objective lens; 9 — motorized microscope stage; 10 — Petri dish containing embryo; 11 — substage condenser; 12 — substage lamp; 13 — CMOS camera; 14 — inverted microscope

A total of 99 embryos were divided into two groups: experimental group (EG) of 63 embryos and concurrent control group (CC group) of 36 embryos. The operator took a picture of the embryo in its initial state, set the trajectory of the laser beam motion for the embryo's ZP microdissection, performed LAH, and took a final picture of the embryo after the procedure. The total time spent on one embryo did not exceed 1.5 min. The embryos usually hatched at the E5 stage, during which they were photographed again.

Statistical data processing

Statistical processing of the results was performed using the Statistica 7.0 software package (Dell; USA) and Microsoft Excel 2013 (Microsoft Corporation; USA). The hypotheses were tested for normality using the Kolmogorov–Smirnov and the Shapiro–Wilk tests. Since the distributions of the data provided in the study were non-normal, nonparametric tests were used for analysis. In this case, median, quartiles (25–75%), and variation (minimum and maximum values of the studied parameters) were considered as significant indicators. The Mann–Whitney U test was used to compare two independent groups; two dependent groups were compared using the Wilcoxon signed-rank test for dependent samples. Significance levels of all statistical parameters were set to 0.05.

RESULTS

Fig. 2A shows a fragment of the embryo's ZP before exposure to laser beam. The primitives (green lines 1–3) set the trajectory of the laser beam motion. Laser exposure of the area along the polyline 1 was essential for breaching of the embryo's ZP integrity during the LAH procedure. About 80–90% of the ZP thickness were cut. Lines 2 and 3 were auxiliary ones (to confirm that the embryo hatched through the drilled hole (Fig. 2B)). The ZP thickness of each embryo of the experimental group at the time of the procedure was measured. The ZP thickness Δ was measured in three different areas with the angular increment of ~90–120°. Similar measurements of the embryo's

ZP thickness were performed at the stage of embryo hatching and after hatching in both experimental (Fig. 2C) and CC (Fig. 2D) groups.

The data on the ZP thickness for the embryos of the experimental and control groups are provided in Fig. 3. As is commonly known, the ZP is stretched during hatching in the natural conditions. Thus, we have shown that the ZP thickness demonstrates a significant decrease in Δ_m (from 6.21 μm (E3.5) to 5.4 μm (E5)) in the control group of animals not exposed to laser beam. No such ZP thinning has been revealed in the experimental group, and the measured Δ_m values are 6.6 μm (E3.5) and 6.2 μm (E5). Statistical processing of the experimental data using the Mann–Whitney U test has confirmed significant differences between the ZP thickness (E5) values observed during the natural hatching cycle and after the LAH procedure.

The ZP thinning coefficient $K = \Delta_{E5}/\Delta_{E3.5}$, where $\Delta_{E3.5}$ and Δ_{E5} are the ZP thickness values of specific embryo obtained 3.5 and 5 days after fertilization, respectively, is one more interesting parameter. The median value of this parameter in the experimental group ($K_{med,e}$) is 0.95. The bars of the bar chart (Fig. 4A) to the right of the $K = 1$ line show that the ZP thickness measured at the stage of hatching is greater than that measured at the time of microsurgery. In certain cases the differences reported reach 23%. This may be due to the fact that the blastocyst demonstrates cyclic volume changes (expansion and collapse) during hatching, thereby stretching the ZP [25]. The ZP thickness measured at the microsurgery stage (E3.5), therefore, corresponded to the stretching phase. In the control group, the ZP thickness was also assessed in the embryos that had reached the blastocyst stage (E3.5). According to Fig. 4B, the ZP of the vast majority of embryos becomes thinner during hatching. The share of embryos with $K > 1$ is less than 20%. Similar to the experimental group, this can be due to the changing thickness of the blastocyst ZP (E3.5) during expansion. The median coefficient values ($K_{med,cc} = 0.84$) also indicate greater ZP thinning in non-treated embryos.

DISCUSSION

The embryo hatching from the ZP is an important step that is essential for further embryo implantation in the uterus. Hatching is preceded by cyclic blastocyst expansion and collapse. The changes in blastocyst volume result in physical impact on the ZP, since these cause ZP stretching and thinning. Exposure to tensile stress and proteases (such as trypsin) synthesized by

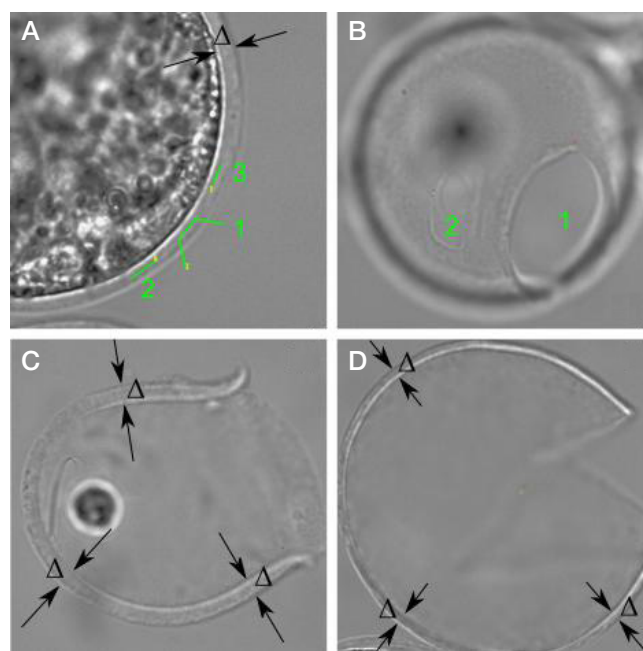


Fig. 2. Embryos before zona microsurgery (A); zona pellucida after hatching (B). 1 — hole in the ZP after blastocyst hatching resulting from incision along the trajectory 1 (on the fragment a); 2 — results of incision along the trajectory 2 (on the fragment a). The zone after hatching of the embryo in the experimental group (C) and CC group (D)

the uterus and/or blastocyst results in the ZP breaching that makes blastocyst hatching possible.

In terms of mechanics, the observed differences between the experimental and control groups can be interpreted in the following way. The breaking strength is a threshold value of mechanical stress applied to the sample; exceeding the threshold results in destruction of the material. As applied to the hatching process, the embryo's ZP is permanently exposed to tensile stress during the blastocyst expansion stage. Exceeding the tensile strength threshold leads to the ZP rupture and initiation of hatching. There are numerous studies aimed at developing models describing the ZP mechanical properties. The approaches used include describing the ZP as a material having linear elastic, hyperelastic, and viscoelastic properties (the detailed review of the present state of the art in analytical and numerical approaches can be found in the recently published report [26]).

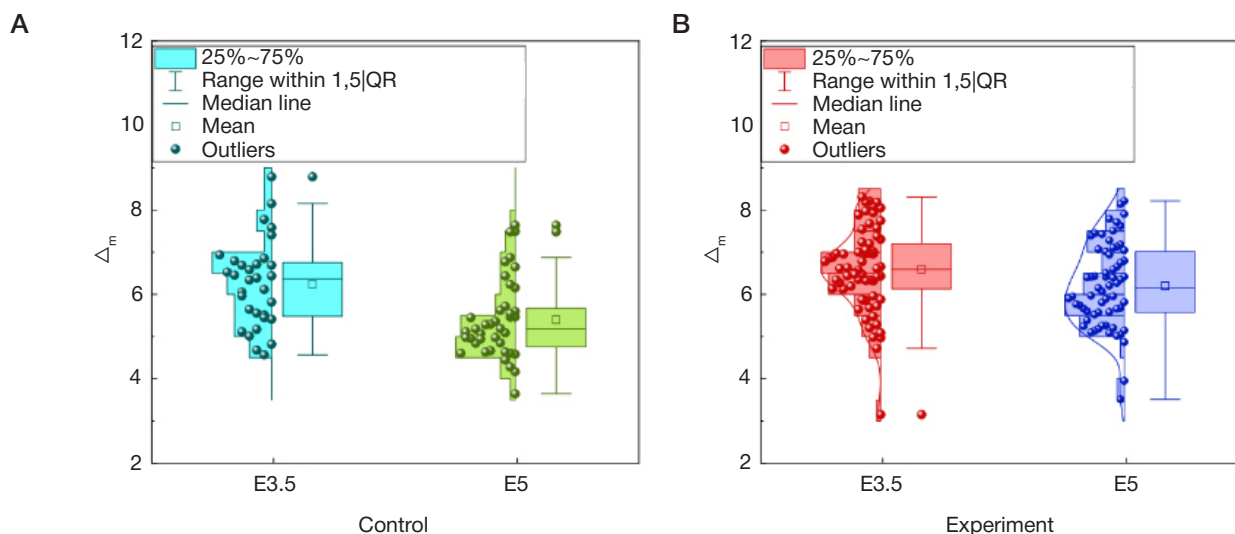


Fig. 3. Changes in the ZP thickness during embryogenesis in the control (A) and experimental (B) groups

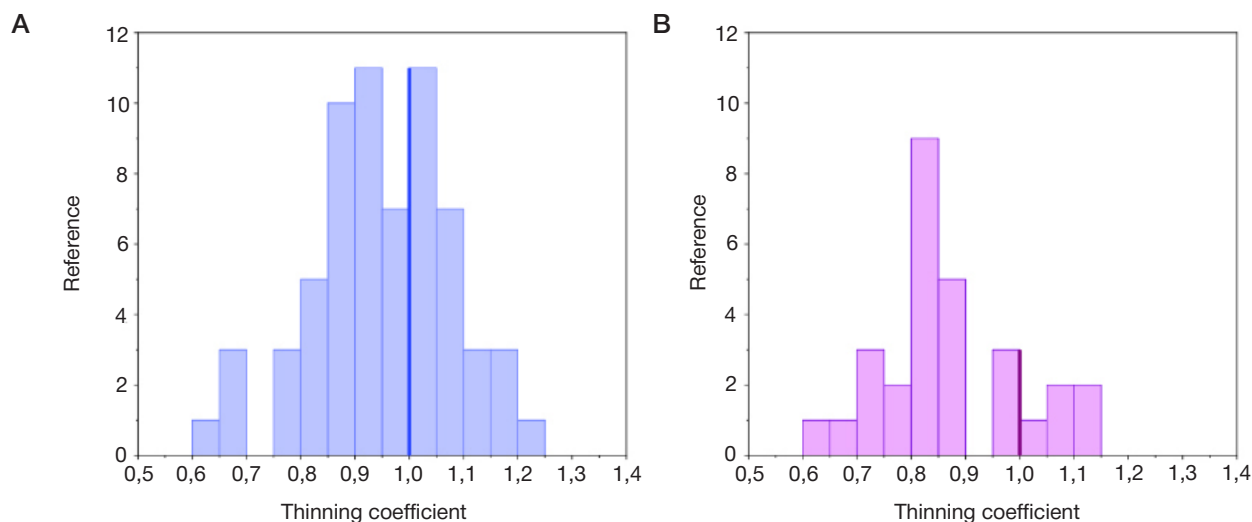


Fig. 4. Distribution of the ZP thinning coefficient in the experimental (A) and control (B) groups

Constructing the model of the mouse embryo ZP mechanical properties lies beyond the scope of this study. However, the data obtained can be analyzed taking into account the current knowledge about the ZP properties. Analysis of the bar charts provided in Fig. 4 appears to be in qualitative agreement with the available models. With an increase in the blastocyst diameter, the tensile stress at the ZP is increased. The ZP radius is increased, while its thickness is reduced. Currently, there are literary data on the Young's modulus (the ratio of the applied stress to the deformation response of the material) values of the mammalian ZP; these values of the mouse oocyte and embryo are 17.9 and 42.2 kPa, respectively [27]. The Young's modulus characterizes the material properties in the linear section of the stress-strain diagram, right up to the yield strength, at which the elastically loaded sample elongates when stretched, but returns to its original form and size when unloaded. When this limit is exceeded, the material ceases to be elastic and starts to deform plastically (does not fully return to its original state). The thinning coefficient values $K < 1$ provided in Fig. 4B indicate plastic deformation after the tensile stress termination. When the stress threshold value (tensile strength) is reached, the zona breaches and the embryo hatches. Breaching of the ZP integrity during LAH results in significantly lower threshold, as evidenced by the ZP thickness mean values Δ_{E5} and the values of the K thinning coefficient that are greater than that of the control group. The paper [25] reports the hypothesis of reduced implantation capability, possibly due to adverse effects of thick ZP on the blastocyst expansion. This hypothesis is consistent with the theory of strength of materials and the need to apply more force per surface area unit to deform a thicker layer of the zona.

The impact of cryopreservation procedures on the state of the ZP of the oocyte/embryo has been studied fairly

extensively. There is abundant evidence that cryopreservation makes their ZP harder [22, 28]. However, the question of how cryopreservation affects the ZP state and properties during the later stages of embryogenesis requires further research. The logical next step of the experiment will be replacing the research object with the embryo subjected to cryopreservation. The data obtained in this study will be used as reference data when studying the ZP thinning in cryopreserved embryos subjected to LAH performed using femtosecond laser pulses at the blastocyst stage.

CONCLUSIONS

This study was focused on assessing the mouse embryo zona pellucida (ZP) thickness both in natural hatching cycle (control group, non-treated embryos) and after the LAH procedure (experimental group). Minimal thermal effects of femtosecond laser beam made it possible to perform microsurgery at the late stage of preimplantation development, at the blastocyst stage before hatching. Measuring the ZP thickness at the blastocyst stage (E3.5) and hatching stage (E5) allowed us to estimate the thinning coefficient of each particular shell. Statistical analysis revealed significant differences in the zona thickness between the experimental and control groups at the blastocyst hatching stage: 5.4 and 6.2 μm , respectively. It was also noted that LAH resulted in almost no stretching of the embryo's ZP: the ZP thickness was 6.6 μm (E3.5) and 6.2 μm (E5), as evidenced by the thinning coefficient median value. We believe that this fact is due to lower tensile stress threshold. The experimental data obtained will provide the basis for comparison during further assessment of the ZP thickness in cryopreserved embryos and embryos grown in media of various compositions.

References

1. Ricardo Loret de Mola J, Garside WT, Bucci J, Tureck RW, Heyner S. Analysis of the human zona pellucida during culture: Correlation with diagnosis and the preovulatory hormonal environment. *J Assist Reprod Genet.* 1997; 14 (6): 332–6. DOI: 10.1007/BF02765837.
2. Eppig JJ. Intercommunication between mammalian oocytes and companion somatic cells. *Bio Essays.* 1991; 13 (11): 569–74. DOI: 10.1002/bies.950131105.
3. Gupta SK. Role of zona pellucida glycoproteins during fertilization in humans. *J Reprod Immunol.* 2015; 108: 90–7. DOI: 10.1016/j.jri.2014.08.006.
4. Dunbar BS. Ovarian Antigens and Infertility. *Am J Reprod Immunol.* 1989; 21 (1): 28–31. DOI: 10.1111/j.1600-0897.1989.tb00994.x.
5. Trounson AO, Moore NW. The survival and development of sheep eggs following complete or partial removal of the zona pellucida. *Reproduction.* 1974; 41 (1): 97–105. DOI: 10.1530/jrf.0.0410097.
6. Balakier H, Sojecki A, Motamedi G, Bashar S, Mandel R, Librach C. Is the zona pellucida thickness of human embryos influenced by

- women's age and hormonal levels? *Fertil Steril*. 2012; 98 (1): 77–83. DOI: 10.1016/j.fertnstert.2012.04.015.
7. Koifman M, Lahav-Baratz S, Shopen L, Idit B, Ishai D, Wiener-Megnazi Z, et al. In Vitro Fertilization Outcomes Following Assisted Hatching of Embryos with Thick Zona Pellucida—A Prospective Randomized Study. *Adv Reprod Sci*. 2014; 2 (4): 76–82. DOI:10.4236/arsci.2014.24009.
 8. Seshagiri PB, Sen Roy S, Sireesha G, Rao RP. Cellular and molecular regulation of mammalian blastocyst hatching. *J Reprod Immunol*. 2009; 83 (1–2): 79–84. DOI: 10.1016/j.jri.2009.06.264.
 9. Tadir Y, Douglas-Hamilton DH, Douglas-Hamilton DH, Douglas-Hamilton DH. Laser Effects in the Manipulation of Human Eggs and Embryos for In Vitro Fertilization. *Methods Cell Biol*. 2007; 82 (06): 409–31. DOI: 10.1016/S0091-679X(06)82014-5.
 10. Sitnikov DS, Ilina IV, Pronkin AA. Assessment of the thermal effect of femtosecond and millisecond laser pulses in microsurgery of mammalian embryos. *Quantum Electron*. 2022; 52 (6): 482–90 DOI: 10.1070/QEL18047.
 11. Ilina IV, Khramova YV, Ivanova AD, Filatov MA, Silaeva YY, Deykin AV, et al. Controlled hatching at the prescribed site using femtosecond laser for zona pellucida drilling at the early blastocyst stage. *J Assist Reprod Genet*. 2021; 38 (2): 517–29. DOI: 10.1007/s10815-020-01998-x.
 12. Ilina IV, Khramova YV, Filatov MA, Sitnikov DS. Femtosecond laser is effective tool for zona pellucida engraving and tagging of preimplantation mammalian embryos. *J Assist Reprod Genet*. 2019; 36 (6): 1251–61. DOI:10.1007/s10815-019-01424-x.
 13. Ilina IV, Khramova YV, Filatov MA, Sitnikov DS. Application of femtosecond laser microsurgery in assisted reproductive technologies for preimplantation embryo tagging. *Biomed Opt Express*. 2019; 10 (6): 2985–95. DOI: 10.1364/BOE.10.002985.
 14. Gilchrist RB, Lane M, Thompson JG. Oocyte-secreted factors: regulators of cumulus cell function and oocyte quality. *Hum Reprod Update*. 2008; 14 (2): 159–77. DOI: 10.1093/humupd/dmm040.
 15. Sun YP, Xu Y, Cao T, Su YC, Guo YH. Zona pellucida thickness and clinical pregnancy outcome following in vitro fertilization. *Int J Gynecol Obstet*. 2005; 89 (3): 258–62. DOI: 10.1016/j.ijgo.2005.02.012.
 16. Lewis EI, Farhadifar R, Farland LV, J. Needleman D, Missmer SA, Racowsky C. Use of imaging software for assessment of the associations among zona pellucida thickness variation, assisted hatching, and implantation of day 3 embryos. *J Assist Reprod Genet*. 2017; 34 (10): 1261–9. DOI: 10.1007/s10815-017-0978-3.
 17. Garside WT, de Mola JRL, Bucci JA, Tureck RW, Heyner S. Sequential analysis of zona thickness during in vitro culture of human zygotes: Correlation with embryo quality, age, and implantation. *Mol Reprod Dev*. 1997; 47 (1): 99–104. DOI: 10.1002/(SICI)1098-2795(199705)47:1<99::AID-MRD13>3.0.CO;2-V.
 18. Marco-Jiménez F, Naturil-Alfonso C, Jiménez-Trigos E, Lavara R, Vicente JS. Influence of zona pellucida thickness on fertilization, embryo implantation and birth. *Anim Reprod Sci*. 2012; 132 (1–2): 96–100. DOI: 10.1016/j.anireprosci.2012.04.008.
 19. Yanez LZ, Han J, Behr BB, Pera RAR, Camarillo DB. Human oocyte developmental potential is predicted by mechanical properties within hours after fertilization. *Nat Commun*. 2016; 7 (1): 10809. DOI: 10.1038/ncomms10809.
 20. Andolfi L, Masiero E, Giolo E, Martinelli M, Luppi S, dal Zilio S, et al. Investigating the mechanical properties of zona pellucida of whole human oocytes by atomic force spectroscopy. *Integr Biol*. 2016; 8 (8): 886–93. DOI: 10.1039/c6ib00044d.
 21. Priel E, Priel T, Szaingurten-Solodkin I, Wainstock T, Perets Y, Zeadna A, et al. Zona pellucida shear modulus, a possible novel non-invasive method to assist in embryo selection during in-vitro fertilization treatment. *Sci Rep*. 2020; 10 (1): 1–10. DOI: 10.1038/s41598-020-70739-y.
 22. Choi JK, Yue T, Huang H, Zhao G, Zhang M, He X. The crucial role of zona pellucida in cryopreservation of oocytes by vitrification. *Cryobiology*. 2015; 71 (2): 350–5. DOI: 10.1016/j.cryobiol.2015.08.012.
 23. Ilina IV, Ovchinnikov AV, Sitnikov DS, Rakityansky MM, Agranat MB, Xramova YuV, Semenova ML. Primenenie femtosekundnykh lazernykh impul'sov v biomedicinskikh kletochnykh tekhnologiyax. *TVT*. 2013; 51 (2): 198–204.
 24. Kirienko KV, Apyrshko VP, Yakovenko SA. Zona pellucida: stroenie, funkci, svojstva (obzor literatury). *Problemy reprodukcii*. 2019; 25 (3): 104–12. Dostupno po ssylke: <https://doi.org/10.17116/repro201925031104>.
 25. Karimian K, Seydewitz R, Töpfer D, Böl M. Poro-viscoelastic behaviour of the zona pellucida: Impact of three-dimensional modelling on material characterisation. *J Mech Behav Biomed Mater*. 2022; 131 (March). DOI: 10.1016/j.jmbbm.2022.105211.
 26. Sun Y, Wan KT, Roberts KP, Bischof JC, Nelson BJ. Mechanical property characterization of mouse zona pellucida. *IEEE Trans Nanobioscience*. 2003; 2 (4): 279–86. DOI: 10.1109/TNB.2003.820273.
 27. Larman MG, Sheehan CB, Gardner DK. Calcium-free vitrification reduces cryoprotectant-induced zona pellucida hardening and increases fertilization rates in mouse oocytes. *Reproduction*. 2006; 131 (1): 53–61. DOI: 10.1530/rep.1.00878.

Литература

1. Ricardo Loret de Mola J, Garside WT, Bucci J, Tureck RW, Heyner S. Analysis of the human zona pellucida during culture: Correlation with diagnosis and the preovulatory hormonal environment. *J Assist Reprod Genet*. 1997; 14 (6): 332–6. DOI: 10.1007/BF02765837.
2. Eppig JJ. Intercommunication between mammalian oocytes and companion somatic cells. *Bio Essays*. 1991; 13 (11): 569–74. DOI: 10.1002/bies.950131105.
3. Gupta SK. Role of zona pellucida glycoproteins during fertilization in humans. *J Reprod Immunol*. 2015; 108: 90–7. DOI: 10.1016/j.jri.2014.08.006.
4. Dunbar BS. Ovarian Antigens and Infertility. *Am J Reprod Immunol*. 1989; 21 (1): 28–31. DOI: 10.1111/j.1600-0897.1989.tb00994.x.
5. Trounson AO, Moore NW. The survival and development of sheep eggs following complete or partial removal of the zona pellucida. *Reproduction*. 1974; 41 (1): 97–105. DOI: 10.1530/jrf.0.0410097.
6. Balakier H, Sojecki A, Motamedi G, Bashar S, Mandel R, Librach C. Is the zona pellucida thickness of human embryos influenced by women's age and hormonal levels? *Fertil Steril*. 2012; 98 (1): 77–83. DOI: 10.1016/j.fertnstert.2012.04.015.
7. Koifman M, Lahav-Baratz S, Shopen L, Idit B, Ishai D, Wiener-Megnazi Z, et al. In Vitro Fertilization Outcomes Following Assisted Hatching of Embryos with Thick Zona Pellucida—A Prospective Randomized Study. *Adv Reprod Sci*. 2014; 2 (4): 76–82. DOI:10.4236/arsci.2014.24009.
8. Seshagiri PB, Sen Roy S, Sireesha G, Rao RP. Cellular and molecular regulation of mammalian blastocyst hatching. *J Reprod Immunol*. 2009; 83 (1–2): 79–84. DOI: 10.1016/j.jri.2009.06.264.
9. Tadir Y, Douglas-Hamilton DH. Laser Effects in the Manipulation of Human Eggs and Embryos for In Vitro Fertilization. *Methods Cell Biol*. 2007; 82 (06): 409–31. DOI: 10.1016/S0091-679X(06)82014-5.
10. Ситников Д. С., Ильина И. В., Пронкин А. А. Оценка теплового воздействия лазерных импульсов фемто- и миллисекундной длительности при выполнении микрохирургических процедур на эмбрионах млекопитающих. *Квантовая Электроника*. 2022; 52 (5): 482–90.
11. Ilina IV, Khramova YV, Ivanova AD, Filatov MA, Silaeva YY, Deykin AV, et al. Controlled hatching at the prescribed site using femtosecond laser for zona pellucida drilling at the early blastocyst stage. *J Assist Reprod Genet*. 2021; 38 (2): 517–29. DOI: 10.1007/s10815-020-01998-x.
12. Ilina IV, Khramova YV, Filatov MA, Sitnikov DS. Femtosecond laser is effective tool for zona pellucida engraving and tagging of preimplantation mammalian embryos. *J Assist Reprod Genet*. 2019; 36 (6): 1251–61. DOI:10.1007/s10815-019-01424-x.
13. Ilina IV, Khramova YV, Filatov MA, Sitnikov DS. Application

- of femtosecond laser microsurgery in assisted reproductive technologies for preimplantation embryo tagging. *Biomed Opt Express*. 2019; 10 (6): 2985–95. DOI: 10.1364/BOE.10.002985.
14. Gilchrist RB, Lane M, Thompson JG. Oocyte-secreted factors: regulators of cumulus cell function and oocyte quality. *Hum Reprod Update*. 2008; 14 (2): 159–77. DOI: 10.1093/humupd/dmm040.
 15. Sun YP, Xu Y, Cao T, Su YC, Guo YH. Zona pellucida thickness and clinical pregnancy outcome following in vitro fertilization. *Int J Gynecol Obstet*. 2005; 89 (3): 258–62. DOI: 10.1016/j.ijgo.2005.02.012.
 16. Lewis EI, Farhadifar R, Farland LV, J. Needleman D, Missmer SA, Racowsky C. Use of imaging software for assessment of the associations among zona pellucida thickness variation, assisted hatching, and implantation of day 3 embryos. *J Assist Reprod Genet*. 2017; 34 (10): 1261–9. DOI: 10.1007/s10815-017-0978-3.
 17. Garside WT, de Mola JRL, Bucci JA, Tureck RW, Heyner S. Sequential analysis of zona thickness during in vitro culture of human zygotes: Correlation with embryo quality, age, and implantation. *Mol Reprod Dev*. 1997; 47 (1): 99–104. DOI: 10.1002/(SICI)1098-2795(199705)47:1<99::AID-MRD13>3.0.CO;2-V.
 18. Marco-Jiménez F, Naturil-Alfonso C, Jiménez-Trigos E, Lavara R, Vicente JS. Influence of zona pellucida thickness on fertilization, embryo implantation and birth. *Anim Reprod Sci*. 2012; 132 (1–2): 96–100. DOI: 10.1016/j.anireprosci.2012.04.008.
 19. Yanez LZ, Han J, Behr BB, Pera RAR, Camarillo DB. Human oocyte developmental potential is predicted by mechanical properties within hours after fertilization. *Nat Commun*. 2016; 7 (1): 10809. DOI: 10.1038/ncomms10809.
 20. Andolfi L, Masiero E, Giolo E, Martinelli M, Luppi S, dal Zilio S, et al. Investigating the mechanical properties of zona pellucida of whole human oocytes by atomic force spectroscopy. *Integr Biol*. 2016; 8 (8): 886–93. DOI: 10.1039/c6ib00044d.
 21. Priel E, Priel T, Szaingurten-Solodkin I, Wainstock T, Perets Y, Zeadna A, et al. Zona pellucida shear modulus, a possible novel non-invasive method to assist in embryo selection during in-vitro fertilization treatment. *Sci Rep*. 2020; 10 (1): 1–10. DOI: 10.1038/s41598-020-70739-y.
 22. Choi JK, Yue T, Huang H, Zhao G, Zhang M, He X. The crucial role of zona pellucida in cryopreservation of oocytes by vitrification. *Cryobiology*. 2015; 71 (2): 350–5. DOI: 10.1016/j.cryobiol.2015.08.012.
 23. Ильина И. В., Овчинников А. В., Ситников Д. С., Ракитянский М. М., Агранат М. Б., Храмова Ю. В., Семенова М. Л. Применение фемтосекундных лазерных импульсов в биомедицинских клеточных технологиях. *ТБТ*. 2013; 51 (2): 198–204.
 24. Кириенко К. В., Апрышко В. П., Яковенко С. А. Zona pellucida: строение, функции, свойства (обзор литературы). *Проблемы репродукции*. 2019; 25 (3): 104–12. Доступно по ссылке: <https://doi.org/10.17116/repro201925031104>.
 25. Karimian K, Seydewitz R, Töpfer D, Böhl M. Poro-viscoelastic behaviour of the zona pellucida: Impact of three-dimensional modelling on material characterisation. *J Mech Behav Biomed Mater*. 2022; 131 (March). DOI: 10.1016/j.jmbbm.2022.105211.
 26. Sun Y, Wan KT, Roberts KP, Bischof JC, Nelson BJ. Mechanical property characterization of mouse zona pellucida. *IEEE Trans Nanobioscience*. 2003; 2 (4): 279–86. DOI: 10.1109/TNB.2003.820273.
 27. Larman MG, Sheehan CB, Gardner DK. Calcium-free vitrification reduces cryoprotectant-induced zona pellucida hardening and increases fertilization rates in mouse oocytes. *Reproduction*. 2006; 131 (1): 53–61. DOI: 10.1530/rep.1.00878.

ADIPOKINES AND MYOKINES AS INDICATORS OF OBESE PHENOTYPES AND THEIR ASSOCIATION WITH THE GUT MICROBIOME DIVERSITY INDICES

Shestopalov AV^{2,3}, Ganenko LA¹ ✉, Grigoryeva TV⁴, Laikov AV⁴, Vasilyev IYu⁴, Kolesnikova IM³, Naboka YuL⁴, Volkova NI¹, Roumiantsev SA^{2,3}

¹ Rostov State Medical University, Rostov-on-Don, Russia

² Center for Molecular Health, Institute of Digital and Translational Biomedicine, Moscow, Russia

³ Pirogov Russian National Research Medical University, Moscow, Russia

⁴ Kazan Federal University, Kazan, Republic of Tatarstan, Russia

Today, metabolically healthy obesity (MHO) and metabolically unhealthy obesity (MUO) are distinguished. Adipose and muscle tissues can determine the obese phenotype due to adipokine and myokine production. Gut microbial community is also involved in MHO. The study was aimed to reveal the features of adipokine and myokine levels and their association with the gut microbiome alpha diversity in patients with MHO and MUO. A total of 265 subjects were divided into two groups: healthy individuals and obese patients. The latter were divided into two subgroups: patients with MHO and patients with MUO. Body mass index, waist circumference, HOMA-IR, adipokine and myokine levels, gut microbiome taxonomic composition, alpha diversity indices were defined in all the surveyed individuals, lipid and carbohydrate metabolism was also assessed. Significant differences in the adipokine and myokine levels and their association with the gut microbiome diversity indicators were revealed in patients with different obese phenotypes. Patients with MHO and MUO showed significantly lower adiponectin levels ($p < 0.05$) and significantly higher leptin and asprosin levels ($p < 0.05$) than healthy individuals. Patients with MUO had lower adiponectin and leptin levels ($p < 0.05$) than patients with MHO. Significantly higher FGF21 levels were observed in patients with MUO. Large-scale correlation analysis revealed the relationship between the glucose levels and the gut microbiome diversity indices that was missing in patients with MUO. This indicated the loss of the microbiota diversity effects on the blood glucose control in individuals with MUO, as well as different regulatory roles in the gut microbiome–liver–muscle/adipose tissue axes of individuals with MHO and MUO played by gut microbiota. The findings show the relationship between the gut microbiome diversity and the obese phenotype.

Keywords: obesity, metabolically healthy obesity, adipokines, myokines, gut microbiome alpha diversity

Funding: the study was conducted as part of the State Assignment № 0373100122119000041, the project "Creation of a bank of blood serum and fecal samples from healthy donors and patients with obesity, metabolic syndrome, type 2 diabetes mellitus, impaired mucosal barrier of the gastrointestinal tract with the aim of identifying candidate species-specific mediators of quorum sensing microbiota systems human modulating endocrine and metabolic function of adipose tissue".

Author contribution: Ganenko LA — study concept, data acquisition and analysis, manuscript writing; Volkova NI — research planning and management, manuscript editing; Roumiantsev SA — study design, manuscript editing; Grigoryeva TV — working with the database, analysis of the results; Laikov AV — data analysis and interpretation of the results; Vasilyev IYu — study concept, manuscript editing; Gaponov AM — literature review, study design, manuscript editing; Naboka YuL — data analysis and interpretation of the results, manuscript editing; Shestopalov AV — search for sources of funding, working with data sets, statistical data processing, manuscript writing.

Compliance with ethical standards: the study was approved by the Ethics Committee of the Rostov State Medical University (protocol № 20/19 of 12 December 2019); the informed consent was submitted by all study participants.

✉ **Correspondence should be addressed:** Lilia A. Ganenko
Nakhichevansky pereulok, 29, Rostov-on-Don, 344022, Russia; ganenko.lilia@yandex.ru

Received: 19.12.2022 **Accepted:** 21.01.2023 **Published online:** 17.02.2023

DOI: 10.24075/brsmu.2023.004

АДИПОКИНЫ И МИОКИНЫ КАК ИНДИКАТОРЫ ФЕНОТИПОВ ОЖИРЕНИЯ И ИХ СВЯЗЬ С ПОКАЗАТЕЛЯМИ РАЗНООБРАЗИЯ МИКРОБИОМА КИШЕЧНИКА

А. В. Шестопалов^{2,3}, Л. А. Ганенко¹ ✉, Т. В. Григорьева⁴, А. В. Лайков⁴, И. Ю. Васильев⁴, И. М. Колесникова³, Ю. Л. Набока⁴, Н. И. Волкова¹, С. А. Румянцев^{2,3}

¹ Ростовский государственный медицинский университет, Ростов-на-Дону, Россия

² Центр цифровой и трансляционной биомедицины «Центр молекулярного здоровья», Москва, Россия

³ Российский национальный исследовательский медицинский университет имени Н. И. Пирогова, Москва, Россия

⁴ Казанский (Приволжский) федеральный университет, Казань, Республика Татарстан, Россия

В настоящее время выделяют метаболически здоровое ожирение (МЗО) и метаболически нездоровое ожирение (МНЗО). Жировая и мышечная ткани могут определять фенотип ожирения за счет выработки адипокинов и миокинов. В формировании МЗО участвует и микробное сообщество кишечника. Целью работы было изучить уровни адипокинов и миокинов и их связь с альфа-разнообразием микробиома кишечника при МЗО и МНЗО. Из 265 обследуемых сформированы две группы: здоровые лица и пациенты с ожирением. Последние были разделены на две подгруппы: пациенты с МЗО и пациенты с МНЗО. У обследуемых определяли индекс массы тела, окружность талии, индекс HOMA-IR, уровень адипокинов и миокинов, таксономический состав микробиома кишечника и индексы альфа-разнообразия, оценивали липидный и углеводный обмен. Выявлены статистически значимые различия уровней адипокинов и миокинов, а также их взаимосвязь с показателями разнообразия микробиома кишечника у пациентов с разными фенотипами ожирения. При МЗО и МНЗО уровень адипонектина был значимо ниже ($p < 0,05$), а лептина и аспросина — выше ($p < 0,05$) по сравнению со здоровыми лицами. Пациенты с МНЗО имели уровни адипонектина и лептина более низкие ($p < 0,05$), чем пациенты с МЗО. При МНЗО статистически значимо выше уровень FGF21. Массовый корреляционный анализ при МЗО показал связь между уровнем глюкозы с индексами разнообразия микробиома кишечника, которая отсутствовала при МНЗО, что указывает на утрату влияния микробиоты кишечника на регуляцию уровня глюкозы крови при МНЗО и о различной регуляторной роли микробиоты кишечника в оси «микробиом кишечника — печень — жировая и мышечная ткани» при МЗО и МНЗО. Полученные данные указывают на взаимосвязь между разнообразием микробиома кишечника и фенотипом ожирения.

Ключевые слова: ожирение, метаболически здоровое ожирение, адипокины, миокины, альфа-разнообразие микробиома кишечника

Финансирование: работа выполнена в рамках реализации госконтракта № 0373100122119000041 по проекту «Создание банка биообразцов сыворотки крови и фекалий от здоровых доноров и пациентов с ожирением, метаболическим синдромом, сахарным диабетом II типа, нарушением мукозального барьера желудочно-кишечного тракта с целью выявления кандидатных видонеспецифических медиаторов систем quorum sensing микробиоты человека, модулирующих эндокринную и метаболическую функцию жировой ткани».

Вклад авторов: Л. А. Ганенко — концепция исследования, получение и анализ данных, написание статьи; Н. И. Волкова — планирование и руководство исследованием, редактирование статьи; С. А. Румянцев — дизайн исследования, редактирование статьи; Т. В. Григорьева — работа с базой данных, анализ результатов; А. В. Лайков — анализ данных и интерпретация результатов; И. Ю. Васильев — концепция исследования, редактирование статьи; А. М. Гапонов — анализ литературы, дизайн исследования, редактирование статьи; Ю. Л. Набока — анализ данных и интерпретация результатов, редактирование статьи; А. В. Шестопалов — поиск источников финансирования, работа с массивом данных, статистическая обработка результатов, написание статьи.

Соблюдение этических стандартов: исследование одобрено этическим комитетом ФГБОУ ВО РостГМУ МЗ РФ (протокол № 20/19 от 12.12.2019); все участники исследования подписали добровольное информированное согласие.

✉ **Для корреспонденции:** Лилия Александровна Ганенко
переулок Нахичеванский, дом 29, г. Ростов-на-Дону, 344022, Россия; ganenko.lilia@yandex.ru

Статья получена: 19.12.2022 **Статья принята к печати:** 21.01.2023 **Опубликована онлайн:** 17.02.2023

DOI: 10.24075/vrgmu.2023.004

Complications of obesity reduce the quality of life and life expectancy [1]. However, obesity is not always associated with metabolic disorders, that is why metabolically healthy obesity (MHO) and metabolically unhealthy obesity (MUO) are distinguished [2]. The prevalence of MHO among obese patients is 6–60% depending on the criteria of MHO [3]. Obesity classification that is based on BMI does not provide a full picture of the health status and potential risk of adverse outcome. This has been documented in the AACE/ACE (American Association of Clinical Endocrinologists and American College of Endocrinology) guidelines (USA, 2014) suggesting to take into account metabolic status when classifying obesity [4]. The adipose and muscle tissues play an important role in maintaining metabolic homeostasis via secretion of biologically active peptides: adipokines and myokines [5]. Imbalance between these insulin sensitivity and adipogenesis increasing and reducing adipokines and myokines may contribute to metabolic complications, such as insulin resistance, slow inflammatory adipose tissue remodeling, extracellular lipid deposition, atherosclerosis, etc. [6]. It is known that adiponectin exerts insulin sensitizing, anti-atherogenic and anti-inflammatory effects [7]. In contrast, such adipokines as leptin and resistin are potential factors of insulin resistance that have pleiotropic effects on food intake, neuroendocrine control of hypothalamus, reproductive function, and energy metabolism [8]. Information about the recently discovered adipokine, asprosin, is extremely fragmented: it is believed that asprosin can affect glucose metabolism, that it is probably associated with obesity, and that asprosin levels can be used as a marker for early diagnosis of diabetes mellitus [9]. Currently, information about the role of myokine (myostatin) in the pathogenesis of obesity and insulin resistance is limited. Some authors suggest using myostatin for identification of MUO [10]. The insulin-responsive myokine, FGF21, functions as a metabolic factor involved in the glucose homeostasis control [11]. Recently the interest of researchers has been drawn to the osteocrin peptide that is secreted by fibroblasts and osteoblast-like cells. Its pathophysiological role is poorly understood [12]. Sporadic results obtained in obese patients with insulin resistance showed that had higher osteocrin levels than healthy individuals [13]. In the last decade, gut microbiota has been considered as a factor affecting the development of obesity. Microbiota can influence the metabolic phenotype via both direct effects on the energy and nutrient availability and modulation of the microorganisms' signalling and metabolic pathways. There is growing evidence that the balance and diversity of microorganisms are essential for both optimal interaction with macroorganism and prevention of extraintestinal diseases [14]. The diversity of microbiome reflects the abundance of various bacterial species. Two types of diversity are distinguished: alpha diversity (within the same biotope) and beta diversity (between distinct biotopes). Alpha diversity is assessed based on the Chao 1, Shannon, Simpson (direct and inverse), Gini–Simpson, and Berger–Parker indices. The Chao 1 index is used to estimate the observed/hidden diversity, the Shannon index is an estimator of the microbiome diversity and evenness (higher index values correspond to wider diversity); the Simpson index describes the probability that any two specimens randomly selected in the indefinitely large community belong to different species (the diversity decreases with the increasing index); the Berger–Parker index is a measure of the species dominance in the microbiome (the larger is the index, the lower is alpha diversity) [15]. Previous studies have shown that the stool microbiome of obese individuals is less diverse than that of lean people [16]. The decrease in microbial diversity in 75% of patients with morbid obesity

and 40% of patients with class I and II obesity has been also shown [17, 18]. Some authors have found a positive correlation between the decrease in the gut microbiome diversity and MUO [19]. Despite the fact that the number of studies aimed at assessing the role of adipokines and myokines in MHO, as well as the relationship between adipokines and myokines and the gut microbiome indicators, is limited, the associations of adiponectin, resistin, FGF21 with MHO reported in the literature [5, 6] have provided the basis for the scientific hypothesis used in our study: various profiles of adipokines and myokines may contribute to phenotypic dissociation of obesity. The study was aimed to reveal the features of adipokine and myokine levels and their association with the gut microbiome diversity indicators in patients with different obese phenotypes.

METHODS

The study was performed in the Rostov State Medical University, Kazan Federal University, and the Center for Molecular Health at the Institute of Digital and Translational Biomedicine. The patients were enrolled between 2019 and 2020. All the subjects were divided into two main groups based on the body mass index (BMI) and waist circumference (WC): healthy individuals (controls) were included in group 1, while obese patients were included in group 2. Then group 2 was divided into two subgroups depending on whether or not metabolic complications were present: subgroup 2a included patients with MHO and subgroup 2b included patients with MUO. Inclusion criteria: age over 18 years; taking no antibiotics, pre- or probiotics within three months before enrollment. Additional inclusion criteria for group 1: $18.5 \text{ kg/m}^2 < \text{BMI} \leq 24.9 \text{ kg/m}^2$; no dyslipidemia, hyperglycemia or arterial hypertension (AH). Additional inclusion criteria for group 2: $\text{BMI} \geq 30 \text{ kg/m}^2$, $\text{WC} > 102 \text{ cm}$ in males and $> 88 \text{ cm}$ in females. Subgroup 2a included patients who met more than three criteria, while subgroup 2b included those who met \geq three criteria of the National Cholesterol Education Program (NCEP), Adult Treatment Panel III (ATPIII) (NCEP-ATP III) including the following indicators: systolic blood pressure (SBP) > 130 and/or diastolic blood pressure (DBP) $> 85 \text{ mm Hg}$, fasting plasma glucose (FPG) $\geq 6.1 \text{ mmol/L}$, triglycerides (TG) $\geq 1.7 \text{ mmol/L}$, high density lipoprotein cholesterol (HDL-C) < 1.29 (females) or < 1.03 (males), waist circumference (WC) $> 102 \text{ cm}$ (males) or $> 88 \text{ cm}$ (females). Exclusion criteria: severe somatic disease, any gastrointestinal disorder, acute condition, depression, alcohol abuse, pregnancy.

Study design

A cohort study was performed. Clinical interview and examination, as well as assessment of anthropometric indicators were performed in all subjects; all of them were through questionnaire survey and the laboratory tests: fasting plasma glucose (FPG), total cholesterol (TC), low density lipoprotein cholesterol (LDL-C), high density lipoprotein cholesterol (HDL-C), triglycerides (TG), adiponectin, leptin, asprosin, resistin, vascular endothelial growth factor (VEGF), irisin, fibroblast growth factor 21 (FGF21), myostatin, osteocrin, and insulin. The insulin resistance index (HOMA-IR) was calculated, the composition of gut microbiome was defined, and the alpha diversity indices of bacterial phylotypes were computed. Blood pressure was measured using the manual blood pressure monitor (Little Doctor LD-60; China) using the standard method by N.S. Korotkov. Biochemical parameters, such as FPG, HDL-C, LDL-C, TG, TC (mmol/L), were assessed by photometry using the Hitachi U-2900 spectrophotometer

Table 1. Clinical and laboratory characteristics of the surveyed individuals of groups 1 and 2

Parameters	Group 1 <i>n</i> = 129	Group 2 <i>n</i> = 136	<i>p</i>
Males	15 (11.6%)	28 (20.6%)	0.621
Females	114 (88.3%)	108 (79.4%)	0.613
Age/years	39.6 ± 4.2	54.6 ± 4.7	0.032
BMI, kg/m ²	20.8 [19; 23]	34 [31; 36]	0.024
WC, cm	74 [69; 75.5]	100 [95; 103]	0.011
SBP, mm Hg	120.5 [90; 125]	135 [125; 145]	0.034
DBP, mm Hg	74.5 [60; 90]	85 [80; 90]	0.001
FPG, mmol/L	3.96 [4.05; 5.1]	5.57 [5.1; 6.93]	0.0001
TC, mmol/L	4.5 [4.1; 5.0]	5.42 [4.62; 6.2]	0.624
LDL-C, mmol/L	3.11 [2.4; 3.21]	3.19 [2.6; 3.64]	0.745
HDL-C, mmol/L	1.93 [1.49; 2.24]	1.23 [1.11; 1.39]	0.031
TG, mmol/L	0.79 [0.57; 1.13]	1.65 [1.33; 2.34]	0.001
Insulin, pg/mL	262 [133.6; 418.2]	390 [170.02; 678.78]	0.001
HOMA-IR	1.86 [1.47; 2.82]	11.7 [5.08; 19.3]	0.001

Note: BMI — body mass index, WC — waist circumference, SBP — systolic blood pressure, DBP — diastolic blood pressure, TC — total cholesterol, LDL-C — low density lipoprotein cholesterol, HDL-C — high density lipoprotein cholesterol, TG — triglycerides, HOMA-IR — Homeostasis Model Assessment of Insulin Resistance.

(Hitachi; Japan) and the Olvex Diagnosticum kits (Russia). Adiponectin, leptin, resistin, asprosin, VEGF, irisin, myostatin, FGF21, osteocrin, and insulin (ng/mL) were quantified by multiplex immunoassay using the Magpix analyzer (BioRad; USA) and the kits manufactured by Milliplex (USA). The concentration of asprosin was determined by ELISA using the ELISA KitForAsprosin (Cloud-Clone.; USA). Faecal samples were collected in accordance with the handbook edited by V.V. Menshikov [20]. Gut microbiome composition was defined by Next-Generation Sequencing (NGS) of the bacterial 16S rRNA gene (V3-V4 variable region) on the MiSeq platform (Illumina; USA) in the paired-end reading mode (2 × 300). Various alpha diversity indices of the bacterial community were used to characterize microbiota.

Statistical analysis

R environment (version 3.2, R Foundation for Statistical Computing; Vienna, Austria) was used for statistical processing. The following was calculated for quantitative indicators: mean ± standard deviation; median and quartiles (25%, 75%); minimum and maximum values of the sample. The average group levels were compared using the Mann–Whitney U test. The median values of the studied parameters were compared using the Kruskal–Wallis test, and the correlation analysis involved the use of Spearman's rank correlation coefficient. The differences were considered significant at *p* < 0.05. Cluster analysis: large-scale correlation analysis was performed in Python v3.8 for each group of patients and the correlations between:

BMI, WC, SBP, DBP, FPG, LDL-C, HDL-C, TG, TC and the levels of adipokines and myokines;

each clinical parameter and microbiota parameters (alpha diversity: species richness (operational taxonomic units (OTUs) with non-zero abundance), Shannon entropy, Berger–Parker dominance index, Simpson index and inverse Simpson index, Gini–Simpson index, Chao1 index;

microbiome parameters and the levels of adipokines and myokines.

The Spearman's rank correlation matrices obtained were clustered together within each group of patients based on the Manhattan distances.

Data availability

The cluster analysis scripts are publicly available from GitHub: https://github.com/ivasilyev/curated_projects/tree/master/ashestopalov/nutrition/obesity_elisa

RESULTS

Clinical and laboratory characteristics of the surveyed individuals of groups 1 and 2 are provided in Table 1.

The control group and obese patients were matched for gender and the TC and LDL-C levels. Furthermore, the subjects of group 1 were younger (*p* = 0.032), they had lower BMI (*p* = 0.024) and WC (*p* = 0.011). Obese patients had higher SBP, DBP, TG, FPG, insulin levels, HOMA (*p* < 0.05) and lower HDL-C (*p* < 0.05) than the control group. Clinical and laboratory characteristics of the surveyed individuals of subgroups 2a and 2b are provided in Table 2.

Subgroups 2a and 2b were matched for the number of males and females, subjects' age, BMI, and WC. When comparing patients with different obese phenotypes, significant differences in various indicators were revealed: SBP, DBP, TG, FPG, insulin, and HOMA were higher (*p* < 0.05) and HDL-C was lower (*p* < 0.05) in the MUO subgroup than in the MHO subgroup. Particularly noteworthy, however, was hyperglycemia in patients of the subgroup 2b that corresponded not to prediabetes, the early carbohydrate metabolism disorder, but to diabetes mellitus. By comparison, normal blood glucose levels were observed in the subgroup 2a, despite insulin resistance revealed in both groups. In the subgroup 2b a more than twofold increase in blood levels of triglycerides suggesting triglyceride storage impairment due to the adipose tissue insulin resistance that resulted in lipotoxicity, i.e. extracellular triglyceride accumulation, was noteworthy.

Comparative analysis of the adipokine and myokine levels in the subjects of groups 1 and 2 revealed significant differences in the levels of adiponectin, leptin, and asprosin. Obese patients had lower adiponectin levels (*p* < 0.05) and higher leptin and asprosin levels (*p* < 0.05) than healthy individuals (Table 3). It is known that leptin is a key mediator of interaction between

Table 2. Clinical and laboratory characteristics of the surveyed individuals of subgroups 2a and 2b

Parameters	Subgroup 2a <i>n</i> = 40	Subgroup 2b <i>n</i> = 55	<i>p</i>
Males	6 (15%)	11 (20%)	0.612
Females	34 (85%)	44 (80%)	0.510
Age, years	49.05 ± 5.1	51.3 ± 3.6	0.734
BMI, kg/m ²	33 [31; 36]	33 [31; 36]	0.591
WC, cm	100 [96; 104]	100 [93; 102]	0.112
SBP, mm Hg	120 [110; 125]	145 [136; 150]	< 0.0001
DBP, mm Hg	75 [70; 80]	90 [90; 95]	< 0.0001
FPG, mmol/L	4.88 [4.57; 5.28]	7.2 [6.14; 8.62]	< 0.0001
HOMA-IR	7.48 [3.3; 12]	14.4 [7.57; 27.37]	0.0003
TC, mmol/L	5.08 [4.31; 6.01]	5.74 [4.57; 6.5]	0.102
LDL-C, mmol/L	3.18 [2.78; 3.53]	3.1 [1.95; 3.79]	0.341
HDL-C, mmol/L	1.3 [1.21; 1.47]	1.2 [1.08; 1.45]	0.022
TG, mmol/L	1.19 [0.91; 1.46]	2.39 [1.77; 3.16]	< 0.0001
Insulin, pg/mL	284.92 [142.25; 529.07]	389.96 [221; 721.57]	0.050

Note: BMI — body mass index, WC — waist circumference, SBP — systolic blood pressure, DBP — diastolic blood pressure, TC — total cholesterol, LDL-C — low density lipoprotein cholesterol, HDL-C — high density lipoprotein cholesterol, TG — triglycerides, HOMA-IR — Homeostasis Model Assessment of Insulin Resistance.

the adipose tissue and the hypothalamic-pituitary axis that exerts orexigenic effect. High leptin levels in the group of obese patients suggest the leptin orexigenic effect inhibition due to resistance to appropriate signals developed by the central nervous system, i.e. these suggest the development of insulin resistance characterized by low satiety, excessive intake of nutrients, and weight gain.

When comparing serum levels of adipokines and myokines in patients with MHO, MUO and healthy donors the following earlier detected trends were observed: patients with MHO and MUO had significantly lower adiponectin levels ($p < 0.05$) and significantly higher leptin and asprosin levels ($p < 0.05$) compared to the control group. Furthermore, patients with MUO had lower adiponectin and leptin levels ($p < 0.05$) than patients with MHO. A significant increase in the levels of FGF21 was also observed in patients with MUO (Table 4). Given its insulin sensitizing effect, the decrease in adiponectin levels fits into the general picture of insulin resistance. The lower leptin levels in patients with MUO that seem paradoxical at first glance are likely to result from the adipose tissue insulin resistance that leads to impaired terminal differentiation into adipocytes, abnormal extracellular triglyceride deposition, and lipotoxicity.

The correlation analysis has revealed positive correlations between the levels of adiponectin and resistin ($r = 0.428$;

$p = 0.001$), FGF21 and myostatin ($r = 0.543$; $p = 0.001$), insulin and leptin ($r = 0.429$; $p = 0.0001$) in healthy donors. This suggests normal balance in the insulin sensitivity regulation system and the adipose and muscle tissue endocrine function.

Positive correlations between the adiponectin levels and the levels of insulin ($r = 0.3$; $p = 0.008$), leptin ($r = 0.3$; $p = 0.008$), resistin ($r = 0.5$; $p < 0.0001$), and VEGF ($r = 0.49$; $p < 0.0001$) were revealed in obese patients. Moreover, there were significant correlations between the levels of the FGF21 myokine and myostatin ($r = 0.37$; $p = 0.0001$), as well as between the levels of insulin and leptin ($r = 0.84$; $p < 0.0001$). The leptin levels were also correlated to the VEGF levels ($r = 0.38$; $p = 0.002$), while resistin levels were correlated to the osteocin levels ($r = 0.33$; $p = 0.0006$). Such correlations are indicative of the imbalances in the regulatory system and the involvement of hypoxia-inducible factor in the regulatory system, since there are positive correlations between adiponectin and leptin and between leptin and VEGF.

Patients with MHO showed the following correlations of osteocin levels: negative correlation with asprosin ($r = -0.43$; $p = 0.02$) and resistin ($r = -0.39$; $p = 0.01$), positive correlation with adiponectin ($r = 0.43$; $p = 0.04$). The relationships were revealed between the levels of adiponectin and myostatin ($r = 0.34$; $p = 0.035$), insulin and leptin ($r = 0.59$; $p < 0.0001$), FGF21 and adiponectin ($r = 0.34$; $p = 0.0003$).

Table 3. Serum levels of adipokines and myokines in healthy individuals and obese patients

Indicators	Group 1 <i>n</i> = 129	Group 2 <i>n</i> = 136	<i>p</i>
Adiponectin, ng/mL	2149800 [62542; 6457800]	591180 [22366; 6457800]	0.05
Leptin, pg/mL	3999.96 [1120.19; 10099.7]	11291.99 [5541.55; 17827.94]	< 0.0001
Resistin, pg/mL	52364.75 [32515.5; 116732]	46147.46 [27968.18; 104077.3]	0.35
Asprosin, pg/mL	0.18 [0; 0.36]	0.35 [0; 0.54]	0.01
VEGF, pg/mL	73.18 [44.93; 139.3]	58.45 [35.45; 143.28]	0.19
Insulin, pg/mL	262 [133.6; 418.2]	390 [170.02; 678.78]	0.001
Osteocin, pg/mL	55.23 [37.7; 74.28]	45.23 [34.15; 69.60]	0.14
Myostatin, pg/mL	0 [0; 0]	0 [0; 0]	0.6
Irisin, pg/mL	0 [0; 0]	0 [0; 0]	0.58
FGF21, pg/mL	0 [0; 56.86]	0 [0; 83.45]	0.14

Table 4. Serum levels of adipokines and myokines in subjects of the group 1 subgroups 2a and 2b

Parameters	Group 1 <i>n</i> = 129	Subgroup 2a <i>n</i> = 40	P_{1p1-2a}	Subgroup 2b <i>n</i> = 55	P_{1p1-2b}	P_{2a-2b}
Adiponectin, ng/mL	214980 [62542; 6457800]	75 618 [25132; 6457800]	< 0.052	57 891 [22616.75; 2606600]	< 0.054	0.003
Leptin, pg/mL	3999.96 [1120.19; 10099.7]	13808.18 [6332.91; 17956.46]	< 0.051	9942.72 [4664.47; 16802.91]	< 0.055	0.002
Insulin, pg/mL	262 [133.6; 418.2]	284 [142.25; 529.07]	0.01	389 [221.22; 721.57]	< 0.054	0.05
Asprosin, pg/mL	0.18 [0; 0.36]	0.46 [0.23; 0.6]	< 0.05	0.38 [0; 0.57]	< 0.05	0.37
FGF21, pg/mL	0 [0; 56.8]	0 [0; 31.44]	< 0.01	13.98 [0; 90.49]	0.005	0.05
Resistin, pg/mL	52364.75 [32515.5; 116732]	48637.48 [33229.66; 97603.33]	0.05	43421.05 [26433.69; 109927.65]	0.06	0.7
VEGF, pg/mL	73.18 [44.93; 139.3]	56.33 [19.89; 145.32]	< 0.05	58.97 [39.61; 163.05]	0.026	0.34
Osteocrin, pg/mL	55.23 [37.7; 74.28]	44.03 [35.91; 59.08]	0.016	48.96 [32.22; 78.6]	0.017	0.57
Myostatin, pg/mL	0 [0; 0]	0 [0; 0]	0.23	0 [0; 0]	0.3	0.6
Irisin, pg/mL	0 [0; 0]	0 [0; 0]	0.034	0 [0; 0]	0.026	0.7

The correlations of osteocrin with asprosin ($r = -0.38$; $p = 0.04$), resistin ($r = 0.48$; $p = 0.001$), and myostatin ($r = 0.33$; $p = 0.03$) were revealed in patients with MUO. There were significant positive correlations between FGF21 and myostatin ($r = 0.37$; $p = 0.005$), insulin and leptin ($r = 0.37$; $p = 0.005$). Thus, the role of osteocrin in regulation of the adipose and muscle tissue endocrine function becomes more and more important with the development of obesity. No correlations of osteocrin have been found in healthy individuals. There are two correlations of osteocrin with adipokines (asprosin and resistin) in the group with MHO and three such correlations that expand the range to the myostatin myokine in the group with MUO. Therefore, obesity is associated with the interrelated alterations in all three mesenchymal stem cell differentiation branches: adipogenic, myogenic, and osteogenic. It should be noted that positive correlations between insulin and leptin are observed in all studied groups. These are maximal in the group with MHO, which suggests that the effects of insulin on the adipose tissue are preserved, and are minimal in the group with MUO, which could be indirect evidence of the adipose tissue insulin resistance. Also noteworthy is the change of the FGF21 regulatory effects with the development of obesity. In healthy donors and patients with MUO, this myokine positively correlates with the other myokine, myostatin, while in patients with MHO is correlates with adiponectin and myostatin. Perhaps the FGF21–adiponectin regulatory axis is one of the compensatory mechanisms in the adipose tissue–muscle tissue system that allows the adipose tissue to retain insulin sensitivity in obese patients and prevent lipotoxicity.

To assess alpha diversity of the bacterial community in the studied groups, we calculated the Simpson and Shannon phylogenetic diversity indices, Chao1 index, and OTUs. Significant differences in the phylogenetic diversity index and Chao1 index between controls and obese patients have been found, which suggest reduced alpha diversity in fecal samples of obese patients. However, there are no differences in the Shannon index between groups 1 and 2 [21, 22].

It should be noted that the Shannon index, Chao1 index, and OTUs were significantly higher in patients with MHO than in the group with MUO and the group of healthy donors. The increased alpha diversity is likely to be a protective mechanism of the microbial community that prevents metabolic disorders in obese individuals.

The large-scale correlation analysis that revealed positively related ($r \geq 0.3$) clusters typical for each obese phenotype was performed in subgroups 2a and 2b. Thus, the following clustering type was typical for the subgroup of patients with MHO: 1) correlations of glucose levels with inverse gut microbiome diversity indices (Berger–Parker index, Gini–Simpson index, inverse Simpson index); 2) correlations of the levels of leptin, insulin, irisin and HOMA values with the VEGF concentrations; 3) correlations of the FGF21 and HDL-C concentrations with the direct gut microbiome diversity indices (Chao1 index, OTUs, Shannon index, Simpson index) (Fig. 1).

Clustering of the correlation between glucose levels and inverse gut microbiome diversity indices demonstrates the relationship between microbiota and glucose levels, it suggests that gut microbiota of individuals with MHO affects glucose concentration and probably keeps glucose at normal levels, despite the presence of obesity. Clustering of the correlation between VEGF levels and the carbohydrate metabolism indicators together with insulin sensitivity shows that hypoxia has a regulatory effect in individuals with MHO. Clustering of the correlation of the direct gut microbiome diversity indices with the FGF21 and HDL-C levels suggests that microbial diversity has a protective effect in individuals with this obese phenotype, probably due to preservation of the microbiota–liver–adipose tissue regulatory axis.

It is important to note that no clustering of the gut microbiota diversity indicators with the glucose levels typical for MHO was observed in patients with the MUO phenotype. This suggests the loss of gut microbiota influence on the regulation of blood glucose levels (Fig. 2). Furthermore, inverse diversity indices in individuals with MUO were highly correlated to BMI, SBP, DBP, LDL-C, TC, HOMA-IR, and insulin, while direct gut microbiome

Table 5. Characteristics of the stool microbiome alpha diversity in the studied groups of patients

Indices	Group 1 (control)	Group 2 (obesity)	Subgroup 2a (MHO)	Subgroup 2b (MUO)
Simpson index	0.981 [0.979–0.982]	0.977 [0.975–0.981]	0.978 [0.971–0.986]	0.976 [0.973–0.981]
Shannon index	7.80 [7.71–7.90]	7.82 [7.63–8.11]	8.28* [7.67–8.76]	7.63† [7.46–7.90]
Chao1 index	4010.16 [3871.53–4256.37]	4018.56* [3647.52–4492.64]	4899.13* [4139.88–5384.25]	3631.75† [3214.01–4118.26]
OTUs	1974.50 [1865.86–2060.00]	2015.00 [1930.17–2285.94]	2479.00* [1982.88–2727.61]	1930.00† [1743.64–2125.33]

Note: the data are presented as median and 95% confidence interval; * — significant differences from group 1 ($p < 0.05$); † — significant differences from patients with MHO ($p < 0.05$)

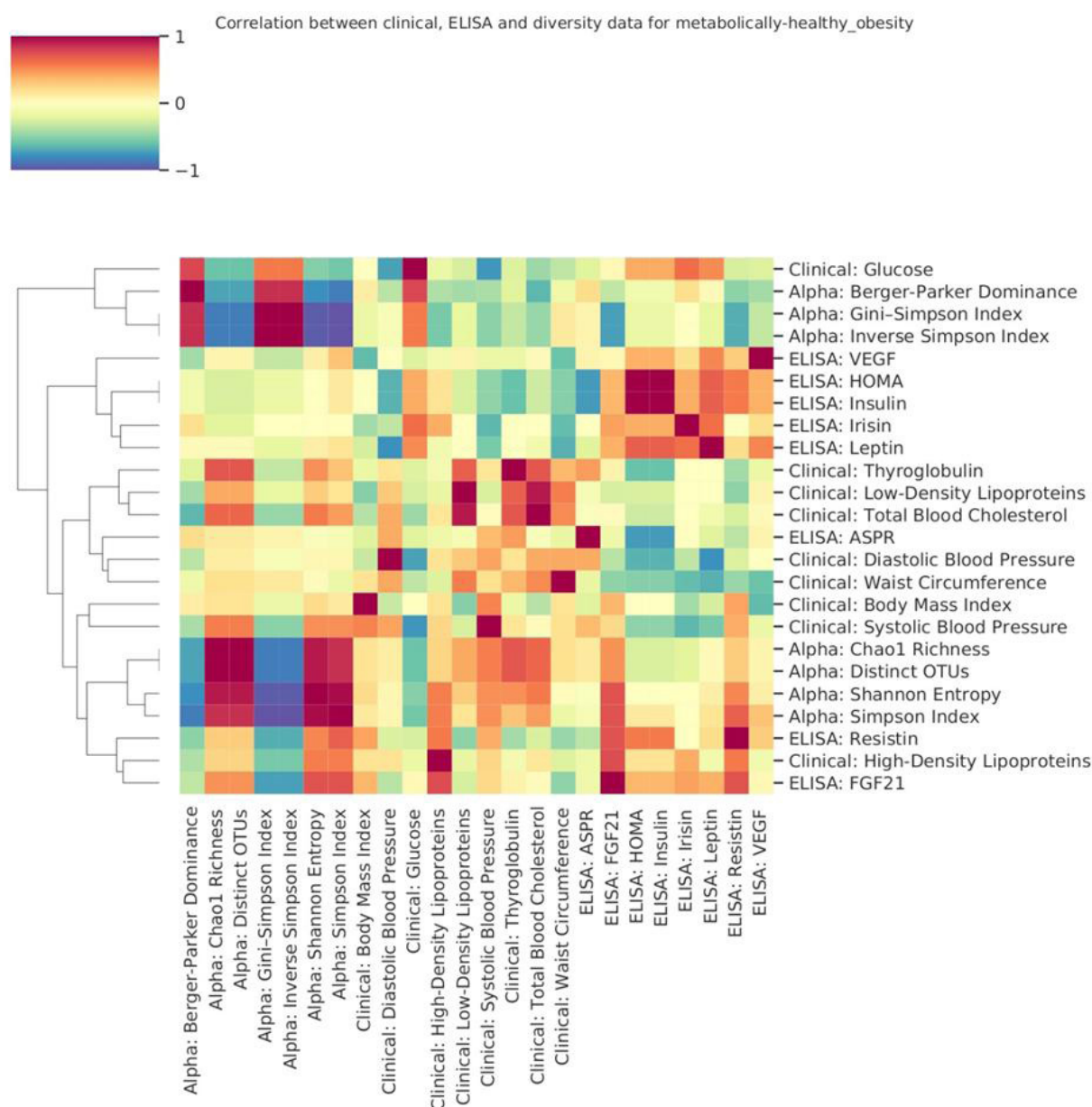


Fig. 1. Clustermap of the correlations between glucose, adipokines, myokines, lipid profile and the gut microbiome diversity indicators for the group of patients with MHO

diversity indices were highly correlated to myostatin, TG, VEGF, FGF21, resistin, and leptin. This suggests that the decrease in the microbial community diversity in individuals with this type of obesity is directly related to the clinical and biochemical manifestations of metabolic syndrome and type 2 diabetes mellitus.

The results obtained suggest that gut microbiota plays different regulatory roles in the gut microbiome–liver–muscle/adipose tissue axis in individuals with various obese phenotypes. The findings also provide evidence of the emergence of abnormal relationships associated with MUO.

DISCUSSION

The roles of microbial community and endocrine factors of adipose and muscle tissues in obesity are quite fully investigated [2, 4, 5]. However, these studies rarely addressed the differences between the obese phenotypes and the correlations of the microbiome characteristics with the adipokine and myokine levels. Our study revealed

alterations in the serum adipokine and myokine profiles consisting of the significant decrease in the adiponectin levels amid the increasing levels of insulin, leptin, and asprosin. This generally reflected the development of insulin resistance, leptin resistance, and, therefore, impaired storage function of adipose tissue and appetite regulation. Downregulation of adiponectin is consistent with the data obtained by other authors [1, 6]. Similar patterns have been previously shown for the levels of leptin and insulin [1, 23]. Higher adiponectin levels and lower leptin levels in healthy individuals are probably due to the lack of terminal adipocyte hypertrophy, preserved adipocyte storage function and metabolic plasticity. That is why such adipocytes must be characterized by high insulin resistance. At the same time, obese individuals may show hyperplasia and hypertrophy of adipocytes, the cytoplasm of which is completely filled with TG. These block further TG deposition in accordance with the negative feedback principle and, consequently, disrupt adipocyte metabolic plasticity [24]. Such remodeling results in ectopic fat accumulation and altered adipocyte morphology, being the triggers of insulin resistance associated with the

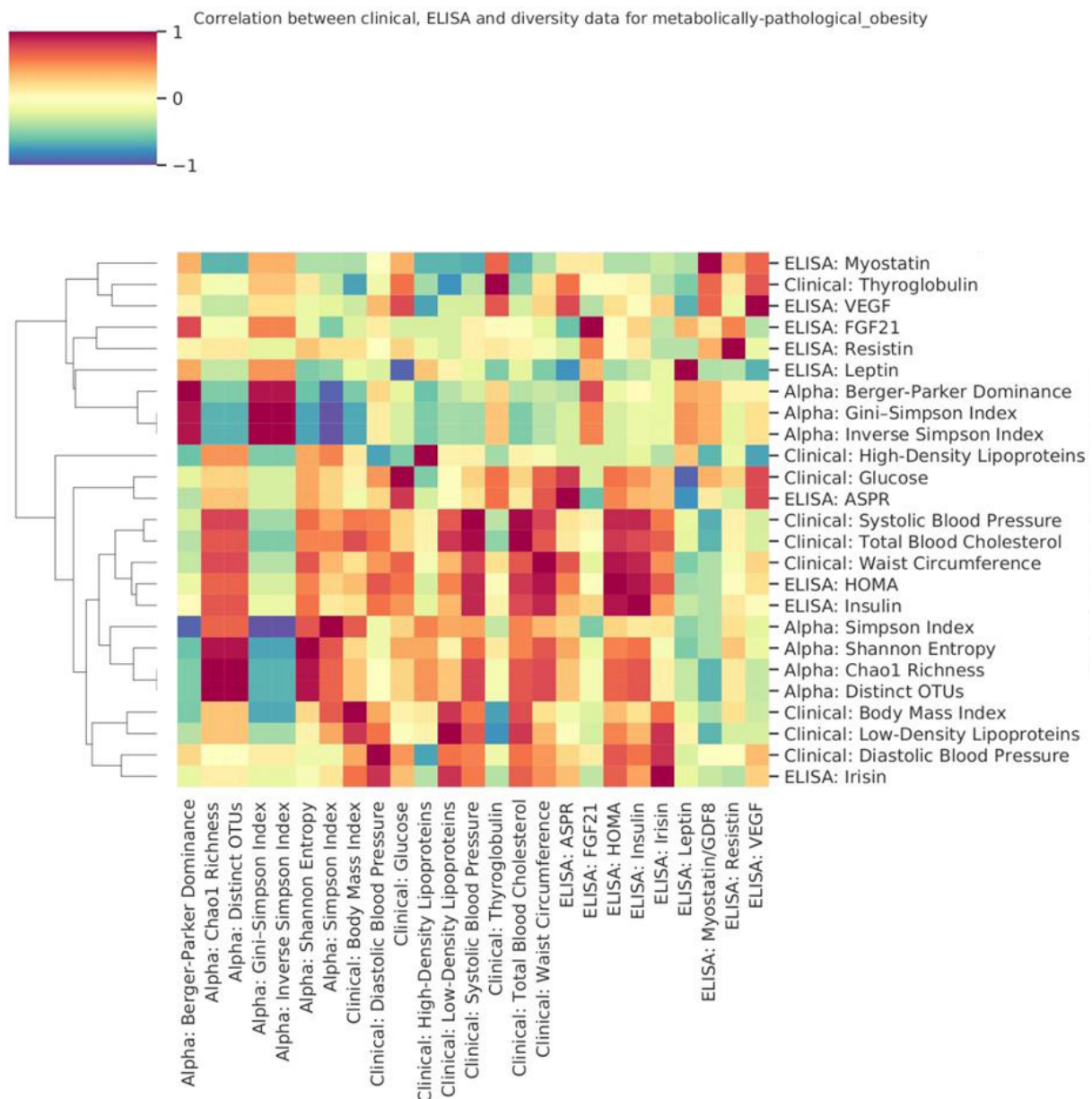


Fig. 2. Clustermap of the correlations between glucose, adipokines, myokines, lipid profile and the gut microbiome diversity indicators for the group of patients with MUO

decreased adiponectin levels and the increased leptin levels. Elevated leptin levels are probably associated with leptin resistance, in which smaller amounts of leptin would reach the brain, thereby decreasing activation of the signaling pathway for body weight regulation. Leptin resistance at the blood-brain barrier (BBB) level is due to the receptor saturation effects caused by excess leptin or reversible inhibition by circulating factors, such as TG [25].

Information about the role of asprosin in obesity is extremely fragmented [26]. The results of this study show higher asprosin levels in obese patients compared to healthy individuals. In the study the levels of asprosin in obese individuals are higher than that in healthy people. It is well-known that asprosin secreted by white adipose tissue increases appetite. Since obesity is associated with the increase in the number of adipocytes, then the asprosin levels increase, which, in turn, results in activation of orexigenic neurons by the agouti-related protein (AgRP) and increased appetite to form a vicious circle [27]. Therefore there are speculations that asprosin can contribute to the development of obesity by affecting food intake.

MHO is characterized by alterations that are similar in all types of obesity, however, lipotoxicity manifestations are minimal. The maximum leptin levels, highest correlation between insulin and leptin, and the relationship between FGF21 and adiponectin are typical for this phenotype. On the one hand, this shows preserved effects of insulin in the adipose tissue, and on the other hand activation of the FGF21–adiponectin regulatory mechanism probably allowing to preserve insulin sensitivity of adipose tissue in individuals with this obese phenotype and to prevent lipotoxicity. The relationship between the gut microbial community diversity and the clinical and laboratory indicators suggests that microbiota is involved in regulation of glucose levels and that the diversity indices have a protective effect on the indicators of cholesterol metabolism, which is probably evidence of preserved microbiota–liver–adipose tissue regulatory axis.

As we have shown earlier, alterations in the share of the main microbiome members, Bacteroidetes and Firmicutes, associated with MHO are less severe than these associated with MUO. Perhaps these alterations are not critical for metabolic

function of the microbial community as a whole, as well as for production of regulatory molecules and metabolites (indoles, kynurenines, short-chain fatty acids, secondary bile acids, vitamins, and essential amino acids), and are compensated by the increased diversity that consequently ensures preservation of the microbiota–liver–adipose tissue regulatory axis.

MUO is characterized by the most severe manifestations of the carbohydrate metabolism disorders, lipotoxicity, and dyslipoproteinemia. Furthermore, patients with MUO have lower adiponectin and leptin levels than patients with MHO. The significantly increased FGF21 levels have been also found in individuals with MUO. Perhaps, elevated FGF21 levels associated with MUO constitute a dysfunctional compensatory mechanism for hyperglycemia, since adipocytes that have reached critical hypertrophy show insulin resistance and are unable to utilise glucose. In this regard, there is a need to form an extra glucose metabolism pathway in order to relieve hyperglycemia. In particular, the increase in the muscle metabolism rate activates glucose utilization by the muscle tissue (myokine FGF21). It is important to note that the missing relationship between the glucose levels and the gut microbiome alpha diversity indicators is a feature of the MUO phenotype. This is indicative of the loss of regulatory effects by the gut microbiome in the microbiota–liver–adipose tissue axis and the emergence of abnormal relationships in individuals with this obese phenotype.

The cause of lower adiponectin concentrations in individuals with MUO compared to MHO is unknown, however, it can be related to the MUO-associated chronic hyperinsulinemia that suppresses adiponectin production by adipose tissue and thereby generates a feedback loop for the decreased insulin secretion caused by insulin resistance [3, 28]. In our study the leptin levels found in patients with MUO were significantly higher than these found in patients with MHO. Such results

were consistent with the data obtained by other authors [29] and were possibly due to abnormal protein synthesis in hypertrophic adipocytes. However, the leptin contribution to the MUO pathogenesis needs to be clarified, since there are studies that have revealed significantly higher leptin levels in patients with MUO [30] or no differences at all [31]. In addition to the common significant correlations, the correlations typical for MUO have been revealed, such as a significant positive correlation between the myostatin and osteocrin levels. In contrast to patients with MHO, the gut microbiome alpha diversity indicators of patients with MUO significantly decreased and no longer correlated with blood glucose levels, while the inverse indices became correlated to the clinical and laboratory indicators of metabolic syndrome and type 2 diabetes mellitus.

CONCLUSIONS

Thus, the levels of leptin, asprosin, and insulin are significantly higher ($p < 0.05$) and adiponectin levels are lower in obese patients than in healthy individuals. Correlation analysis revealed imbalances in the regulatory system involving the hypoxia-inducible factor and interrelated changes in the adipogenic, myogenic, and osteogenic mesenchymal stem cell differentiation. Large-scale correlation analysis allowed us to reveal the loss of the microbiota diversity protective effects on metabolic processes in individuals with MUO. Further study of the relationship between gut microbiota and both lipid metabolism and carbohydrate indicators would contribute to further improvement of the therapeutic strategy for obesity and associated metabolic disorders through the development of the microbiome-based therapy of obesity. Furthermore, the data obtained may be used for early prevention of metabolic disorders and MUO conversion into MHO.

References

- Frühbeck G, Catalán V, Rodríguez A, Gómez-Ambrosi J. Adiponectin-leptin ratio: A promising index to estimate adipose tissue dysfunction. Relation with obesity-associated cardiometabolic risk. *Adipocyte*. 2018; 7 (1): 57–62. DOI: 10.1080/21623945.2017.1402151.
- Iacobini C, Pugliese G, Blasetti Fantauzzi C, et al. Metabolically healthy versus metabolically unhealthy obesity. *Metabolism*. 2019; 92: 51–60. DOI: 10.1016/j.metabol.2018.11.009.
- Smith GI, Mittendorfer B, Klein S. Metabolically healthy obesity: facts and fantasies. *J Clin Invest*. 2019; 129 (10): 3978–89. DOI: 10.1172/JCI129186.
- Garvey WT, Garber AJ, Mechanick JL, et al. The AACE Obesity Scientific Committee. American association of clinical endocrinologists and American college of endocrinology position statement on the 2014 advanced framework for a new diagnosis of obesity as a chronic disease. *Endocr Pract*. 2014; 20 (9): 977–89. DOI: 10.4158/EP14280.PS.
- Graf C, Ferrari N. Metabolic Health-The Role of Adipo-Myokines. *Int J Mol Sci*. 2019; 20 (24): 6159. DOI: 10.3390/ijms20246159.
- Bakhal A. Adipokines--targeting a root cause of cardiometabolic risk. *QJM*. 2008; 101 (10): 767–76. DOI: 10.1093/qjmed/hcn066.
- Doumatey AP, Bentley AR, Zhou J, Huang H, Adeyemo A, Rotimi CN. Paradoxical Hyperadiponectinemia is Associated With the Metabolically Healthy Obese (MHO) Phenotype in African Americans. *J Endocrinol Metab*. 2012; 2 (2): 51–65. DOI: 10.4021/jem95W.
- Bluher S. Metabolically healthy obesity from childhood to adulthood — does weight status alone matter? *Metabolism*. 2014; 63: 1084–109.
- Wang HY. Plasma asprosin concentrations are increased in individuals with glucose dysregulation and correlated with insulin resistance and first-phase insulin secretion. *Mediators of Inflammation*. 2018; ID 9471583.
- Amor M, Itariu BK, Moreno-Viedma V, Keindl M, Jürets A, Prager G, et al. Serum Myostatin is Upregulated in Obesity and Correlates with Insulin Resistance in Humans. *Exp Clin Endocrinol Diabetes*. 2019; 127 (8): 550–6.
- Staiger H, Keuper M, Berti L, Hrabe de Angelis M, Häring HU. Fibroblast Growth Factor 21-Metabolic Role in Mice and Men. *Endocr Rev*. 2017; 38 (5): 468–88.
- Hu C, Zhang X, Zhang N, Wei WY, Li LL, Ma ZG, et al. Osteocrin attenuates inflammation, oxidative stress, apoptosis, and cardiac dysfunction in doxorubicin-induced cardiotoxicity. *Clin Transl Med*. 2020; 10 (3): e124.
- Fu J, Li Y, Esangbedo IC, Li G, Feng D, Li L, et al. Circulating Osteonectin and Adipokine Profiles in Relation to Metabolically Healthy Obesity in Chinese Children: Findings From BCAMS. *J Am Heart Assoc*. 2018; 7 (23): e009169. DOI: 10.1161/JAHA.118.009169.
- Rinninella E, Raoul P, Cintoni M, Franceschi F, Miggiano GAD, Gasbarrini A, et al. What is the healthy gut microbiota composition? A changing ecosystem across age, environment, diet, and diseases. *Microorganisms*. 2019; 7 (1): 14. DOI: 10.3390/microorganisms7010014.
- Stoma IO, Karpov IA. *Мікробіом людини*. Мінск: Доктор Дізаїн, 2018; 122 с. Russian.
- Bombin A, Yan S, Bombin S, Mosley JD, Ferguson JF. Obesity influences composition of salivary and fecal microbiota and

- impacts the interactions between bacterial taxa. *Physiological Reports*. 2022; 10: e15254. Available from: <https://doi.org/10.14814/phy2.15254>.
17. Aron-Wisnewsky J, Prifti E, Belda E, et al. Major microbiota dysbiosis in severe obesity: fate after bariatric surgery. *Gut*. 2019; 68 (1): 70–82. DOI: 10.1136/gutjnl-2018-316103.
 18. Cotillard A, Kennedy SP, Kong LC, Edi Prifti, Nicolas Pons, Emmanuelle Le Chatelier, et al. Dietary intervention impact on gut microbial gene richness. *Nature*. 2013; 500 (7464): 585–8. DOI: 10.1038/nature12480. Erratum in: *Nature*. 2013; 502 (7472) 580.
 19. Everard A, Belzer C, Geurts L, et al. Cross-talk between *Akkermansia muciniphila* and intestinal epithelium controls diet-induced obesity. *Proc Natl Acad Sci USA*. 2013; 110 (22): 9066–71. DOI: 10.1073/pnas.1219451110.
 20. Menshikov VV, редактор. *Методики клинических лабораторных исследований. Справочное пособие. Том 3. М.: Лабора, 2009; 880 с. Russian.*
 21. Gaponov AM, Volkova NI, Ganenko LA, Naboka YuL, Markelova MI, Sinyagina MN, i dr. Osobennosti mikrobioma tolstoj kishki u pacientov s ozhireniem pri ego razlichnyx fenotipax. *Zhurnal mikrobiologii, ehpidemiologii i immunobiologii*. 2021; 98 (2): 144–155. Dostupno po ssylke: <https://doi.org/10.36233/0372-9311-66>. Russian.
 22. Kolesnikova IM, Gaponov AM, Ganenko LA, Volkova NI, Grigoreva TV, Lajkov AV, i dr. Vzaimosvyaz' soderzhaniya nejrotrofov kishhechnogo mikrobioma pri razlichnyx metabolicheskix tipax ozhireniya. *Zhurnal ehvolucionnoj bioximii i fiziologii*. 2022; 58 (54): 298–310. Russian.
 23. Yosae S, Khodadost M, Esteghamati A, et al. Adiponectin: An Indicator for Metabolic Syndrome. *Iran J Public Health*. 2019; 48 (6): 1106–15.
 24. Gustafson B, Hedjazifar S, Gogg S, Hammarstedt A, Smith U. Insulin resistance and impaired adipogenesis. *Trends Endocrinol Metab*. 2015; 26 (4): 193–200. DOI: 10.1016/j.tem.2015.01.006.
 25. Izquierdo AG, Crujeiras AB, Casanueva FF, Carreira MC. Leptin, obesity, and leptin resistance: where are we 25 years later? *Nutrients*. 2019; 11 (11): 2704. DOI: 10.3390/nu11112704.
 26. Yuan M, Li W, Zhu Y, et al. Asprosin: A novel player in metabolic diseases. *Front Endocrinol (Lausanne)*. 2020; 11: 64. DOI: 10.3389/fendo.2020.00064.
 27. Ugur K, Aydin S. Saliva and blood asprosin hormone concentration associated with obesity. *Int J Endocrinol*. 2019; 2019: 2521096. DOI: 10.1155/2019/2521096.
 28. Elisha B, Karelis AD, Imbeault P, et al. Effects of acute hyperinsulinaemia on total and high-molecular-weight adiponectin concentration in metabolically healthy but obese postmenopausal women: a Montreal-Ottawa New Emerging Team (MONET) study. *Diabetes Metab*. 2010; 36 (4): 319–21. DOI: 10.1016/j.diabet.2010.03.004.
 29. Ung UJ, Choi M-S. Obesity and its metabolic complications: the role of adipokines and the relationship between obesity, inflammation, insulin resistance, dyslipidemia and nonalcoholic fatty liver disease. *International Journal of Molecular Sciences*. 2014; 15 (4): 6184–223. Available from: <https://doi.org/10.3390/ijms15046184111,112>.
 30. Jamar G, Caranti DA, de Cassia Cesar H, et al. Leptin as a cardiovascular risk marker in metabolically healthy obese: Hyperleptinemia in metabolically healthy obese. *Appetite*. 2017; 108: 477–82. DOI: 10.1016/j.appet.2016.11.013.
 31. Fu J, Li Y, Esangbedo IC, et al. Circulating osteonectin and adipokine profiles in relation to metabolically healthy obesity in chinese children: findings from BCAMS. *J Am Heart Assoc*. 2018; 7 (23): e009169. DOI: 10.1161/JAHA.118.009169.

Литература

1. Frühbeck G, Catalán V, Rodríguez A, Gómez-Ambrosi J. Adiponectin-leptin ratio: A promising index to estimate adipose tissue dysfunction. Relation with obesity-associated cardiometabolic risk. *Adipocyte*. 2018; 7 (1): 57–62. DOI: 10.1080/21623945.2017.1402151.
2. Iacobini C, Pugliese G, Blasetti Fantauzzi C, et al. Metabolically healthy versus metabolically unhealthy obesity. *Metabolism*. 2019; 92: 51–60. DOI: 10.1016/j.metabol.2018.11.009.
3. Smith GI, Mittendorfer B, Klein S. Metabolically healthy obesity: facts and fantasies. *J Clin Invest*. 2019; 129 (10): 3978–89. DOI: 10.1172/JCI129186.
4. Garvey WT, Garber AJ, Mechanick JL, et al. The AACE Obesity Scientific Committee. American association of clinical endocrinologists and American college of endocrinology position statement on the 2014 advanced framework for a new diagnosis of obesity as a chronic disease. *Endocr Pract*. 2014; 20 (9): 977–89. DOI: 10.4158/EP14280.PS.
5. Graf C, Ferrari N. Metabolic Health-The Role of Adipo-Myokines. *Int J Mol Sci*. 2019; 20 (24): 6159. DOI: 10.3390/ijms20246159.
6. Bakhai A. Adipokines--targeting a root cause of cardiometabolic risk. *QJM*. 2008; 101 (10): 767–76. DOI: 10.1093/qjmed/hcn066.
7. Doumatey AP, Bentley AR, Zhou J, Huang H, Adeyemo A, Rotimi CN. Paradoxical Hyperadiponectinemia is Associated With the Metabolically Healthy Obese (MHO) Phenotype in African Americans. *J Endocrinol Metab*. 2012; 2 (2): 51–65. DOI: 10.4021/jem95W.
8. Bluher S. Metabolically healthy obesity from childhood to adulthood — does weight status alone matter? *Metabolism*. 2014; 63: 1084–109.
9. Wang HY. Plasma asprosin concentrations are increased in individuals with glucose dysregulation and correlated with insulin resistance and first-phase insulin secretion. *Mediators of Inflammation*. 2018; ID 9471583.
10. Amor M, Itariu BK, Moreno-Viedma V, Keindl M, Jürets A, Prager G, et al. Serum Myostatin is Upregulated in Obesity and Correlates with Insulin Resistance in Humans. *Exp Clin Endocrinol Diabetes*. 2019; 127 (8): 550–6.
11. Staiger H, Keuper M, Berti L, Hrabec de Angelis M, Häring HU. Fibroblast Growth Factor 21-Metabolic Role in Mice and Men. *Endocr Rev*. 2017; 38 (5): 468–88.
12. Hu C, Zhang X, Zhang N, Wei WY, Li LL, Ma ZG, et al. Osteocrin attenuates inflammation, oxidative stress, apoptosis, and cardiac dysfunction in doxorubicin-induced cardiotoxicity. *Clin Transl Med*. 2020; 10 (3): e124.
13. Fu J, Li Y, Esangbedo IC, Li G, Feng D, Li L, et al. Circulating Osteonectin and Adipokine Profiles in Relation to Metabolically Healthy Obesity in Chinese Children: Findings From BCAMS. *J Am Heart Assoc*. 2018; 7 (23): e009169. DOI: 10.1161/JAHA.118.009169.
14. Rinnella E, Raoul P, Cintoni M, Franceschi F, Miggiano GAD, Gasbarrini A, et al. What is the healthy gut microbiota composition? A changing ecosystem across age, environment, diet, and diseases. *Microorganisms*. 2019; 7 (1): 14. DOI: 10.3390/microorganisms7010014.
15. Стома И. О., Карпов И. А. *Микробиом человека. Минск: Доктор Дизайн, 2018; 122 с.*
16. Bombin A, Yan S, Bombin S, Mosley JD, Ferguson JF. Obesity influences composition of salivary and fecal microbiota and impacts the interactions between bacterial taxa. *Physiological Reports*. 2022; 10: e15254. Available from: <https://doi.org/10.14814/phy2.15254>.
17. Aron-Wisnewsky J, Prifti E, Belda E, et al. Major microbiota dysbiosis in severe obesity: fate after bariatric surgery. *Gut*. 2019; 68 (1): 70–82. DOI: 10.1136/gutjnl-2018-316103.
18. Cotillard A, Kennedy SP, Kong LC, Edi Prifti, Nicolas Pons, Emmanuelle Le Chatelier, et al. Dietary intervention impact on gut microbial gene richness. *Nature*. 2013; 500 (7464): 585–8. DOI: 10.1038/nature12480. Erratum in: *Nature*. 2013; 502 (7472) 580.
19. Everard A, Belzer C, Geurts L, et al. Cross-talk between *Akkermansia muciniphila* and intestinal epithelium controls diet-induced obesity. *Proc Natl Acad Sci USA*. 2013; 110 (22): 9066–71. DOI: 10.1073/pnas.1219451110.
20. Меньшиков В. В., редактор. *Методики клинических лабораторных исследований. Справочное пособие. Том 3. М.: Лабора, 2009; 880 с.*
21. Гапонов А. М., Волкова Н. И., Ганенко Л. А., Набока Ю. Л., Маркелова М. И., Синягина М. Н., и др. Особенности

- микробиома толстой кишки у пациентов с ожирением при его различных фенотипах. Журнал микробиологии, эпидемиологии и иммунобиологии. 2021; 98 (2): 144–155. Доступно по ссылке: <https://doi.org/10.36233/0372-9311-66>.
22. Колесникова И. М., Гапонов А. М., Ганенко Л. А., Волкова Н. И., Григорьева Т. В., Лайков А. В. и др. Взаимосвязь содержания нейротрофов кишечного микробиома при различных метаболических типах ожирения. Журнал эволюционной биохимии и физиологии. 2022; 58 (54): 298–310.
 23. Yosae S, Khodadost M, Esteghamati A, et al. Adiponectin: An Indicator for Metabolic Syndrome. Iran J Public Health. 2019; 48 (6): 1106–15.
 24. Gustafson B, Hedjazifar S, Gogg S, Hammarstedt A, Smith U. Insulin resistance and impaired adipogenesis. Trends Endocrinol Metab. 2015; 26 (4): 193–200. DOI: 10.1016/j.tem.2015.01.006.
 25. Izquierdo AG, Crujeiras AB, Casanueva FF, Carreira MC. Leptin, obesity, and leptin resistance: where are we 25 years later? Nutrients. 2019; 11 (11): 2704. DOI: 10.3390/nu11112704.
 26. Yuan M, Li W, Zhu Y, et al. Asprosin: A novel player in metabolic diseases. Front Endocrinol (Lausanne). 2020; 11: 64. DOI: 10.3389/fendo.2020.00064.
 27. Ugur K, Aydin S. Saliva and blood asprosin hormone concentration associated with obesity. Int J Endocrinol. 2019; 2019: 2521096. DOI: 10.1155/2019/2521096.
 28. Elisha B, Karelis AD, Imbeault P, et al. Effects of acute hyperinsulinaemia on total and high-molecular-weight adiponectin concentration in metabolically healthy but obese postmenopausal women: a Montreal-Ottawa New Emerging Team (MONET) study. Diabetes Metab. 2010; 36 (4): 319–21. DOI: 10.1016/j.diabet.2010.03.004.
 29. Ung UJ, Choi M-S. Obesity and its metabolic complications: the role of adipokines and the relationship between obesity, inflammation, insulin resistance, dyslipidemia and nonalcoholic fatty liver disease. International Journal of Molecular Sciences. 2014; 15 (4): 6184–223. Available from: <https://doi.org/10.3390/ijms15046184111,112>.
 30. Jamar G, Caranti DA, de Cassia Cesar H, et al. Leptin as a cardiovascular risk marker in metabolically healthy obese: Hyperleptinemia in metabolically healthy obese. Appetite. 2017; 108: 477–82. DOI: 10.1016/j.appet.2016.11.013.
 31. Fu J, Li Y, Esangbedo IC. et al. Circulating osteonectin and adipokine profiles in relation to metabolically healthy obesity in chinese children: findings from BCAMS. J Am Heart Assoc. 2018; 7 (23): e009169. DOI: 10.1161/JAHA.118.009169.

MAIN STATE INDUSTRIAL POLICY MEASURES FOR THE PHARMACEUTICAL INDUSTRY OF THE RUSSIAN FEDERATION

Gaydin TY^{1,2}, Geller EV², Rozhnova SA, Gaydina TA² ✉

¹ Department of Competition and Industrial Policy, Faculty of Economics, Lomonosov Moscow State University, Moscow, Russia

² Pirogov Russian National Research Medical University, Moscow, Russia

Due to the changes in the modern world, it is necessary to develop the domestic pharmaceutical industry, which is a task especially important in the context of implementation of the import substitution policy. The article classifies the main measures the state industrial policy has for the pharmaceutical industry; these measures cover informational and consulting aspects, research and technical parts, innovations and economic matters. Practical actions and their possible consequences are considered for each group of the industrial policy measures: encouragement of domestic consumption, regulation of imports, stimulation and support of exports, stimulation of technological development, public-private partnerships, support of the development of intersectoral territorial production complexes (clusters), direct state support of investment activities, tax incentives for investors.

Keywords: pharmaceutical industry, competition support, industrial policy, innovation, consumer welfare.

Author contribution: Gaydin TY, Geller EV — literature analysis, study conduct, manuscript authoring; Rozhnova SA, Gaydina TA — literature analysis, study planning and conduct, manuscript authoring.

✉ **Correspondence should be addressed:** Timofey Yu. Gaydin
Ostrovityanova, 1, Moscow, 117997, Russia; gaydin@econ.msu.ru

Received: 30.01.2023 **Accepted:** 17.02.2023 **Published online:** 28.02.2023

DOI: 10.24075/brsmu.2023.007

ОСНОВНЫЕ МЕРЫ ГОСУДАРСТВЕННОЙ ПРОМЫШЛЕННОЙ ПОЛИТИКИ В ФАРМАЦЕВТИЧЕСКОЙ ОТРАСЛИ РОССИЙСКОЙ ФЕДЕРАЦИИ

Т. Ю. Гайдин^{1,2}, Е. В. Геллер², С. А. Рожнова², Т. А. Гайдина² ✉

¹ Московский государственный университет имени М. В. Ломоносова, Москва, Россия

² Российский национальный исследовательский медицинский университет имени Н. И. Пирогова, Москва, Россия

Ввиду изменений в современном мире необходимо развитие отечественной фармацевтической отрасли, что особенно актуально при проведении политики импортозамещения. В работе классифицированы основные меры промышленной политики государства в фармацевтической отрасли: информационно-консультационные, научно-технические, инновационные и экономические. Для каждой группы мер промышленной политики рассмотрены практические действия и их возможные последствия: стимулирование внутреннего потребления, регулирование импорта, стимулирование и поддержка экспорта, стимулирование технологического развития, государственно-частное партнерство, поддержка развития межотраслевых территориально-производственных комплексов (кластеров), прямая государственная поддержка инвестиций, налоговые инвестиционные стимулы.

Ключевые слова: фармацевтическая отрасль, поддержка конкуренции, промышленная политика, инновации, благосостояние потребителя

Вклад авторов: Т. Ю. Гайдин, Е. В. Геллер — анализ литературы, проведение исследования, подготовка рукописи; С. А. Рожнова, Т. А. Гайдина — анализ литературы, планирование и проведение исследования, подготовка рукописи.

✉ **Для корреспонденции:** Тимофей Юрьевич Гайдин
ул. Островитянова, д. 1, г. Москва, 117997, Россия; gaydin@econ.msu.ru

Статья получена: 30.01.2023 **Статья принята к печати:** 17.02.2023 **Опубликована онлайн:** 28.02.2023

DOI: 10.24075/vrgmu.2023.007

Russian Pharmaceutical Industry

Pharmaceutical companies have always found production of drugs an investment appealing sector of the Russian economy, since Russian market is one of the largest markets for medicines worldwide and it continues to grow. June 2021 through June 2022, the size of the commercial drugs market of the country was about 1.3 trillion rubles. In rubles, it has increased by 29.2% first six months of 2022 over first six months of 2021 [1]. Pharmaceutical industry is strategically important: health of the population hinges on timely provision of high-quality drugs and cannot be critically dependent on imports. Over the past 9 years, 62 integrated pharmaceutical production complexes have been opened in Russia and 16 factories launched; there are over 500 pharmaceutical companies currently in business that stably produce drugs with sanctions in the background, but this is not enough to foster competition, it is necessary to pursue an industrial policy aimed at developing the pharmaceutical market [2]. In Russia, foreign companies, such as OTCPharm, Bayer, Stada, GlaxoSmithKline, Sanofi, remain the leading players, and they specialize not only in sales

and promotion but also in the development and production of pharmaceuticals [3].

Given the current political and epidemiological conditions and the fact that foreign pharmaceutical companies are superior to their Russian national counterparts, it can be said that industrial policy is an important practical tool for the Russian economy. During the initial adaptation, import substitution efforts proved to be insufficiently effective and rather costly [4].

This article defines the industrial policy measures that have to do with informational and consulting aspects, research and technical parts, innovations and economic factors.

Industrial policy measures

The industrial policy measures being implemented in Russia (and within its pharmaceutical industry in particular) were developed with the current political and epidemiological circumstances in mind (see Table) [5, 6].

In addition to the above industrial policy measures, it is necessary to pursue a staffing policy, since economic sustainability of pharmaceutical companies depends on

Table. Industrial policy measures and tools of state support. (According to: Kalinin A. Developing a balanced industrial policy: structuring goals, objectives, tools. Questions of Economics. 2012; (4): 132–146.)

#	Industrial policy measures	Tools of state support
1	Encouragement of consumption of domestic drugs	State purchasing of products from domestic producers
2	Regulation of drug imports	Non-tariff regulation of imports, technological barriers
3	Drug exports stimulation and support	Tax incentives for the exports, simplified customs procedures
4	Stimulation of technological development	Provision of resources to support innovations and technological development
5	Public private partnerships	Joint ventures
6	Support of development of intersectoral territorial production complexes (clusters)	Organizational and financial support of organization and development of clusters Organization of cooperation between educational and research institutions, producers and industry bodies
7	Direct support of investments by the government	Interest rate or cost subsidies, milder deposit requirements, other preferences
8	Tax incentives for investments	Privileges

competitive human resources. Their skills, professional training and qualifications ensure improvement of the production efficiency. The demand for highly qualified personnel has long exceeded supply thereof, and the labor market has been seeing a significant shortage of the respective labor resources [7].

Regulations allow sales of drugs in foreign packaging in the Russian Federation until December 31, 2023, subject to the availability of labeling in Russian [8]. In addition, drug suppliers are required to give a 6-month advance notice of their plans to leave the pharmaceutical market [9].

Stimulation of domestic consumption was analyzed in one of the studies investigating group buying of medicines in low- and middle-income countries [10]. The authors of that study looked into the structure of pharmaceutical markets in India (Kerala state), the Philippines, Senegal, Serbia, South Africa (states of KwaZulu-Natal, Northern, Western and Eastern Capes), Tunisia and Zambia. The data covered purchases of 40 drugs from 16 therapeutic areas (most of them — generics) made in 2015 through 2017. The results of the study allowed identification of two consistent patterns. First, the increased demand for drugs produced in low- and middle-income regions reinforces the position of their producers as awardees of the public procurement contracts. Secondly, centralized buying means purchasing of large amounts, which, for governments, translates into volume discounts. Thus, centralized bulk orders of pharmaceuticals in the public sector drive the prices down [10]. It is possible to stimulate national consumption of domestically produced drugs under the following conditions: population of the country has access to all necessary drugs; producers have sufficient capacities and human resources; and supporting them does not cause critical damage to the economy as a whole.

Otherwise, reducing the prices requires regulation of imports of drugs. For example, in the US, purchases of prescription drugs account for 10% of the total healthcare spending: in 2016, the prescription drug sales there amounted to over \$448 billion. A study by the Kaiser Family Foundation established that in 2019, the average spending by Medicare beneficiaries on various hematologic drugs was as follows: venetoclax — \$8712/year, imatinib — \$8983/year, acalabrutinib — \$10,175/year, midostaurin — \$11,830/year, lenalidomide — \$14,461/year. Both consumers and policy makers have underscored the significant differences in cost of drugs in the US and other industrialized countries. Many of these drugs are new, there are yet no generics and biosimilar medicines that could put pressure on their prices. In order to drive the said consumer prices down, it was proposed to allow additional large-scale imports of drugs

from the following countries: Australia, Canada, Israel, Japan, New Zealand, Switzerland, South Africa, EU member states and member states of the European Economic Area [11].

In Europe, the US and other countries with strict patent laws, competing producers are not allowed to produce generic drugs or biosimilar medicines even if they are made only for export to a country where the respective patents are invalid, have been obtained or have expired. This situation encourages producers of generics to systematically grow their capacities in potential export markets and not in Europe or the US, while the patents still have to expire. European market is expected to gain from non-renewal of patents in other countries, the respective benefits taking the form of additional exports worth about \$1 billion per year and about 25000 new jobs [12]. In Russia, holder of a pharmaceutical patent is protected legally as per the international standards. However, in some cases, patent law conflicts such factors as the security of the state, protection of life and health of the citizens, public welfare and technological progress. In this connection, the state implements mechanisms to regulate such conflicts, such as limitation of effect of the patent law in the form of compulsory licensing [13].

In recent years, as part of implementation of the European Union's industrial policy there was established a public-private partnership called Innovative Medicines Initiative (IMI), which seeks to actively develop innovative drugs. The objectives of IMI are to accelerate the development of more effective and safer drugs by designing reliable and validated study patterns, to eliminate the poorly predictable preclinical models, to develop new biomarkers and drug targets and to create tools and methods enabling prediction of adverse reactions to drugs. With around €5 billion in funding, IMI can boost drug development in Europe by 2024. Currently, the initiative supports 86 consortiums comprised of 593 research groups that are members of the European Federation of Pharmaceutical Industries and Associations (EFPIA), as well as 1214 academic partnership groups and 249 other partnership groups. IMI is engaged in all types of pharmaceutical research, including development of biomarkers, drugs against infectious diseases and diseases of the central nervous system [14].

In Russia, pharmaceutical clusters have been created since 2010 as part of implementation of the industrial policy [15]. One of the main exporters working with the Kaluga pharmaceutical cluster is Liston, a vendor that supplies medical products to 35 countries and operates in more than 50 countries. The cluster also cooperates with Eurobiomed, Bavaria and MediconValley. The export revenue of residents of the Kaluga region's pharmaceutical, biotechnological and biomedical cluster

is expected to double by 2024 and amount to \$160 million while employing 11.3 thousand people, but the real foreign policy situation may adjust the estimated export figures: the trade with the European and American companies shrinks and new trade relations between Russia and countries of the East and South Asia evolve [16, 17]. Therefore, it is important to mention the Chinese and Korean experience of implementation of the industrial policy measures. Some of the key measures in China are beneficial lending, tax cuts, subsidies and relaxed requirements for companies wishing to enter the market. The industrial policy can improve the efficiency of resource allocation and promote industrial development [18]. South Korea has adopted the Western model of industrial policy measures, which include, for example, barriers to imports [19].

Seeking to stimulate research and development of the new drugs, the government of the Russian Federation will provide subsidies to pharmaceutical companies. There are two main subsidies allocation strategies: subsidies for innovative resources and subsidies for innovative products. For companies, subsidies mean better profits, and for the state — stimulation of innovations by the companies and improvement of the social welfare [20].

There are also tax incentives supporting investments into the pharmaceutical industry in Russia. For example, the

government of Moscow issued a decree that decreases the income tax from 20 to 16.5% for pharmaceutical facilities that received the status of an industrial pharmaceutical production complex. These support measures ensure creation of highly paid jobs and the further development of industrial production [21].

CONCLUSION

In today's difficult economic and foreign policy conditions, additional analysis and implementation of industrial policy measures enable expansion of the possibilities available to the domestic pharmaceutical production facilities. From the perspectives of both the pharmaceutical companies and the state, the most appealing industrial policy measures are those design to support of development of intersectoral territorial production complexes (clusters), stimulate and support exports. Organization of pharmaceutical clusters translated into new cooperation ties with 35 countries and the possible creation of 11.3 thousand jobs. Exports to the Southeastern part of the globe, China, Republic of Korea, will support expansion of the production capacities of domestic pharmaceutical companies. Implementation of comprehensive industrial policy measures enable creation of the best prerequisites for development of the pharmaceutical industry, which is socially significant.

References

1. Dannye roznichnogo audita farmacevticheskogo rynka RF DSM Group. 2022. [citirovano 2023 Yanvar' 28] Dostupno po ssylke: <https://dsm.ru/docs/analytics/lyun'%202022%20tlog.pdf>. Russian.
2. Solodova R. Analitika ot GxP News. 2022. [citirovano 2022 Dekabr' 24]. Dostupno po ssylke: <https://gxpnews.net/2022/06/farmotrasl-rossii-na-nachalo-2022-goda/>. Russian.
3. DSM Group. Farmaceuticheskij ryok Rossii: Dekabr' 2022 g. 2022. [citirovano 2023 Yanvar' 28]. Dostupno po ssylke: <https://dsm.ru/marketing/free-information/analytic-reports/>. Russian.
4. Oborin MS. Problemy i perspektivy importozameshheniya v farmacevticheskoy otrasli. Vestnik NGIEl. 2021; 5 (120): 101–10. DOI: 10.24412/2227-9407-2021-5-101-110. Russian.
5. Kurdin A, Shastitko A. The new industrial policy: a chance for the BRICS countries. BRICS Journal of Economics. 2020; 1 (1): 60–80. DOI: 10.38050/2712-7508-2020-5.
6. Kalinin A. Postroenie sbalansirovannoy promyshlennoy politiki: voprosy strukturirovaniya celej, zadach, instrumentov. Voprosy ehkonomiki. 2012; (4): 132–146. DOI: 10.32609/0042-8736-2012-4-132-146. Russian.
7. Korzh NV, Shkatova KV, Supikov V. N. Sovremennye tendencii razvitiya rossijskogo rynka truda. Izvestiya vysshix uchebnyx zavedenij. Povolzhskij region. Obshhestvennye nauki. 2022; 2 (62): 40–51. Russian.
8. Postanovlenie Pravitel'stva Rossijskoj Federacii ot 05.04.2022 # 593 «Ob osobennostyax obrashheniya lekarstvennyx sredstv dlya medicinskogo primeneniya pri vozniknovenii defektury ili riska vozniknoveniya defektury v svyazi s vvedeniem v otnoshenii Rossijskoj Federacii ogranichitel'nyx mer ehkonomicheskogo xaraktera». 2023. [citirovano 2023 Mart 02]. Dostupno po ssylke: <http://publication.pravo.gov.ru/Document/View/0001202204110030?index=0&rangeSize=1>. Russian.
9. Federal'nyj zakon #323 ot 21.11.2011 «Ob osnovax oxrany zdorov'ya grazhdan v RF». 2023. [citirovano 2023 Mart 02]. Dostupno po ssylke: <https://www.zakonrf.info/zakon-o-zdorovyegrazhdan/>. Russian.
10. Pooled Procurement of Drugs in Low and Middle Income Countries. [citirovano 2023 Yanvar' 28]. Dostupno po ssylke: https://www.tse-fr.eu/sites/default/files/TSE/documents/doc/wp/2019/wp_tse_999.pdf.
11. Scheckel CJ, Vincent Rajkumar S. Drug importation: limitations of current proposals and opportunities for improvement. Blood Cancer Journal. 2021; 11 (7): 132. DOI: 10.1038/s41408-021-00522-3.
12. Minssen T, Kesselheim AS, Darrow JJ. An export-only exception to pharmaceutical patents in Europe: should the United States follow suit? Nat Biotechnol. 2019; 37 (1): 21–22. DOI: 10.1038/nbt.4324.
13. Gaydin TY, Rozhnova SA. Compulsory licensing in pharmaceutical industry: current state of affairs and prospects. Bulletin of RSMU. 2021;(2);5–10. DOI: 10.24075/brsmu.2021.011.
14. Schuhmacher A, Gassmann O, McCracken N, Hinder M. Open innovation and external sources of innovation. An opportunity to fuel the R&D pipeline and enhance decision making?. Journal of Translational Medicine. 2018; 16 (1): 119. DOI: 10.1186/s12967-018-1499-2.
15. Sokolova SV, Kareva NN, Ivanov AS. Farmaceuticheskij ryok: klasternyj vektor razvitiya. Problemy sovremennoj ehkonomiki. 2017; 4 (64): 173–8. Russian.
16. Dorozhkina TV, Pilgun YaS. Osobennosti razvitiya Kaluzhskogo farmacevticheskogo klastera v usloviyax vneshnix vyzovov: pandemiya koronavirusa. Ehkonomika i biznes: teoriya i praktika. 2020; 51 (63): 169–72. DOI: 10.24411/2411-0450-2020-10400. Russian.
17. Dorozhkina TV, Tatarchenko KR, Kuznecova AA. Nacproekt «Mezhdunarodnaya kooperaciya i ehksport»: smeshhenie akcenta na regional'nyj uroven'. Vestnik obrazovatel'nogo konsorciuma Srednerusskij universitet. Seriya: Ehkonomika i upravlenie. 2022; (20): 16–18. Russian.
18. Chen J, Xie L. Industrial policy, structural transformation and economic growth: evidence from China. Front Bus. Res China. 2019; 13 (18): <https://doi.org/10.1186/s11782-019-0065-y>.
19. Lane N. Manufacturing Revolutions: Industrial Policy and Industrialization in South Korea. 2022. 2023. [citirovano 2023 Mart 02]. Dostupno po ssylke: <http://dx.doi.org/10.2139/ssrn.3890311>.
20. Huang Z, Lan Y, Zha X. Research on government subsidy strategies for new drug R&D considering spillover effects. PloS One. 2022; 17 (2): e0262655. DOI: 10.1371/journal.pone.0262655.
21. Postanovlenie Pravitel'stva Moskvy ot 11.02.2016 N 38-PP «O merax po realizacii promyshlennoj i investicionnoj politiki v gorode Moskve». 2023. [citirovano 2023 Mart 02]. Dostupno po ssylke: <https://www.mos.ru/depr/documents/view/269724220/>. Russian.

Литература

1. Данные розничного аудита фармацевтического рынка РФ DSM Group. 2022. [цитировано 2023 Январь 28]. Доступно по ссылке: <https://dsm.ru/docs/analytics/Июнь%202022%20Итог.pdf>.
2. Солодова Р. Аналитика от GxP News. 2022. [цитировано 2022 Декабрь 24]. Доступно по ссылке: <https://gxnews.net/2022/06/farmotrasl-rossii-na-nachalo-2022-goda/>.
3. DSM Group. Фармацевтический рынок России: Декабрь 2022 г. 2022. [цитировано 2023 Январь 28]. Доступно по ссылке: <https://dsm.ru/marketing/free-information/analytic-reports/>.
4. Оборин М. С. Проблемы и перспективы импортозамещения в фармацевтической отрасли. Вестник НГИЭИ. 2021; 5 (120): 101–110. DOI: 10.24412/2227-9407-2021-5-101-110.
5. Kurdin A, Shastitko A. The new industrial policy: a chance for the BRICS countries. BRICS Journal of Economics. 2020; 1 (1): 60–80. DOI: 10.38050/2712-7508-2020-5.
6. Калинин А. Построение сбалансированной промышленной политики: вопросы структурирования целей, задач, инструментов. Вопросы экономики. 2012; (4): 132–146. DOI: 10.32609/0042-8736-2012-4-132-146.
7. Корж Н. В., Шкатова К. В., Супиков В. Н. Современные тенденции развития российского рынка труда. Известия высших учебных заведений. Поволжский регион. Общественные науки. 2022; 2 (62): 40–51.
8. Постановление Правительства Российской Федерации от 05.04.2022 № 593 «Об особенностях обращения лекарственных средств для медицинского применения при возникновении дефектуры или риска возникновения дефектуры в связи с введением в отношении Российской Федерации ограничительных мер экономического характера». 2023. [цитировано 2023 Март 02]. Доступно по ссылке: <http://publication.pravo.gov.ru/Document/View/0001202204110030?index=0&rangeSize=1>.
9. Федеральный закон №323 от 21.11.2011 «Об основах охраны здоровья граждан в РФ». 2023. [цитировано 2023 Март 02]. Доступно по ссылке: <https://www.zakonrf.info/zakon-o-zdorovye-grazhdan/>.
10. Pooled Procurement of Drugs in Low and Middle Income Countries. [цитировано 2023 Январь 28]. Доступно по ссылке: https://www.tse-fr.eu/sites/default/files/TSE/documents/doc/wp/2019/wp_tse_999.pdf.
11. Scheckel CJ, Vincent Rajkumar S. Drug importation: limitations of current proposals and opportunities for improvement. Blood Cancer Journal. 2021; 11 (7): 132. DOI: 10.1038/s41408-021-00522-3.
12. Minssen T, Kesselheim AS, Darrow JJ. An export-only exception to pharmaceutical patents in Europe: should the United States follow suit? Nat Biotechnol. 2019; 37 (1): 21–22. DOI: 10.1038/nbt.4324.
13. Гайдин Т. Ю., Рожнова С. А. Принудительное лицензирование в фармации: текущее регулирование и перспективы. Вестник РГМУ. 2021; (2): 5–11. DOI: 10.24075/vrgmu.2021.011.
14. Schuhmacher A, Gassmann O, McCracken N, Hinder M. Open innovation and external sources of innovation. An opportunity to fuel the R&D pipeline and enhance decision making? Journal of Translational Medicine. 2018; 16 (1): 119. DOI: 10.1186/s12967-018-1499-2.
15. Соколова С. В., Карева Н. Н., Иванов А. С. Фармацевтический рынок: кластерный вектор развития. Проблемы современной экономики. 2017; 4 (64): 173–8.
16. Дорожкина Т. В., Пильгун Я. С. Особенности развития Калужского фармацевтического кластера в условиях внешних вызовов: пандемия коронавируса. Экономика и бизнес: теория и практика. 2020; 51 (63): 169–72. DOI: 10.24411/2411-0450-2020-10400.
17. Дорожкина Т. В., Татарченко К. Р., Кузнецова А. А. Нацпроект «Международная кооперация и экспорт»: смещение акцента на региональный уровень. Вестник образовательного консорциума Среднерусский университет. Серия: Экономика и управление. 2022; (20): 16–18.
18. Chen J, Xie L. Industrial policy, structural transformation and economic growth: evidence from China. Front Bus. Res China. 2019; 13 (18): <https://doi.org/10.1186/s11782-019-0065-y>.
19. Lane N. Manufacturing Revolutions: Industrial Policy and Industrialization in South Korea. 2022. 2023. [цитировано 2023 Март 02]. Доступно по ссылке: <http://dx.doi.org/10.2139/ssrn.3890311>.
20. Huang Z, Lan Y, Zha X. Research on government subsidy strategies for new drug R&D considering spillover effects. PloS One. 2022; 17 (2): e0262655. DOI: 10.1371/journal.pone.0262655.
21. Постановление Правительства Москвы от 11.02.2016 N 38-ПП «О мерах по реализации промышленной и инвестиционной политики в городе Москве». 2023. [цитировано 2023 Март 02]. Доступно по ссылке: <https://www.mos.ru/depr/documents/view/269724220/>.

MIDTERM SEVERE FOREFOOT DEFORMITY TREATMENT OUTCOMES IN ELDERLY PATIENTS

Egiazaryan KA, Ratyev AP, Miroshnikova EA, Zhavoronkov EA, Abilemets AS ✉

Pirogov Russian National Research Medical University, Moscow, Russia

Severe complex deformities of the forefoot in elderly patients with no rheumatoid arthritis result in the pronounced decrease in quality of life, chronic pain, reduced mobility, failure to get shoes for everyday use, exacerbation of the concomitant somatic diseases. The use of conventional joint preservation techniques in such patients often leads to the deformity relapse, persistent pain, and the need for revision surgery that is often impossible due to worsening of the patients' general somatic status and local functional status. The study was aimed to improve surgical outcomes in elderly patients with no rheumatoid arthritis who had severe forefoot deformities. The prospective cohort study that involved allocation to the retrospective group for comparison of surgical outcomes in 65 patients was carried out in 2016–2019. The results obtained before and after surgery were assessed using the FFI, AOFAS Hallux, and AOFAS Lesser Toes scores. The Maryland scores were used to assess the outcomes during the postoperative period. The study revealed significant differences in treatment outcomes based on the AOFAS Hallux ($p = 0.0001$), AOFAS Lesser Toes ($p = 0.0001$), FFI ($p = 0.0001$), and Maryland ($p = 0.0001$) scores. In view of the elderly patients' specific nature, the radical surgical techniques that do not ensure joint preservation may be considered as effective and predictable methods of correction aimed at reducing the rate of revision surgeries. These techniques represent a one-step method to improve the quality of life of elderly patients.

Keywords: flat-valgus foot, metatarsalgia, forefoot

Author contribution: Egiazaryan KA — statement of the problem of managing the patients, manuscript editing; Ratyev AP — study concept, literature review, interpretation of the treatment outcomes; Miroshnikova EA — developing the study concept, theoretical justification of treatment, surgical treatment and monitoring of patients, data acquisition and analysis; Zhavoronkov EA — treatment of patients, postoperative management, assessment of medium-term treatment outcomes; Abilemets AS — surgical treatment, monitoring of patients, data acquisition and analysis, assessment of midterm treatment outcomes, manuscript editing.

Compliance with ethical standards: the study was approved by the Ethics Committee of Pirogov Russian National Research Medical University (protocol No. 181 of 28 January 2018). All patients submitted the informed consent to study participation.

✉ **Correspondence should be addressed:** Alexey S. Abilemets
Ostrovityanov, 1, Moscow, 117997, Russia; abilemets@mail.ru

Received: 02.02.2023 **Accepted:** 20.02.2023 **Published online:** 28.02.2023

DOI: 10.24075/brsmu.2023.008

СРЕДНЕСРОЧНЫЕ РЕЗУЛЬТАТЫ ЛЕЧЕНИЯ ТЯЖЕЛОЙ ДЕФОРМАЦИИ ПЕРЕДНЕГО ОТДЕЛА СТОПЫ У ПАЦИЕНТОВ ПОЖИЛОГО ВОЗРАСТА

К. А. Егизарян, А. П. Ратьев, Е. А. Мирошникова, Е. А. Жаворонков, А. С. Абилец ✉

Российский национальный исследовательский медицинский университет имени Н. И. Пирогова, Москва

Комплексные тяжелые деформации переднего отдела стопы у пожилых пациентов, не страдающих ревматоидным артритом, характеризуются выраженным снижением качества жизни, формированием хронического болевого синдрома, снижением общей мобильности с невозможностью подбора обуви для ежедневного использования, усугублением течения сопутствующих соматических заболеваний. Использование классических, сохраняющих сустав техник у данных пациентов зачастую приводит к рецидиву деформации, стойкому сохранению болевого синдрома, необходимости ревизионных вмешательств, часто невозможных из-за усугубления общесоматического или местного статуса пациента. Целью исследования было улучшить результаты хирургического лечения пациентов пожилого возраста, не страдающих ревматоидным артритом, с тяжелой деформацией переднего отдела стопы. Проведено проспективное когортное исследование с выделением ретроспективной группы сравнения результатов оперативного лечения 65 пациентов, с 2016 по 2019 г. Результаты до и после операции оценивали по шкалам FFI, AOFAS Hallux, AOFAS Lesser Toes. Оценку результатов в послеоперационном периоде проводили по шкале Maryland. В исследовании получены статистически значимые различия результатов лечения по шкалам AOFAS Hallux ($p = 0,0001$), AOFAS Lesser Toes ($p = 0,0001$), FFI ($p = 0,0001$), Maryland ($p = 0,0001$). В связи со специфичностью пожилых пациентов радикальные методики, не сохраняющие сустав, могут быть рассмотрены как эффективный предсказуемый способ коррекции, направленный на сокращение ревизионных вмешательств, и являются одноэтапным методом улучшения качества жизни пожилых пациентов.

Ключевые слова: плоско-вальгусная деформация, метатарзалгия, передний отдел стопы

Вклад авторов: К. А. Егизарян — постановка проблематики лечения данных пациентов, редактирование статьи; А. П. Ратьев — концепция исследования, работа с литературой, интерпретация результатов лечения; Е. А. Мирошникова — разработка концепции исследования, теоретическое обоснование лечения пациентов, оперативное лечение и наблюдение за пациентами, сбор и анализ данных; Е. А. Жаворонков — лечение пациентов, послеоперационное ведение, оценка среднесрочных результатов лечения; А. С. Абилец — оперативное лечение, наблюдение за пациентами, сбор и анализ данных, оценка среднесрочных результатов лечения, редактирование статьи.

Соблюдение этических стандартов: исследование одобрено этическим комитетом РНИМУ им. Н. И. Пирогова Минздрава России (протокол № 181 от 28 января 2018 г.). Все пациенты подписали информированное согласие на участие в исследовании.

✉ **Для корреспонденции:** Алексей Сергеевич Абилец
ул. Островитянова, д. 1, г. Москва, 117997, Россия; abilemets@gmail.com

Статья получена: 02.02.2023 **Статья принята к печати:** 20.02.2023 **Опубликована онлайн:** 28.02.2023

DOI: 10.24075/vrgmu.2023.008

Surgical treatment of elderly patients with forefoot deformities is a challenging task. The static complex deformity that involves deformities of two or more rays of the foot together with severe hallux valgus and rigid lesser ray deformities is difficult to correct by conventional surgical methods.

When developing the treatment tactics, it is necessary to take into account not only the foot deformity and the bone tissue quality together with the features of selecting metal fixators [1], but also the neurocirculatory status of the limb, local functional status of the soft tissues, the presence and course

of chronic concomitant disorders, taking various medications in order to ensure compensation, the need to minimize the patient's hypodynamia, his/her social status and ability to adequately execute the more or less complex postoperative instructions [2].

It is worth choosing more predictable tactics of surgical correction in order to minimize the risk of the deformity relapse, chronic pain, and the need for revision surgical interventions.

Regardless of numerous options for correction of severe static complex forefoot deformities, there is still no consensus on management of elderly patients [3]. The currently existing treatment tactics are often based on the surgeon's personal experience only [4].

Given high perioperative risk, it is recommended to use conservative therapy in many elderly patients. However, conservative treatment of patients with no risk of surgical intervention fails to restore the patients' motor activity or improve their quality of life. Furthermore, it is often impossible due to high cost and inaccessibility of orthopaedic devices [5]. Moreover, some authors note the increased injury rate in elderly patients that is associated with alterations of gait stereotype due to severe foot deformities [6], while surgical treatment makes it possible to restore the patients' freedom of movement and improve their quality of life despite all the risks [7].

Regardless of the fact that satisfactory forefoot deformity treatment outcomes can be generally achieved by surgical correction, the share of adverse outcomes is still high (25–33%) [8]. It would be several times higher in the group of elderly patients, that is why the revision surgery rate would also increase.

The attempts to correct severe deformities in these patients by conventional joint preservation techniques often lead to failure because of the morphological features of persistent deformity, such as severe cicatricial adhesion of the sesamoids, which cannot be corrected without aggressive loosening of soft tissues, the need for pronounced lateralization of the first metatarsal distal fragment and the failure of fixation due to osteoporosis of various origins and minimal bone contact after the bone fragment displacement, because of the high risk of the first metatarsal head avascular necrosis associated with abnormal vascularization, development of severe degenerative arthrosis of first metatarsophalangeal joint after correction due to underestimation of the initial injury to the cartilage and subchondral bone [9]. All of this leads to progressive first ray deformity and abnormalities of the stance and pushoff phase [10], incomplete PASA correction, and the development or recurrence of pre-existing transfer metatarsalgia [11], the development of extensive soft tissue damage associated with abnormal circulation due to massive releases [12], symptomatic pseudarthrosis [13]. The rigid dislocations of the lesser toe proximal phalanges with the contracture formation and shortening of the toe neurovascular bundles increase the risk of tissue necrosis and toe gangrene after the dislocation management involving insufficient shortening of the ray [14]. The degenerative damage to the fixing soft tissue structures, such as the plantar plate and the collateral ligaments of metatarsophalangeal joints increase the intraoperative time and the soft tissue injury when attempting to restore these structures using grafting or suture, while lesser metatarsal osteotomy often results in symptomatic pseudarthrosis with severe metatarsalgia [15].

All the above circumstances result in the need to rely on more predictable surgical methods and the methods that make it more likely to avoid revision surgery and provide radical treatment to rid the patient of symptoms when choosing the surgical treatment tactics for this extremely complex group of

patients. The radical surgical technique that does not ensure joint preservation that has been first proposed for treatment of patients with rheumatoid arthritis is one of such methods.

The study was aimed to improve surgical outcomes in elderly patients with no rheumatoid arthritis who had severe forefoot deformities using the surgical technique that did not ensure joint preservation.

METHODS

Study design

The prospective cohort study that involved allocation to the retrospective group for comparison of surgical outcomes in patients who received treatment at the Department of Traumatology, Orthopedics and Military Field Surgery (Pirogov Russian National Research Medical University) and the University Clinic of Traumatology and Orthopedics (City Clinical Hospital № 1, Moscow) was carried out in 2016–2019. The average period of the treatment outcome estimation in the control group was 34.26 ± 9.48 months, while the average period of the treatment outcome estimation in the index group was 27.73 ± 6.31 months.

All the patients were operated by the same surgical team under spinal anesthesia. The follow-up examination of the patient after surgery was conducted by the surgical team members at weeks 6, 12, 24 after surgery and during the patient's last visit. The post-surgical instrumental examination of the feet that involved the forefoot radiography in the anteroposterior and oblique projections was also performed at weeks 6, 12, 24 and during the patient's last visit.

Patients

The study involved 65 patients, among them all were females. This can be explained by predominance of symptomatic foot deformities in women. The average age of the studied patients was 72.69 ± 5.54 years.

Inclusion criteria: age over 65 years; no established diagnosis of rheumatoid arthritis; severe first ray foot deformity according to the Coughlin classification; rigid hammertoe deformity of one or more lesser toes with dislocation of the metatarsophalangeal joint that cannot be fixed during clinical assessment; no clinical effects of conservative therapy.

Exclusion criteria: age under 65 years; history of surgical correction of the forefoot; mild-to-moderate first ray foot deformity according to the Coughlin classification; elastic deformities of the lesser toes.

Reconstructive surgery of single foot was performed in all groups. The patients were divided into two groups in accordance with the applied technique.

The control patients were operated using the conventional joint preservation techniques. The control group included 35 patients.

The following surgical methods were considered as conventional.

Correction of the first ray of the foot in the control group:

- distal metadiaphyseal osteotomy of the first metatarsal (SCARF, Chevron, Maestro);
- Akin osteotomy of the great toe proximal phalanx;
- Lapidus procedure;
- metatarsophalangeal joint resection arthroplasty.

The correction options were used in combinations (Table 1).

Correction of the lesser rays of the foot in the control group was performed by the following methods:

Table 1. Characteristics of the first ray surgeries

Characteristics of methods	Total number of patients	Number of cases, abs	Share of cases, %
Distal osteotomies + Akin osteotomy	35	22	62.9%
Lapidus procedure + distal osteotomy	35	16	45.7%
Metatarsophalangeal joint resection arthroplasty	35	5	14.3%

– distal minimally invasive metatarsal osteotomy (DMMO);
 – Weil osteotomy without bone fixation in accordance with our patented method (RF patent No. 2705233);
 – Weil osteotomy with bone fixation;
 – resection arthroplasty of the proximal interphalangeal joints of the lesser toes (Table 2).

Patients of the index group ($n = 30$) were operated using the technique that did not ensure joint preservation known as the Hoffman-Clayton procedure, which included arthrodesis of the first metatarsophalangeal joint, 2nd–5th metatarsal head resection, resection arthroplasty of the proximal interphalangeal joints involving transcutaneous fixation of the 2nd–5th toes with wires in the metatarsal canals, or using our patented method (RF patent № 2742447), which included arthrodesis of the first metatarsophalangeal joint and fixation with a plate, 2nd–4th metatarsal head resection, resection arthroplasty of the proximal interphalangeal joints involving transcutaneous fixation of the 2nd–4th toes with wires in the metatarsal canals, minimally invasive oblique proximal diaphyseal osteotomy of the fifth metatarsal without metal fixation.

Postoperative management of patients

On day two after surgery the patient was bandaged to ensure elastic toe fixation in the position of metatarsophalangeal joint overcorrection (plantar flexion) in the control group or the position set by metal fixators in the index group.

On day 14 the dressings were changed and the stitches were removed from the postoperative wound, the patient was bandaged again to ensure the position of metatarsophalangeal joint overcorrection till day 28 after surgery. After that the dressings were removed in both groups. In the index group the fixing wires were also removed on day 28 after the intervention.

All the patients were allowed the operated limb loading since the next day after surgery using special orthopedic shoes. The guidelines on wearing orthopedic shoes varied depending on the type of the first metatarsal reconstructive surgery type. Shoes had been used for 6 weeks after distal osteotomy or for 8 weeks after the first metatarsophalangeal joint arthrodesis and the Lapidus procedure.

Methods for assessment of the results

The following preoperative and postoperative radiological parameters were assessed:

- hallux valgus angle (HVA; the angle between the longitudinal axes of the first metatarsal and the first proximal phalanx of the hallux);
- intermetatarsal angle (IMA; the angle between the longitudinal axes of the first and second metatarsals);

Table 2. Characteristics of the main lesser ray surgeries

Characteristics of methods	Total number of patients	Number of cases, abs	Share of cases, %
DMMO	35	6	17.1%
Weil osteotomy without bone fixation	35	17	65.4%
Weil osteotomy with bone fixation	35	9	34.6%
Resection arthroplasty	35	26	74.3%

– proximal articular set angle (PASA; the angle formed by the articular surface of the first metatarsal head and the longitudinal axis of the first metatarsal).

The function of the foot was assessed before and after surgery using the following scores: FFI (Foot Functional Index), AOFAS (American Orthopaedic Foot and Ankle Society Score) Lesser Toes, AOFAS (American Orthopaedic Foot and Ankle Society Score) Hallux. The results were also assessed using the Maryland score during the postoperative period.

According to the results obtained (Table 3), there were no significant intergroup differences in the main preoperative assessment criteria. However, it should be noted that statistical processing has revealed differences in the PASA and IMA scores. This can be explained by errors of positioning for radiography and small size of the patient sample.

Statistical analysis

When comparing two groups based on the numerical indicators, the mean values and standard deviations were used in the $M \pm S$ format. The nonparametric Mann-Whitney U test was used to compare two groups by quantitative variables. Statistical significance of intergroup differences for binary and categorical variables was defined using the Pearson's chi-squared (χ^2) test. Analysis of the dependent variables for comparison of two periods was based on the nonparametric Wilcoxon signed-rank test. The significance level was set at 0.05. Statistical data processing was performed using the Statistica 10 and SAS JMP 11 software packages.

RESULTS

The data obtained (Table 4) suggest that there were significant differences in all the indicators between two comparison groups. The most significant were the differences in the FFI scores between the controls and the index group (on average by 26.0%; $p < 0.0001$); the AOFAS Lesser Toes scores between the index group and the controls (on average by 33.1%; $p < 0.0001$); the AOFAS Hallux scores between the index group and the controls (on average by 19.6%; $p < 0.0001$).

The analysis of the dynamic changes in these parameters before and after treatment is provided in Table 5.

The findings suggest that all the indicators have changed significantly. The most significant are the changes in the FFI scores (in the control group) (on average by 34.5%; $p < 0.0001$); the AOFAS Lesser Toes scores (in the control group) (on average by 29.9%; $p < 0.0001$); the AOFAS Hallux scores (in the control group) (on average by 43.0%; $p < 0.0001$).

Statistical processing has also revealed the risk factors that most often lead to satisfactory and adverse treatment

Table 3. Comparison of two groups based on the radiological criteria and foot function assessment results obtained using the assessment scales before surgery

Indicator	Group		Significance level <i>p</i>
	Control group	Index group	
	(<i>n</i> = 35)	(<i>n</i> = 30)	
Scores			
AOFAS Hallux before surgery	18.77 ± 11.44	16.03 ± 5.80	0.8312
AOFAS Lesser Toes before surgery	19.63 ± 13.61	18.10 ± 5.86	0.4009
FFI before surgery	68.74 ± 12.93	72,87 ± 12,66	0.2009
Radiological criteria			
HVA before surgery	54.26 ± 6.55	55.67 ± 9.13	0.7366
IMA before surgery	19.77 ± 1.99	17.93 ± 2.79	0.0055
PASA before surgery	33.60 ± 7.61	37.57 ± 7.05	0.0168

outcomes based on the AOFAS Hallux, AOFAS Lesser Toes, FFI scores of the control group obtained before surgery.

The AOFAS Hallux and AOFAS Lesser Toes scores below 75 were considered as satisfactory and adverse treatment outcomes. The FFI scores above 40% were considered as satisfactory and bad.

Significance of the indicator effects on the target binary variable was determined using the Pearson's chi-squared (χ^2) test. All the factors were sorted in descending order of significance (χ^2 statistics) to select the key indicators of the risk of such events, as AOFAS Hallux < 75, AOFAS Lesser Toes < 75, FFI > 40.

Age over 70 appeared to be a significant risk factor in all the studied groups.

AOFAS Lesser Toes — $p = 0.0005$

AOFAS Hallux — $p = 0.03$

FFI — $p = 0.002$

DISCUSSION

The world literature describes numerous options for surgical correction of severe valgus forefoot deformities and various combinations of methods. However, selection of options for correction does not take into account the patient's age, circulatory status of the limb, the patient's rehabilitation potential, and concomitant disorders. Decompensation of concomitant disorders often makes it impossible to perform revision surgery, thus leading to persistence of pain syndrome, decrease in the elderly patient's daily activity, reduced quality of life, and the need for continuous use of anti-inflammatory drugs. Elimination of pain and prevention of the foot deformity relapse are the main goals of the surgical treatment of severe deformities in elderly patients. Thus, it has been shown that cosmetic results were less important than elimination of pain and the possibility to increase the distance traversed [16]. It is

necessary to choose more controllable, predictable, and reliable methods of surgical correction to ensure elimination of pain in this group of patients. Arthrodesis of the metatarsophalangeal joint and lesser metatarsal head resection are one of the options for severe forefoot deformities in patients with rheumatoid arthritis. This procedure that does not ensure joint preservation allows to achieve persistent elimination of pain, radical correction of the deformity, and the increase in the patient's daily activity.

However, a few sources assume that surgical treatment of this type can also be suitable for correction of severe rigid forefoot deformities in elderly patients.

Thus, assessment of 13 patients (15 feet; the average follow-up period was 44.3 months after surgery; the range was 20–76 months) showed that the average postoperative satisfaction score was 9.0 (out of 10) [17]. None of the patients in this cohort needed reoperative surgery. The pain score was significantly reduced: from 6.2 before surgery to 1.9 after surgery ($p < 0.001$). Radiological parameters (1.2 IMA, HVA) improved after surgery ($p < 0.05$), the first metatarsophalangeal joint arthrodesis union was achieved in all 15 feet.

In the retrospective study of 39 patients (56 feet) with severe non-rheumatic forefoot deformities, 13 patients (20 feet) underwent first metatarsophalangeal joint arthrodesis and lesser metatarsal head resection, 20 patients (26 feet) underwent first metatarsophalangeal joint arthrodesis and Weil osteotomy of the metatarsal [18]. The average follow-up period was 24 months. The criteria of the patients' condition after surgery were assessed using the AOFAS and SF-36 scores. Postoperative satisfaction was 92% in patients after first metatarsophalangeal joint arthrodesis and lesser metatarsal head resection and 91% in patients after first metatarsophalangeal joint arthrodesis and lesser metatarsal osteotomy. However, the quantity of revision surgeries was not estimated in the studied groups. The total SF score was 80.7 and 76, respectively. The researchers concluded that surgery of this type could be recommended

Table 4. Comparison of two groups based on the radiological criteria and foot function assessment results obtained using the assessment scales after surgery

Indicator	Group		Significance level <i>p</i>
	Control group	Index group	
	(<i>n</i> = 35)	(<i>n</i> = 30)	
Scores			
AOFAS Hallux after surgery	61.80 ± 13.99	81.40 ± 4.54	< 0.0001
AOFAS Lesser Toes after surgery	49.49 ± 13.76	82.60 ± 3.34	< 0.0001
Maryland MFS	67.49 ± 7.02	88.40 ± 3.45	< 0.0001
Maryland MFS	34.20 ± 12.59	8.20 ± 4.62	< 0.0001
HVA after surgery	26.20 ± 8.32	12.93 ± 5.53	< 0.0001
IMA after surgery	11.20 ± 2.49	12.67 ± 2.35	0.015

Table 5. Estimation of the dynamic changes in the studied criteria before and after surgery

Group	Indicator	M ± S, before	M ± S, after	Dynamic changes	Differences between mean values (before –after)	Significance level <i>p</i>
Control group	AOFAS Hallux	18.77 ± 11.44	61.80 ± 13.99	229.22%	43.03	< 0.0001
Control group	AOFAS Lesser Toes	19.63 ± 13.61	49.49 ± 13.76	152.11%	29.86	< 0.0001
Control group	FFI	68.74 ± 12.93	34.20 ± 12.59	–50.25%	–34.54	< 0.0001
Control group	HVA	54.26 ± 6.55	26.20 ± 8.32	–51.71%	–28.06	< 0.0001
Control group	IMA	19.77 ± 1.99	11.20 ± 2.49	–43.35%	–8.57	< 0.0001
Control group	PASA	33.60 ± 7.61	21.06 ± 4.93	–37.33%	–12.54	< 0.0001
Index group	AOFAS Hallux	16.03 ± 5.80	81.40 ± 4.54	407.69%	65.37	< 0.0001
Index group	AOFAS Lesser Toes	18.10 ± 5.86	82.60 ± 3.34	356.35%	64.5	< 0.0001
Index group	FFI	72.87 ± 12.66	8.20 ± 4.62	–88.75%	–64.67	< 0.0001
Index group	HVA	55.67 ± 9.13	12.93 ± 5.53	–76.77%	–42.74	< 0.0001
Index group	IMA	17.93 ± 2.79	12.67 ± 2.35	–29.37%	–5.26	< 0.0001

for treatment of chronic pain associated with severe non-rheumatic forefoot deformities.

In the retrospective study of 193 patients of whom 85 were elderly people, all patients underwent examination 6 months and 2 years after surgery [19]. Conventional surgical techniques for correction of deformities, such as SCARF osteotomy of first metatarsal, osteotomy of the proximal phalanx of the hallux (Akin osteotomy), and the lesser metatarsal Weil osteotomy, were used in all the patients. No significant differences in postoperative satisfaction between the cohorts of young, middle-aged, and elderly patients were revealed based on the AOFAS and Sf-36 scores. However, it should be noted that the number of bed-days in the hospital was higher in elderly patients than in other groups, the return visits due to pain in the operated feet and hospital readmissions were more frequent in the group of elderly patients. The most important fact was that the group of elderly patients had a 5 times higher risk of the deformity relapse.

In our study, the index group included 30 patients, all the them were operated using the proposed method or our patented method (RF patent № 2742447).

The treatment outcomes were assessed using the AOFAS Lesser Toes, AOFAS Hallux, FFI, Maryland scores, the average follow-up period was 27.73 ± 6.31 months. In the intervention group, we managed to ensure a significant increase in the AOFAS Hallux score (from 16.03 ± 5.80 to 81.40 ± 4.54); the average increase for the parameter was 65.37; the AOFAS Lesser Toes score increased from 18.10 ± 5.86 to 82.60 ± 3.34, the average increase for the parameter was 64.5; as for the FFI score, we managed to improve the foot function from

72.87 ± 12.66% to 8.20 ± 4.62% (average values), the improvement was 64.67% (average values). When assessing the foot function after surgery, the average Maryland score was 88.40 ± 3.45, which corresponded to beneficial outcome. We managed to ensure significant differences in treatment outcomes compared to the control group based on the AOFAS Lesser Toes, AOFAS Hallux, FFI, Maryland scores. None of the patients needed revision surgery due to recurrent metatarsalgia or transfer metatarsalgia, hallux valgus relapse, rigid hammertoe deformity, osteotomy or arthrodesis non-union.

The described treatment outcomes, patients' satisfaction, and no need for revision surgery were achieved due to rational selection of the surgical technique for correction of static complex forefoot deformities in this extremely complex group of elderly patients. All the operated patients stayed mobile throughout the postoperative period, which was extremely important for elderly people. After surgery the daily activity levels and the maximum distance traveled without pain improved in all patients; the patients faced no difficulties when selecting footwear for everyday use, it was no longer necessary to select or purchase the highly complex orthopedic shoes.

CONCLUSIONS

The proposed option for correction of static complex forefoot deformities in elderly patients can be used in clinical practice. Despite its radical nature, the option has made it possible to achieve persistent elimination of pain, reduce the risk of reoperative surgery, and restore mobility in elderly patients with no rheumatoid arthritis.

References

- Bobrov DS, Slinyakov Lyu, Chenskij AD, Matvienko MI, Xlodaev MYu, Xurcilava ND. Rigidnyj 1-j palec stopy: klinika, diagnostika i lechenie (analiticheskij obzor literatury). Kafedra travmatologii i ortopedii. 2014; 3 (11): 4–12. Russian.
- Egiazaryan KA, Miroshnikova EA, Zhavoronkov EA, Ratev AP, Abilemec AS. Analiz rezul'tatov operativnogo lecheniya slozhnyx kompleksnyx deformacij perednego otdela stopy u pacientov starshej vozrastnoj gruppy. Politravma. 2021; 3: 46–53. Russian.
- Deenik A, Verburg A, Willem Louwerens J, de Waal Malefijt M, de Bie R. Evidence of Treatment Algorithms for Hallux Valgus. JSM Foot Ankle 1(1): 1003 (2016)
- Robinson AHN, Limbers JP. Modern concepts in the treatment of hallux valgus. J Bone Joint Surg. 2005; 87 (8): 1038–45.
- Mansur H, Cardoso V, Nogueira T, Castro I. Relationship between quality of life and radiological parameters after hallux valgus correction. Acta Ortopedica Brasileira. 2020; 28 (2): 65–68.
- Muchna A, Najafi B, Wendel CS, Schwenk M, Armstrong DG, Mohler J. Foot problems in older adults associations with incident falls, frailty syndrome, and sensor-derived gait, balance, and physical activity measures. J Am Podiatr Med Assoc. 2018; 108 (2): 126–139. DOI: 10.7547/15-186.
- S/O K S RZE, Lee M, Chen J, Meng NYE. Do patients aged 70 years and older benefit from hallux valgus surgery? J Foot Ankle Surg. 2022; 61 (2): 310–13. Available from: <https://doi.org/10.1053/j.jfas.2021.08.009>.
- Fleischer AE, Yorath MC, Joseph RM, Baron A, Nordquist T, Moore BJ, et al. Impact of podiatry resident experience level in hallux valgus surgery on postoperative outcomes. J Surg

- Research. 2014; 189 (2): 262–7. Available from: <https://doi.org/10.1016/j.jss.2014.03.005>.
9. Bock P, Kristen KH, Kröner A, Engel A. Hallux valgus and cartilage degeneration in the first metatarsophalangeal joint. The Journal of bone and joint surgery. British volume. 2004; 86 (5): 669–73. Available from: <https://doi.org/10.1302/0301-620x.86b5.14766>.
 10. Coetzee JC. Scarf osteotomy for hallux valgus repair: the dark side. Foot & Ankle international. 2003; 24 (1): 29–33. Available from: <https://doi.org/10.1177/107110070302400104>.
 11. Maceira E, Monteagudo M. Transfer metatarsalgia post hallux valgus surgery. Foot and ankle clinics. 2014; 19 (2): 285–307. Available from: <https://doi.org/10.1016/j.fcl.2014.03.001>.
 12. Solan MC, Davies MS. Revision surgery of the lesser toes. Foot and Ankle Clinics. 2011; 16 (4): 621–45. Available from: <https://doi.org/10.1016/j.fcl.2011.09.002>.
 13. Herzog JL, Goforth WD, Stone PA, Paden MH. A modified fixation technique for a decompressional shortening osteotomy: a retrospective analysis. The Journal of Foot and Ankle Surgery. 2014; 53 (2): 131–6. Available from: <https://doi.org/10.1053/j.jfas.2013.12.018>.
 14. Solan MC, Davies MS. Revision surgery of the lesser toes. Foot and Ankle Clinics. 2011; 16 (4): 621–45. Available from: <https://doi.org/10.1016/j.fcl.2011.09.002>.
 15. Herzog JL, Goforth WD, Stone PA, Paden MH. A modified fixation technique for a decompressional shortening osteotomy: a retrospective analysis. The Journal of Foot and Ankle surgery. 2014; 53 (2): 131–6. Available from: <https://doi.org/10.1053/j.jfas.2013.12.018>.
 16. Schneider W, Knahr K. Surgery for hallux valgus. The expectations of patients and surgeons. International Orthopaedics. 2001; 25 (6): 382–5. Available from: <https://doi.org/10.1007/s002640100289>.
 17. Nixon DC, McKean RM, Klein SE, Johnson JE, McCormick JJ. Rheumatoid Forefoot Reconstruction in the Nonrheumatoid Patient. Foot & Ankle International. 2017; 38 (6): 605–11. Available from: <https://doi.org/10.1177/1071100717696253>.
 18. Giunta JC, Mouton T, Fessy MH, Besse JL. Rheumatoid forefoot reconstruction in nonrheumatic patients: lesser metatarsal head resection versus osteotomy. The Journal Foot and Ankle Surgeons. 2021; 60 (2): 252–7. Available from: <https://doi.org/10.1053/j.jfas.2020.03.004>.
 19. Goh GS, Tay AYW, Thever Y, Koo, K. Effect of age on clinical and radiological outcomes of hallux valgus surgery. Foot & Ankle International. 2021; 42 (6): 798–804. Available from: <https://doi.org/10.1177/1071100720982975>.

Литература

1. Бобров Д. С., Слиняков Л. Ю., Ченский А. Д., Матвиенко М. И., Хлодаев М. Ю., Хурцилава Н. Д. Ригидный 1-й палец стопы: клиника, диагностика и лечение (аналитический обзор литературы). Кафедра травматологии и ортопедии. 2014; 3 (11): 4–12.
2. Егизарян К. А., Мирошникова Е. А., Жаворонков Е. А., Ратьев А. П., Абиелемез А. С. Анализ результатов оперативного лечения сложных комплексных деформаций переднего отдела стопы у пациентов старшей возрастной группы. Политравма. 2021; 3: 46–53.
3. Deenik A, Verburg A, Willem Louwerens J, de Waal Malefijt M, de Bie R. Evidence of Treatment Algorithms for Hallux Valgus. JSM Foot Ankle 1(1): 1003 (2016)
4. Robinson AHN, Limbers JP. Modern concepts in the treatment of hallux valgus. J Bone Joint Surg. 2005; 87 (8): 1038–45.
5. Mansur H, Cardoso V, Nogueira T, Castro I. Relationship between quality of life and radiological parameters after hallux valgus correction. Acta Ortopedica Brasileira. 2020; 28 (2): 65–68.
6. Muchna A, Najafi B, Wendel CS, Schwenk M, Armstrong DG, Mohler J. Foot problems in older adults associations with incident falls, frailty syndrome, and sensor-derived gait, balance, and physical activity measures. J Am Podiatr Med Assoc. 2018; 108 (2): 126–139. DOI: 10.7547/15-186.
7. S/O K S RZE, Lee M, Chen J, Meng NYE. Do patients aged 70 years and older benefit from hallux valgus surgery? J Foot Ankle Surg. 2022; 61 (2): 310–13. Available from: <https://doi.org/10.1053/j.jfas.2021.08.009>.
8. Fleischer AE, Yorath MC, Joseph RM, Baron A, Nordquist T, Moore BJ, et al. Impact of podiatry resident experience level in hallux valgus surgery on postoperative outcomes. J Surg Research. 2014; 189 (2): 262–7. Available from: <https://doi.org/10.1016/j.jss.2014.03.005>.
9. Bock P, Kristen KH, Kröner A, Engel A. Hallux valgus and cartilage degeneration in the first metatarsophalangeal joint. The Journal of bone and joint surgery. British volume. 2004; 86 (5): 669–73. Available from: <https://doi.org/10.1302/0301-620x.86b5.14766>.
10. Coetzee JC. Scarf osteotomy for hallux valgus repair: the dark side. Foot & Ankle international. 2003; 24 (1): 29–33. Available from: <https://doi.org/10.1177/107110070302400104>.
11. Maceira E, Monteagudo M. Transfer metatarsalgia post hallux valgus surgery. Foot and ankle clinics. 2014; 19 (2): 285–307. Available from: <https://doi.org/10.1016/j.fcl.2014.03.001>.
12. Solan MC, Davies MS. Revision surgery of the lesser toes. Foot and Ankle Clinics. 2011; 16 (4): 621–45. Available from: <https://doi.org/10.1016/j.fcl.2011.09.002>.
13. Herzog JL, Goforth WD, Stone PA, Paden MH. A modified fixation technique for a decompressional shortening osteotomy: a retrospective analysis. The Journal of Foot and Ankle Surgery. 2014; 53 (2): 131–6. Available from: <https://doi.org/10.1053/j.jfas.2013.12.018>.
14. Solan MC, Davies MS. Revision surgery of the lesser toes. Foot and Ankle Clinics. 2011; 16 (4): 621–45. Available from: <https://doi.org/10.1016/j.fcl.2011.09.002>.
15. Herzog JL, Goforth WD, Stone PA, Paden MH. A modified fixation technique for a decompressional shortening osteotomy: a retrospective analysis. The Journal of Foot and Ankle surgery. 2014; 53 (2): 131–6. Available from: <https://doi.org/10.1053/j.jfas.2013.12.018>.
16. Schneider W, Knahr K. Surgery for hallux valgus. The expectations of patients and surgeons. International Orthopaedics. 2001; 25 (6): 382–5. Available from: <https://doi.org/10.1007/s002640100289>.
17. Nixon DC, McKean RM, Klein SE, Johnson JE, McCormick JJ. Rheumatoid Forefoot Reconstruction in the Nonrheumatoid Patient. Foot & Ankle International. 2017; 38 (6): 605–11. Available from: <https://doi.org/10.1177/1071100717696253>.
18. Giunta JC, Mouton T, Fessy MH, Besse JL. Rheumatoid forefoot reconstruction in nonrheumatic patients: lesser metatarsal head resection versus osteotomy. The Journal Foot and Ankle Surgeons. 2021; 60 (2): 252–7. Available from: <https://doi.org/10.1053/j.jfas.2020.03.004>.
19. Goh GS, Tay AYW, Thever Y, Koo, K. Effect of age on clinical and radiological outcomes of hallux valgus surgery. Foot & Ankle International. 2021; 42 (6): 798–804. Available from: <https://doi.org/10.1177/1071100720982975>.